Manuscript submitted to Tectonics :

The western Andes at ~20–22°S: A contribution to the quantification of crustal shortening and kinematics of deformation

Tania Habel – Université de Paris, Institut de physique du globe de Paris, CNRS, F-75005 Paris, France – **taniahabel@gmail.com**

Martine Simoes – Université de Paris, Institut de physique du globe de Paris, CNRS, F-75005 Paris, France – **simoes@ipgp.fr**

Robin Lacassin – Université de Paris, Institut de physique du globe de Paris, CNRS, F-75005 Paris, France – **lacassin@ipgp.fr**

Daniel Carrizo – GeoEkun SpA, Santiago 7500593, Chile – **carrizo@geoekun.com**

Germán Aguilar – Advanced Mining Technology Center, Facultad de Ciencias Físicas y Matemáticas, Universidad de Chile, Avenida Tupper 2007, Santiago, Chile – **german.aguilar@amtc.cl**

This manuscript has been re-submitted for publication to Tectonics on 2022-02-07. This is the revised version of our initial manuscript submitted to the same journal (on 2020-12-17) after a first round of peer-review.

Any comments can be sent to the corresponding authors:

simoes@ipgp.fr

lacassin@ipgp.fr

The western Andes at ~20–22°S: A contribution to the quantification of crustal shortening and kinematics of deformation.

T. Habel[1], M. Simoes[1], R. Lacassin[1], D. Carrizo[2,3], and G. Aguilar[2]

[1]Université de Paris, Institut de physique du globe de Paris, CNRS, F-75005 Paris, France

[2]Advanced Mining Technology Center, Facultad de Ciencias Físicas y Matemáticas, Universidad de Chile, Avenida Tupper 2007, Santiago, Chile

[3]now at GeoEkun SpA, Santiago 7500593, Chile

Corresponding authors: Robin Lacassin (lacassin@ipgp.fr) & Martine Simoes (simoes@ipgp.fr)

Key Points:

- New data on the kinematics of shortening of the West Andean Fold-and-Thrust-Belt and Andean Basement Thrust at ~20–22°S
- Multi-kilometric shortening across the western Andes after ~68 Ma, implying significant contribution in the early stages of Andean orogeny
- Significant slowing-down of deformation rates after ~29 Ma, starting possibly by ~44 Ma

Abstract

The Andes are an emblematic active Cordilleran orogen. It is admitted that mountain-building in the Central Andes at ~20°S started by Late-Cretaceous to Early-Cenozoic along the subduction-margin, and propagated eastward. In general, the structures sustaining the uplift of the West Andean flank are dismissed, and their contribution to mountain-building remains poorly solved. Here, we focus on two sites along the western Andes at ~20–22°S, where structures are well exposed. We combine mapping from high-resolution satellite-images with field-observations and numerical trishear-forward-modeling to provide quantitative constraints on the kinematic evolution of the western Andes. Our results confirm the existence of two main structures: (1) the Andean Basement Thrust, a west-vergent thrust system placing Andean Paleozoic basement over Mesozoic strata; and (2) a series of west-vergent folds pertaining to the West Andean Fold-and-Thrust-Belt, deforming primarily Mesozoic units. Once restored, we estimate that both structures accommodate together at least ~6–9 km of shortening across the sole ~7–17 km-wide outcropping fold-and-thrust-belt. This multi-kilometric shortening represents only a fraction of the total shortening accommodated along the whole western Andes. The timing of the main deformation recorded in the fold-and-thrust-belt can be bracketed sometime between ~68 and ~29 Ma – and possibly between ~68 and ~44 Ma – from dated folded geological layers, with a subsequent significant slowing-down of shortening-rates. Even though negligible when compared to total shortening across the whole orogen, the contribution of the structures of the West Andes has been likely significant at the earliest stages of Andean mountain-building before deformation was transferred eastward.

1. Introduction

One of the most active convergent plate boundaries is located along the western margin of South America (Figure 1). There, the oceanic Nazca plate plunges beneath the South American continent, with a convergence rate currently of ~8 cm/yr at ~20ºS, according to the NUVEL-1A model (DeMets et al., 1994). The major part of this convergence is absorbed by the subduction megathrust in the form of large earthquakes (magnitude $M_w \geq 8$). A small fraction of this convergence – presently about 1 cm/yr at 20°S (e.g. Brooks et al., 2011; Norabuena et al., 1998) – contributes to the deformation of the upper plate over millions of years and to the formation of one of the largest reliefs at the Earth's surface: the Andean Cordilleras and the Altiplano-Puna plateau in between.

Andean mountain-building initiated by Late Cretaceous-Early Cenozoic along the western Andes of the Bolivian Orocline (between 16–22°S), and proceeded since then with the progressive eastward propagation of deformation onto the South American continent (e.g. Anderson et al., 2017; Armijo et al., 2015; Barnes et al., 2008; Barnes & Ehlers, 2009; Charrier et al., 2007; DeCelles et al., 2015; Eichelberger et al., 2013; Elger et al., 2005; Faccenna et al., 2017; Kley & Monaldi, 1998; McQuarrie et al., 2005; Oncken et al., 2006; Sheffels, 1990; and references therein). Most local and mountain-wide previous studies have essentially focused on the structures of the Altiplano-Puna plateau and on those of the various cordilleras to the east, but those located along the western flank of the orogen have remained up to now under-studied and their contribution to the significant topographic relief (Figure 1) and crustal thickness (e.g. Allmendinger et al., 1990; Introcaso et al., 1992; Isacks, 1988) of this part of the orogen poorly understood.

In most classical models of Andean mountain-building, the western flank is described as a passive monoclinal-like crustal-scale flexure (e.g., Isacks, 1988; Lamb, 2011, 2016; McQuarrie, 2002). However, in the late 1980's, Mpodozis and Ramos (1989) described west-vergent thrusting on the western Andean margin as potential major tectonic structures. Later, other authors described various thrusts, mostly west-vergent, at several localities along the western Andean flank (e.g. Charrier et al., 2007; Farías et al., 2005; Fuentes et al., 2018; Garcia & Hérail, 2005; Martínez et al., 2021; Muñoz & Charrier, 1996; Victor et al., 2004), but they generally gave these thrusts a minor role in the building of the western flank of the orogen. Only further south, at the latitude of Santiago de Chile (~33°30'S), a clear west-verging fold-and-thrust-belt (fold-and-thrust-belt hereafter simplified as FTB) has been documented along the western Andes (Armijo et al., 2010; Riesner et al., 2017, 2018). This FTB emerges at the active San Ramon Fault in front of the capital city of Santiago de Chile, and has absorbed a significant amount of shortening (Riesner et al., 2017). It has been proposed to link this western FTB to a crustal-scale west-verging thrust (the West Andean Thrust or WAT) thought to have played a major role in the initiation of orogenic building (Armijo et al. 2010, Riesner et al. 2018, 2019), although this interpretation is still debated (e.g. Astini & Dávila, 2010; Barrionuevo et al., 2021; Lossada et al., 2020).

We note that at 33º30'S, the orogen is relatively younger and narrower than in the Bolivian Orocline further north. In contrast, at ~20–22°S, where the Andes-Altiplano system is much wider and structurally more complex, the contribution of similar west-vergent structures along the western Andes is probably small compared to the >300 km total shortening (e.g. Anderson et al., 2017; Barnes & Ehlers, 2009; Eichelberger et al., 2013; Elger et al., 2005; Faccenna et al., 2017; Kley & Monaldi, 1998; McQuarrie et al., 2005; Oncken et al., 2006; Sheffels, 1990) across the entire >650 km wide orogen, but their role at the start of orogenic building may have been significant (Armijo et al., 2015). At this latitude, Victor et al. (2004) showed the existence of west-vergent thrusts rooting on a deep decollement dipping eastward beneath the western Andes. They also estimated that these structures absorbed ~3 km of shortening. However, this relatively minor shortening only characterizes the deformation affecting the post ~29 Ma Altos de Pica Formation deposited above the Choja erosional surface (or Choja Pediplain). The Mesozoic series beneath this surface appear much more deformed (e.g. Armijo et al., 2015; Blanco & Tomlinson, 2013) but this deformation remains to be precisely described and quantified. One of the difficulties in such quantification is that a very large part of the deformation is hidden under blanketing mid-upper Cenozoic deposits and volcanics (Armijo et al., 2015; Farías et al., 2005; SERNAGEOMIN, 2003; Victor et al., 2004). A quantitative analysis of this deformation and its kinematics is only possible at the few sites along the western flank where deformed Mesozoic series crop out and which are accessible despite the hostile desert conditions in North Chile.

In this study, we provide quantitative data to better constrain the geometry of structures, the shortening they accommodated and their kinematics of deformation over time in two of the few areas along the west Andean flank where erosion of the Cenozoic units allows for exposures of the underlying deformed Mesozoic layers (Figure 1). The Pinchal area, at ~21°30'S, exhibits a major west-vergent thrust that brings the Paleozoic basement of the Cordillera Domeyko over a FTB of Mesozoic units. These structures have never been described in detail. In the Quebrada Blanca zone, ~80 km further north, the excellent exposure of the FTB affecting the Mesozoic series allows for a more quantitative estimate of the shortening and of the timing of the main deformation episodes. Despite our detailed and quantitative approach, these two study areas only give a limited minimal vision of total deformation of this region, as their spatial extent remains minor at the scale of the whole western Andean flank (Figure 1). We find that the shortening of these structures is multi-kilometric, revealing that the contribution of the west Andean flank to Andean mountain building is not negligible. Additionally, we show that the main deformation recorded by folded Mesozoic units occurred sometime between ~68 and ~29 Ma (and possibly between ~68 Ma and ~44 Ma), further emphasizing that these structures mostly participated to the early stages of mountain-building.

2. Geological Context of the Andes (~20–22°S)

2.1 General geological framework

The Central Andean mountain-belt extends parallel to the Peru–Chile trench (Figure 1), where the Nazca oceanic plate subducts slightly obliquely beneath the South American continent. Spreading out north–south over several thousands of kilometers, the morpho-tectonic structure of the belt varies not only across the range, but also along its ~north–south axis.

At ~20–22°S, the mountain-belt is characterized by its largest width (>650 km), highest average elevation (~4–4.5 km above sea level, hereafter a.s.l., Figure 1), thickest crust (70–80 km, e.g. Tassara et al., 2006; Wölbern et al., 2009; Yuan et al., 2000) and greatest total shortening (>300 km, e.g. Anderson et al., 2017; Eichelberger et al., 2013; Elger et al., 2005; McQuarrie et al., 2005; Sheffels, 1990). Here, the Andean margin along the western border of the continent is described by three major morpho-tectonic ensembles, which are, from west to east: (1) the subduction margin (including the Peru–Chile Trench, the oceanward forearc, and the Coastal Cordillera that reaches altitudes >1 km and that corresponds to the former Mesozoic volcanic arc); (2) the Atacama Bench or Central Depression (at an altitude of ~1 km, corresponding to a modern continental forearc basin, particularly well expressed in the morphology and topography of North Chile); and (3) the strictly speaking Andean orogen, including the current volcanic arc and the Altiplano plateau reaching elevations over 4000 m a.s.l. at ~20°S (e.g. Charrier et al., 2007; McQuarrie et al., 2005; Oncken et al., 2006). Following the terminology of Armijo et al. (2010, 2015), the morpho-tectonic units located west of the Andean orogen constitute the Marginal Block (i.e. the oceanward forearc, the Coastal Cordillera and the Atacama Bench) (Figure 1).

At ~20–22°S latitude, the Andean orogen itself is composed of several major tectono-stratigraphic ensembles, which are, from west to east: (1) the Western Cordillera (Figure 1), including the Cordillera Domeyko and the modern volcanic arc (following here the terminology of e.g. Armijo et al., 2015; McQuarrie, 2002; Eichelberger et al., 2013; Garzione et al., 2017; Oncken et al., 2006); (2) the Altiplano Plateau, a high-elevation internally drained low-relief basin; (3) the Eastern Cordillera, a bi-vergent portion of the East Andean FTB; (4) the Interandean zone (or Cordillera Oriental); and (5) the Subandean ranges, east of which the South American craton underthrusts the Andes (e.g. Armijo et al., 2015; Isacks, 1988; McQuarrie et al., 2005; Oncken et al., 2012). The building of the Andean mountain-belt *stricto sensu* proceeded since the Late Cretaceous - Early Cenozoic at ~20–22ºS and was associated with crustal shortening and thickening (e.g. Amilibia et al., 2008; Andriessen & Reutter, 1994; Armijo et al., 2015; Arriagada et al. 2006; Barnes et al., 2008; Bascuñan et al., 2016; Charrier et al., 2007; DeCelles et al., 2015; Faccenna et al., 2017; Henriquez et al., 2019; McQuarrie et al., 2005; Mpodozis et al., 2005; Oncken et al., 2006). Based on the regional syntheses and reviews by McQuarrie et al. (2005), Oncken et al. (2006), Charrier et al. (2007), Armijo et al. (2015), Garzione et al. (2017) and Horton (2018), the across-strike growth of the orogen may be summarized as follows: (1) by Late Cretaceous, the Mesozoic arc and backarc basin (formed during the early Andean cycle) is located at the position of the present-day forearc, and most of the current Andes shows mainly flat topography; (2) by Late Cretaceous - Early Cenozoic, orogenic growth initiates and deformation primarily affects the western margin of the present-day Altiplano; (3) by ~45–30 Ma, shortening vanishes along the western flank of the Andes, and is transferred to the Eastern Cordillera; (4) by ~25 Ma, deformation ends in the Eastern Cordillera and migrates into the Interandean Belt; (5) from ~10 Ma until present, deformation within the Subandean Belt proceeds with the underthrusting of the Brazilian Craton beneath the Andes. It is therefore clear that the Andean shortening started along the western Andes and subsequently propagated eastward, progressively enlarging the orogen to form the different cordilleras and the Altiplano plateau in between.

Different authors investigated crustal shortening and thickening at ~20–22°S at the scale of the whole Andean mountain-belt. From these earlier studies, total crustal shortening is estimated to ~360 km (e.g. Anderson et al., 2017; Barnes & Ehlers, 2009; Eichelberger et al., 2013; Elger et al., 2005; Kley & Monaldi, 1998; McQuarrie et al., 2005; Sheffels, 1990). This crustal shortening contributed to crustal thickening. With a crustal thickness of ~70–80 km (e.g. Heit et al., 2007; Tassara et al., 2006; Wölbern et al., 2009; Yuan et al., 2000; Zandt et al., 1994) beneath the Western Cordillera, the Altiplano and the Eastern Cordillera at these latitudes, the crust is over-thickened compared to the ~45 km thick crust of the South America craton (e.g. Wölbern et al., 2009).

2.2 Geological setting of the Western flank of the Andes at ~20–22°S

The Andean western flank is formed of three tectono-stratigraphic units at ~20–22°S, aside from the present-day volcanic arc. Starting from the East (oldest and deepest units, exposed at high altitudes) to the West (youngest units, lower altitudes), these are (Figure 1): (1) Andean basement consisting of metamorphic rocks of Precambrian and Paleozoic ages; (2) volcano-sedimentary deposits of Mesozoic age (Triassic–Cretaceous), folded and deformed in a FTB, and (3) unconformably overlain by less-deformed mid-upper Cenozoic (Oligocene – Quaternary) volcanics and sedimentary cover. Magmatic intrusions locally alter these different units, and are mostly Cenozoic (SERNAGEOMIN, 2003). This along-strike structuration of the western Andean flank at these latitudes is here only given to the first-order as Mesozoic strata may be locally trapped in between two basement units, and Cenozoic layers may be unconformably overlying older strata even to the east (Figure 1). Laterally, and in particular further south (i.e. south of the city of Calama, ~22°27'), it should be noted that the structural organization of the western flank of the Andes is more complex, and the description proposed here does not directly apply.

The pre-Andean basement rocks formed during the Late Proterozoic and Paleozoic, when the Amazonian craton was progressively assembled from various terranes (e.g. Charrier et al., 2007; Lucassen et al., 2000; Ramos, 1988; Rapela et al., 1998). At the end of this period of subduction and continental accretion, intensive magmatic activity (volcanism and major granite intrusions) welded together the basement during the Late Carboniferous to Early Permian (Charrier et al., 2007; Ramos, 2008; Vergara & Thomas, 1984).

The Mesozoic deposits (Triassic to Cretaceous), found today along the west Andean flank, formed in a proto-Andean arc and backarc basin system during the early period of the Andean cycle (e.g. Charrier et al., 2007; Mpodozis & Ramos, 1989). Marine and continental sediments are interbedded with volcano-magmatic rocks (Aguilef et al., 2019; SERNAGEOMIN, 2003). These Mesozoic units attain locally thicknesses up to ≥10 km (e.g. Buchelt & Tellez, 1988; Charrier et al., 2007; Mpodozis & Ramos, 1989).

A regional erosional surface called the Choja Pediplain (Galli-Olivier, 1967) developed during the Eocene to Early Oligocene (~50–30 Ma) (e.g. Armijo et al., 2015; Victor et al., 2004). Above this angular unconformity, the up to ~1600 m thick (Labbé et al., 2019) Cenozoic deposits of the Altos de Pica Formation (Galli & Dingman, 1962) are composed of continental clastic sediments, interbedded with volcanic layers (Victor et al., 2004). The oldest documented age within the Altos de Pica Formation is of ~24–26 Ma from dated ignimbrites (Farías et al., 2005; Victor et al., 2004). From there, an age of ~27–29 Ma for the base of the Altos de Pica Formation is inferred regionally when extrapolated to the basal erosional surface using an average sedimentation rate. The youngest ignimbrites within the Altos de Pica Formation are dated at ~14–17 Ma (Middle Miocene) (Vergara & Thomas, 1984; Victor et al., 2004). Based thereon and in addition to other younger dated ignimbrites (Baker, 1977; Vergara & Thomas, 1984), Victor et al. (2004) deduced from stratigraphic correlations that the development of the Altos de Pica Formation finished by ~5–7 Ma (Late Miocene) at ~20–22ºS.

The Paleozoic basement of the Western Cordillera is disrupted at places in the form of various basement highs boarded by reverse faults (Figure 1), such as the Sierra del Medio to the east and the Sierra de Moreno to the the west at ~22°S (e.g. Haschke & Günther, 2003; Henriquez et al., 2019; Puigdomenech et al., 2020; Tomlinson et al., 2001) – not to be confused with the north–south trending strike-slip Domeyko Fault System, also called West Fissure System (or Falla Oeste) (e.g. Charrier et al., 2007; Reutter et al., 1996; Tomlinson & Blanco, 1997a, 1997b) along the Late Cretaceous - Early Cenozoic magmatic arc, east and out of our field study area. At ~21°30’S, the geological map of Skarmenta and Marinovic (1981) indicates a west-vergent thrust bringing the Paleozoic basement over folded Mesozoic units. Such thrust contact is in structural continuity with other similar basement thrusts locally described further north and south by other authors (Aguilef et al., 2019; Haschke & Günther, 2003; SERNAGEOMIN, 2003; Skarmenta & Marinovic, 1981). These basement thrusts, if pertaining to a common thrust system, would imply significant crustal shortening across the western Andean margin, yet to be further documented in the field.

Using apatite fission track dating, Maksaev and Zentilli (1999) proposed significant exhumation of the basement units between 50 Ma and 30 Ma, possibly related to basement overthrusting. Older exhumation ages (Late Cretaceous to Early Cenozoic (U-Th)/He zircon and apatite ages) are however provided by Reiners et al. (2015) for the western Andean basement at

~21°42'S, but from only one sample and without modeling. Together, these ages indicate that data remain missing to better quantify the exhumation, uplift and timing of deformation of the basement thrusts reported along this flank of the Andes.

In the folded sedimentary series further west, Victor et al. (2004) determined ~3 km of shortening recorded by the Cenozoic deposits of the Altos de Pica Formation, i.e. accumulated between ~29 Ma and ~5–10 Ma. However, these authors did not take into account the deformation of the underlying more deformed Mesozoic units. They interpret the underlying structures and folding as part of a system of west-vergent thrusts, re-analyzed recently by other authors (Fuentes et al., 2018; Martinez et al., 2021), but the poor quality of the seismic profiles at these depths renders these interpretations quite tenuous and disputable. Haschke and Günther (2003) estimated that >9 km of shortening across the western flank in the outcropping Sierra de Moreno area (~21°45'S) occurred since the Late Cretaceous to Eocene on a west- and east-verging thrust system. It follows that even if published data hint at the existence of a west-verging fault system along the western Andean front at ~20–22°S, its geometry, kinematics and total amount of shortening have not yet been satisfactorily evaluated.

Unconformable mid-upper Cenozoic clastic sediments and ignimbrites commonly hide the folded Mesozoic layers and their contact with the basement. Investigation is thus limited to sparse areas of few tens of km of extent, only where the interplay of erosion, canyon incision and exhumation has removed this Cenozoic cover and allows for structural observations (Aguilef et al., 2019; SERNAGEOMIN, 2003) (Figure 1). In this study, we focus on two relatively accessible outcrop sites (Figure 1): (1) At ~21°30'S, where the Paleozoic basement thrusts over the Mesozoic according to Skarmenta and Marinovic (1981). This zone will be referred to as the Pinchal area (next to Cerro Pinchal, 4193 m a.s.l.). (2) At ~20°45'S, where the FTB composed of deformed Mesozoic units has been significantly eroded and allows observations. This zone is hereafter named Quebrada Blanca area, after its largest canyon.

3. Data and Methods

3.1 Available Data

The most detailed existing geological map for the Pinchal area is the Quillagua map (1:250,000 scale, Skarmenta and Marinovic, 1981), which only provides very large-scale information but hints for the existence of a major west-vergent basement thrust. For the Quebrada Blanca area, the recent Guatacondo map (1:100,000 scale, Blanco & Tomlinson, 2013) provides detailed and updated information on the stratigraphy and structure. There, the folded Mesozoic rocks are well exposed on a relatively wide area (~15 km east–west extent) and their structure has been preliminarily mapped and qualitatively described by Blanco and Tomlinson (2013), Armijo et al. (2015) and Fuentes et al (2018).

Enhanced cartographic details can be deduced from high-resolution satellite imagery. We use Google Earth imagery (Landsat 7, DigitalGlobe) whose resolution varies from a few meters to a few tens of meters depending on the zones. In addition, this work benefits from very high-resolution imagery from the European Pléiades satellites. Using the MicMac software suite (Rosu et al., 2014; Rupnik et al., 2016), we calculate high-resolution DEMs from tri-stereo Pléiades imagery, with a 0.5 m resolution. These DEMs are down-sampled to a resolution of 2m to enhance data treatment and calculations (e.g. stratigraphic projection and image processing). Relative vertical accuracy may reach ~1m, depending on local slope.

Field observations acquired during two field surveys in March 2018 and January 2019 complete the dataset and permit the verification of the large-scale data acquired from maps and satellite imagery. Difficult accessibility and field logistics in the remote and desert Pinchal area only allow detailed field observations on a relatively limited area. Observation points and the off-road track followed to reach our field site in the Pinchal area are provided as supplementary material.

3.2 Establishing structural maps

We establish structural maps for the two investigated sites. We use an approach based on the 3D-mapping of stratigraphic layers on satellite imagery (Armijo et al., 2010; Riesner et al., 2017). More precisely, layers are traced and correlated on Google Earth satellite images. The so-obtained georeferenced traces are projected on the DEM-derived topographic map, and compared with geological maps, mainly for stratigraphic and age references. Field observations allow ground verifications and provide supplementary details, such as the existence of minor thrusts and folds, the observation of polarity criteria or the local measurement of dip angles.

The approach used here is mainly limited by local geological complications. Continuous mapping of Mesozoic strata is indeed locally complicated where incision of Cenozoic strata is limited, where magmatic intrusions and associated hydrothermalism alter the surrounding structural geometries, where soft layers with no well-expressed bedding such as marls are present (ex: Pinchal area), or where small landslides or recent sediment deposits hide the underlying deformation pattern. Therefore, geometrical observations and detailed mapping of the structures may be locally difficult, in some zones impossible. These difficulties cause uncertainties in precisely correlating mapped layers and may result in metric to decametric errors (if correlating a layer with its neighbor by error) but do not modify our large-scale (km) results and interpretations.

3.3 Building structural cross-sections

We use structural measurements, field observations and the obtained structural map to build cross-sections of the two investigated areas.

In the Pinchal area – because of limited canyon incision, marls, and frequent blanketing of the structures by Cenozoic cover – we build our structural cross-sections mainly from field observations (strike and dip angles, polarity criteria, first-order stratigraphic column), with additional information taken from satellite imagery.

In contrast, in the Quebrada Blanca area, we mostly build our subsurface cross-section from mapping on satellite imagery. Here, we follow the approach already proposed in Armijo et al. (2010) and described in detail in Riesner et al. (2017). The mapped georeferenced horizons are projected on the high-resolution Pléiades DEMs. Using a 3D-modeler, the horizons can be visualized interactively. In order to precisely assess the local average dip and strike angles of deformed Mesozoic layers, we project these layers along swath profiles chosen where Mesozoic strata crop out the best, where folds are mostly cylindrical and where incision (and therefore topographic relief) is most significant. It should be noticed that river incision is here significantly lower (a few hundred meters at most) than at the latitude of Santiago de Chile (~33°30'S) where this approach has been previously employed (Riesner et al., 2017, 2018). In any case, we successfully obtain the overall sectional geometry of layers, and by comparing with the structural map, we determine the approximate locations of the major synclinal and anticlinal fold axes. By respecting the classical structural rule of constant layer thickness, we derive fold geometries.

The limits of our interpretations mostly relate to the difficulty of unambiguously correlating stratigraphic layers, and to the fact that, in reality, layers may not always keep constant thicknesses. As incision and local topographic relief are reduced to a few hundred meters at most, the construction of cross-sections is mostly restricted to extrapolating surface dip angles at depth.

3.4 Crustal shortening and kinematic modeling

We use our subsurface cross-sections to estimate the minimum shortening across the investigated sites. We employ a simple line-length-balancing approach to determine shortening related to folding. However, we have no precise indication on the structure and geometry of layers at depth, in particular within the footwall of thrusts or within the hanging wall nearby the interpreted propagating faults. Given this, thrust offsets can not be precisely documented from field observations only. To solve this and get a more complete view on shortening estimates, we model anticlinal geometries interpreted to be related to fault-propagation using a numerical trishear approach (e.g. Allmendinger, 1998; Erslev, 1991). We use the code FaultFold Forward (version 6) (Allmendinger, 1998) in order to jointly model thrust displacement and anticlinal folding. Trishear models the deformation distributed within a triangular zone located at the tip of a propagating fault (Erslev, 1991). This forward modeling relies on a set of parameters that are here adjusted by trial and error to fit structural geometries. By adding sedimentary layers at various steps during ongoing deformation, we model syntectonic deposition and subsequent deformation, in order to reproduce deformation of Cenozoic layers. Additional information on trishear modeling, together with the range of tested parameters, are provided in supplementary material. We recognize that our best-fit model parameters may not be unique. This is not expected to impact much estimated total shortening as this result depends mostly on final cross-sections. This point will be further discussed in section 7.3 and in the supporting information.

Deformation is expressed in terms of shortening (in km) but also in terms of relative shortening (in %). Relative shortening is hereafter defined as the ratio of the estimated shortening by the initial length of the undeformed section.

4. Basement thrust and deformed Mesozoic series within the Pinchal area (~21º30'S)

4.1 Field observations

Our observations confirm the existence of a major basement thrust in the Pinchal area. Because our observations may seem in contradiction with previous stratigraphic and structural interpretations of the folded Mesozoic series along the Western Andean flank, we hereafter describe in detail our field observations. We subsequently discuss and compare them to previous interpretations, and propose a solution reconciling these observations with a priori regional stratigraphic knowledge.

4.1.1 Stratigraphic observations

We propose a first-order stratigraphic column from our structural, stratigraphic and sedimentary field observations. In the landscape, the three main tectono-stratigraphic units are clearly distinguishable (Figure 2): (1) the metamorphic basement, (2) the continuous Mesozoic sedimentary series (with a continuum from continental upward to marine facies) and (3) the continental Cenozoic cover. The first-order stratigraphic column (Figure 3) is hereafter described from the oldest to the youngest units. Detailed field pictures of identified and individualized sedimentary formations are provided in supplementary material to complement the forthcoming stratigraphic descriptions. We acknowledge not to have any constraint on the absolute ages of these series, but the relative stratigraphic ages are deduced from the kilometer-scale structural geometry and from clear sedimentary or structural polarity criteria observed in the field (further details below). We also indicate that thicknesses are inferred only locally, and that we cannot exclude thickness variations within the sedimentary series over our study area.

The Paleozoic basement (Figure S1) dominates the eastern part of the Pinchal area, and is composed of mainly coarse-grain granodiorites and diorites, as well as metamorphic rocks comprising gneisses, migmatites and mica-schist, consistent with documented characteristics of the basement in the area (Skarmenta & Marinovic, 1981).

The older part of the outcropping Mesozoic series consists of continental deposits, with a high content of Paleozoic lithics and volcano-clastic and tuffitic low-rounded conglomerates, of greenish, beige and brownish colors, and clast-sizes varying from a few millimeters to few decimeters (Figure S2). At places, these rocks bear sedimentary polarity criteria such as grain-grading, grain-sorting, cross-bedding and tangential beds (Figure S3). In the eastern part of the Pinchal area, we locally observed below this series some dark green detrital pelites (lutites) (Figure S4). On the basis of petrographic and sedimentological correlations, these detrital Mesozoic sediments resemble to units mapped as Triassic north of the Pinchal zone (between 21º–21º30'S) in the Quehuita area (Aguilef et al., 2019).

In paraconformity, a characteristic limestone layer marks the beginning of a marine sequence within the Mesozoic series, evidencing a marine transgression process. We hereafter refer to this layer as the "calcareous crest" as it is prominent in the landscape (Figure 2) and as such can be easily used as a reference marker in the field or in satellite images. The base of the calcareous crest is characterized by the presence of silex layers or nodules (Figure S5). Upsection, numerous stromatolites (Figure S6) and bivalves (Figure S7) are found within the unit. Its thickness varies between a few meters (less than 10 m) in the eastern part, to ~10–20 m to the west.

The calcareous crest is overlain by thin-bedded (cm–dm) limestone layers of rose-beige color (Figure S8), over a thickness of ~50–100 m. Going upsection, the marine series becomes progressively more marly, limestone layers become more rare and the color more beige, evidencing a deeper marine paleo-environment bearing fossiliferous marl layers. Belemnite fossils were encountered in the lower part of this limestone-to-marl sequence. Characteristic calcareous oval concretions of variable diameter (cm to m) (Figure S9), are pervasive at the transition from marly limestones to marls. The marls bear ammonite fossils, which we have not identified. These Ammonite species could be *Perisphinctes*, *Euaspidoceras*, *Mirosphinctes* and *Gregoryceras*, according to the notice of the Quillagua geological map (Skarmenta & Marinovic, 1981) if applicable here. In this case they would be associated with a Middle Jurassic age (Bajocian to Callovian). The series from the thin-bedded limestones to the top of the beige marls is ~200 m thick, along one of the canyons and sections investigated in the field (Quebrada Tania).

Upsection, the beige marls become progressively more calcareous again, with the presence of thin limestone layers (Figure S10). Finally, this marine sequence ends with black marls containing layers of beige sandstones (mm to few cm – rarely dm – thick) (Figure S11), indicative of a detrital component in a probable deep seated basin, comparable to the "flysch" series in the Alpine basins (Homewood & Lateltin, 1988). This unit is hereafter called "black flysch", and has a minimum thickness of ~50 m.

Continental-clastic Cenozoic deposits (Altos de Pica Formation), unconformably overlie the folded Mesozoic series over the Choja erosional surface (Galli & Dingman, 1962; Galli-Olivier, 1967; Victor et al., 2004) (Figures 2 and 3). They are mainly composed of alluvial fan facies that were sourced from the mountain front immediately to the east, with different aggradational terraces. Locally, ignimbrites are observed to cover these clastic series. We encountered red arenites at the base of the Cenozoic series in the western part of the Pinchal area (Figure S12). The age of the oldest sedimentary deposits above this erosional surface is regionally inferred to be ~27–29 Ma (Victor et al., 2004, see also section 2.2).

4.1.2 Structural Observations

The structural map of Figure 4 illustrates the main stratigraphic and structural features observed in the field and by mapping on satellite imagery. Two ~east–west cross-sections show detailed surface observations along two accessible representative canyons: Quebrada Tania and Quebrada Martine (Figure 5a,b). The Quebrada Tambillo incises deeper into folded units, and as such surface structural observations can be further extrapolated at depth (Figure 5c).

The easternmost part of our study area is marked by a major west-vergent thrust bringing the metamorphic basement over the Mesozoic units. This basement thrust is hereafter named the Pinchal Thrust. The west-vergent thrust-nature of the shear zone between the Paleozoic basement and the Mesozoic units is observable in the field (Figures 2 and 6). The characteristic C/S-fabric ("Cisaillement/Schistosité") – underlines the penetrative shearing of the basement rocks within and nearby the thrust shear zone, and indicates a top-to-the-west thrusting direction (Figure 7a). The Pinchal Thrust roughly follows a north-south direction (Figure 4). This major contact often resumes to a single basement thrust (Figure 5a,c), but may also show local geometrical complexities, with secondary thrusts and branches, eventually involving basement with stripes of trapped Mesozoic units, as for example along Quebrada Martine (Figure 5b).

West of the Pinchal Thrust, a series of folds involving folded Mesozoic units is observable (Figures 2 and 4). From east to west, an asymmetric and overturned syncline is first found (Figure 8a), followed by a relatively symmetric anticline (Figure 8b). The eastern limb of the syncline, right beneath the Pinchal Thrust, is inverted and locally highly faulted and folded (Figures 5 and 7b-c). Within this inverted limb, the series goes westward (and upsection) from sheared lutites beneath the Pinchal Thrust followed by Mesozoic detrital series with conglomerates, to the Mesozoic marine series from the calcareous crest upsection to the marly limestones. The overturned strata are steeply dipping (50–70ºE). Penetrative small-scale deformation can be observed pervasively within the marine Mesozoic series, in the form of numerous local small folds, kinematically indicative of an inverted fold limb (used here as a structural polarity criterium) (Figure 7b), and local secondary shear zones and thrusts (Figure 7c).

Going westward, as observed in detail along Quebrada Tania (Figure 5a), the eastern part of the black flysch bears small-scale folds characteristic of the inverted fold limb, whereas normal limb folds (used here also as structural polarity criteria) are observed slightly further west: the axis of the overturned west-vergent syncline therefore passes through the black flysch. Part of the Mesozoic series is missing, as overthrusting within the flysch and (marly) limestones is observed frequently along Quebrada Tania (Figure 5a). The overturned syncline is therefore found to be broken by a secondary thrust fault striking approximately parallel to the Pinchal Thrust and roughly coinciding with the synclinal fold axis (Figures 4-5). Westward, the normal western limb of the syncline encompasses the whole Mesozoic series from the black flysch down-section to the Mesozoic volcano-detrital series, with more gentle dip angles (20–40ºE) (Figures 2 and 5). Penetrative deformation is observed to be limited here.

The continental Mesozoic layers of the normal limb of the syncline flatten toward the west. The section along Quebrada Tambillo (Figure 5c) shows a broad, overall symmetrical, anticlinal fold (Figure 8b). Its fold axial plane is steep, dipping ~80°E. The western flank of this large anticline is marked by smaller, secondary folds with westward decreasing wavelength and amplitude. Field logistics did not permit further detailed structural observations within this anticline.

The Mesozoic sediments immediately west of the basement are unconformably covered by sheet-like, river-incised Cenozoic fluvial deposits, forming aggradational terraces deposited above erosional surfaces at different elevations, of varying spatial extent and of probably different ages (Figure 2b). The majority of these erosional surfaces shows a westward tilt (Figure

5c). Further west, the Cenozoic deposits become thicker and bury the westward extent of the folded Mesozoic units. Westward thickening of the Cenozoic layers is clearly observable in Quebrada Tambillo and indicates the presence of growth strata at the front of the anticline deforming the Mesozoic series (Figures 5c and 8b).

4.1.3 Comparison to previous stratigraphic and structural interpretations

In the Pinchal area, a major basement thrust was reported in the Quillagua 1:250,000 geological map (Skarmenta & Marinovic, 1981). In this map, the Mesozoic units are interpreted as pertaining to the Jurassic Quinchamale formation, deposited in a backarc basin context and composed of an Oxfordian (~157–163 Ma) and a younger Kimmeridgian (~152–157 Ma) sub-unit. Based on this age interpretation and relying on a regionally established Mesozoic stratigraphy where marine sequences are followed upward by younger clastic deposits, Skarmenta & Marinovic (1981) interpreted the main structure of the Pinchal zone as an anticline.

Our field investigations confirm the existence of a basement thrust, but contradict the earlier interpretation of the structure of the folded Mesozoic series and of the local Mesozoic stratigraphy. Even though we do not know the absolute ages of the folded sedimentary series, our structural and sedimentary field observations allow for clearly constraining the relative stratigraphic ages of Mesozoic units, from either structural or sedimentary polarity criteria, and unambiguously indicate that detrital continental units are here geometrically and stratigraphically below a marine sequence (Figure 3). In the case that the marine strata are Jurassic in age from their likely fossiliferous content, the older continental clastic units could be Triassic, by comparison to recent observations not far from the Pinchal area (Aguilef et al., 2019). These ages need to be confirmed by future chronological and stratigraphic analyses.

Given this, even though the stratigraphic sequence we observe in Pinchal may look in contradiction with the regionally known stratigraphy, it may rather be viewed as complementary: the detrital component observed here below marine series may be older than the marine-to-continental upward succession that has been well described regionally. In this sense, the Pinchal area may provide a key outcrop to refine our knowledge of older series.

In any case, we recall that relative ages are only needed here for the scope of this study to decipher the general structure and deformation pattern.

4.2 Structural Interpretation

The cross-section of Quebrada Tambillo (Figure 5c) summarizes our interpretation of the sub-surface structural geometry of the Pinchal area. Tectonic shortening in the Pinchal area is evidenced by the presence of the Pinchal Thrust and by the folded and faulted Mesozoic strata.

Based on the dip angle of the C/S-fabric in the Pinchal Thrust shear-zone (Figure 7a) and on the mapping of the Pinchal Thrust on satellite imagery, we estimate that the Pinchal Thrust has a subsurface dip angle of ~40ºE, even though locally flatter such as along Quebradas Tania and Martine (Figures 5a-b). All secondary strands of the Pinchal Thrust are expected to root at depth onto the main shear-zone. The secondary thrust breaking the core of the syncline is roughly parallel to the Pinchal Thrust (Figure 4) and is probably a frontal splay fault of the basement thrust. It is therefore expected to also connect onto it at depth. A similar reasoning is proposed to all small-scale thrusts and décollements observed within the inverted synclinal limb, in particular along Quebrada Tania.

Considering that the folds west of the Pinchal Thrust develop above underlying thrusts that connect onto a common detachment is a reasonable and classical assumption for fold-and-thrust-belts (hereafter simplified as FTB). This detachment is expected to root at least at the base of the outcropping Mesozoic series, or deeper (Figure 5c). Assuming that the layer thickness is constant over our study area, it can be extrapolated that such detachment is located at least 2 km beneath the topographic surface (i.e. at ~0.2 km a.s.l.), or deeper. To the West of our field area, at the front of the anticline, the small-scale folds with westward decreasing wavelength and amplitude (Figure 8b) are interpreted as the possible expression of disharmonic folding within the forelimb of the anticline and/or of a thrust ramping-up toward the sub-surface at the front of the anticline (Figure 5c).

Because of the internal shortening of the thrust sheet, with the pervasive presence of small-scale folding and thrusting, in particular within the inverted limb of the overthrusted syncline, our shortening estimate only represents a minimum value. Using the simplified cross-section along Quebrada Tambillo (Figure 5c), line-length balancing results in a minimum of ~1 km of shortening absorbed by folding only across the two folds documented here, from the Pinchal Thrust to the front of the anticline. A significant – but unconstrained – amount of shortening related to the pervasive deformation observed in the field (Figures 5a-b and 7b-c) is to be added, as well as the thrust offsets on the faults of the FTB and on the Pinchal Thrust. An estimate of the contribution of thrusting within the FTB will be provided below by modeling (section 6.2).

The minimum thickness of the Mesozoic series is ~2.2 km, as estimated from the normal limb of the syncline along the Quebrada Tambillo section. Thus, it can be considered that the strict minimum exhumation of the basement is equally of ~2.2 km. Assuming a 40°E dip angle for the ABT, this yields a strict minimum displacement of ~2.6 km on this thrust, which has to be added to the minimum shortening estimated from the folding of the Mesozoic series.

5. Structure of the folded Mesozoic series within the Quebrada Blanca area (~20°45'S)

5.1 Stratigraphy of the Quebrada Blanca area

The stratigraphy of the western Andean flank at ~20°45'S is well described in the Guatacondo geological map (Blanco & Tomlinson, 2013). Unlike in the Pinchal area, basement rocks do not crop out in the investigated zone nearby the Quebrada Blanca (Figure 9), but larger scale maps (e.g. SERNAGEOMIN, 2003) show Paleozoic basement units further east and higher in the topography (Figure 1).

The Mesozoic units of the Quebrada Blanca are of Jurassic to Cretaceous age (Blanco & Tomlinson, 2013), have been deposited in a back-arc basin context in successive transgression–regression sequences (Charrier et al., 2007), and are subdivided into three formations: (1) The Late Oxfordian Majala Formation, a clastic unit of sandstones, shales and subordinately stromatolitic limestones of transitional marine origin (Blanco et al., 2012; Blanco & Tomlinson, 2013; Galli-Olivier, 1967); (2) the Late Jurassic / Early Cretaceous Chacarilla Formation, a continental (fluvial) clastic sequence (Blanco & Tomlinson, 2013; Dingman & Galli, 1965); and (3) the Late Cretaceous Cerro Empexa Formation, an andesitic volcanic and continental sedimentary unit (Blanco et al., 2000; Blanco & Tomlinson, 2013; Dingman & Galli, 1965). The Majala and Chacarilla Formations are both of reddish and beige colors and predominantly bear detritic sediments. The Cerro Empexa Formation appears greyish and massive in the field. In the Quebrada Blanca area, uranium-lead (U/Pb) dated zircons from this formation bear ages between ~75 and ~68Ma (Blanco et al., 2012; Blanco & Tomlinson, 2013; Tomlinson et al., 2015) (Figure 9).

The Cenozoic deposits of the Altos de Pica Formation here also unconformably overlie the Mesozoic series, over the Choja Pediplain angular unconformity (Galli-Olivier, 1967) (see also section 2.2). The age of the basal deposits of the Altos de Pica Formation is estimated regionally to ~27–29 Ma (Blanco & Tomlinson, 2013; Victor et al., 2004).

Magmatic intrusions and hydrothermalism occur locally, and hide the eastern continuation of the folded Mesozoic series. Some of these intrusions are dated by uranium-lead (U/Pb) on zircons at ~44 Ma (Blanco & Tomlinson, 2013) (Figure 9).

5.2 Structural observations

The structural map of the Quebrada Blanca area (Figure 9) highlights the main stratigraphic and structural elements observed in the field and by mapping from satellite imagery. Although the cartography of the folds is complicated by the persistent Cenozoic cover (notably in the west and south), and by magmatic intrusions and hydrothermalism (particularly to the east), three large-scale folds are clearly observable: a wide syncline in the center (Higueritas syncline), bounded by two anticlines to the west (Chacarilla anticline) and east (fold names from Blanco & Tomlinson, 2013; Fuentes et al. 2018). The scale of these major folds is multi-kilometric (Figure 9). The cross-section of Figure 10 illustrates the asymmetry of the folds. Both anticlinal folds have steeper western limbs (dip angles vary mostly between ~50–80ºW), whereas their eastern limbs have more gentle dip angles (varying mostly between ~20–50ºW) (Figure 10a). Despite the fact that the eastern flank of the eastern anticline is widely hidden by magmatic intrusions and hydrothermalism, its southern part is well observed in the field and mapped (Figure 9). The central Higueritas syncline is wider and more symmetric, with dip angles of ~40–50° on both limbs. The anticlines involve the Majala and Chacarilla Formations, while the core of the syncline bears the Cerro Empexa Formation. Overall, the folded series – and in particular the anticlines – document a clear west-vergence of the folds (Figure 10c). From our projection of the strata mapped on satellite imagery, the Mesozoic series are observed to be all concordant (Figures 10a-b). The cross-section of the Guatacondo map (Blanco & Tomlinson, 2013) proposes an angular unconformity of <10º between the Jurassic and Cretaceous units, at the base of the Cerro Empexa formation, however not observed here from our large-scale high-resolution mapping. As this unconformity does not produce any evident change in the geometry of layers from Jurassic to Cretaceous, we consider it to be minor for our analysis, in particular with respect to the main large-scale folding documented here.

In the field, we observe small-scale deformation within both anticlines (Figure 10). A series of anticlines with westward decreasing amplitude and wavelength (of a few tens to a few hundreds of meters – to be compared to the ~4 km wavelength of the main anticline) are observable on the western edge of the Chacarilla anticline (Figures 10c and 11). In the field, at least one of these small-scale folds seems affected by a minor thrust. Additionally, within the eastern large-scale anticline, a thrust-affected small-scale fold is observed (Figures 10c and 12), and confirms the west-vergence at this smaller scale.

The Cenozoic detrital units are unconformably deposited above the folded Mesozoic series. Thin sheet-like river-incised Cenozoic surfaces remain in the central part, becoming more dominant to the South and West (Figure 9). These superficial erosional surfaces show an overall westward tilt (Figure 11). Westward thickening of the Cenozoic layers deposited above the erosional Choja surface is clearly observed at the front of the western anticline (Figure 11) and reveals the presence of growth strata.

5.3 Structural interpretations

As for the Pinchal area and by analogy with other FTBs, we interpret the Quebrada Blanca area folds as related to ramp thrusts rooting onto a deep detachment (Figure 10c). The detachment probably roots at least at the base of the observed Late Jurassic series, or possibly deeper. Assuming constant layer thicknesses over the study area, it can be extrapolated that the detachment locates at least 4 km beneath the current topographic surface (i.e. at least at –2 km a.s.l.). To the East of our investigated area and in order to balance the proposed cross-section, the detachment is interpreted to deepen. An alternative interpretation would be that the detachment keeps a shallow eastward dip angle with some local thickening beneath the eastern anticline. The secondary frontal folds with westward decreasing wavelength (Figures 10c and 11) can be explained as disharmonic folds within the forelimb of the large western anticline and/or be interpreted as reflecting the existence of a shallow thrust (Figure 10c). Such a feature is also in good agreement with secondary (steeper) thrusts affecting the center of anticlines (Figure 10).

Line-length-balancing of the cross-section of Figure 10c results in ~3.8 km of shortening solely related to folding. This value is only a minimum as it does not account neither for slip on the interpreted thrusts nor for the observed small-scale deformation.

6. Kinematics of shortening of the folds and thrusts at the Pinchal and Quebrada Blanca sites

6.1 Timing of deformation

The time frame for the tectonic deformation observed within the two investigated sites can be bounded from our data, and more specifically from our results at the Quebrada Blanca site (Figure 10c). Indeed, our field observations and 3D-mapping do not reveal any relevant angular unconformity within the folded Mesozoic series in both study areas. The main deformation and folding of the investigated FTB therefore post-dates the deposition of these series. In the Quebrada Blanca area, the youngest folded Mesozoic layers that form the core of the mapped syncline belong to the Cerro Empexa Formation and bear maximum U-Pb ages of 68.9±0.6 Ma and 68±0.4 Ma (Blanco & Tomlinson, 2013) (Figures 9 and 10c). Here, we can therefore conclude that the main deformation of the documented folds post-dates ~68 Ma. This does not preclude that minor deformation happened locally earlier, as suggested by the minor unconformities reported from previous field works (Blanco & Tomlinson, 2013; Martínez et al., 2021).

Magmatic intrusions dated at ~44 Ma intrude the folded Mesozoic units, and appear cartographically not affected by folding (Blanco & Tomlinson, 2013) (Figure 9). This possibly suggests that the major part of the folding occurred during the ~68–44 Ma time interval. However, without additional observations of the deformation – or not – of these intrusions (geometry of the contact with surrounding host units, mineral deformation…), we cannot unequivocally conclude here from this simple cartographic observation.

Even though we suspect that the deformed series of the Pinchal zone are Triassic to Jurassic (section 4.1), we do not have any absolute ages of the folded units. Therefore, we postulate that the main deformation here also post-dates ~68 Ma by analogy to our observations at the Quebrada Blanca.

The FTB is unconformably covered by the Cenozoic deposits of the Altos de Pica Formation at both investigated sites. This is also the case for the Pinchal Thrust and secondary thrusts at few places in the Pinchal zone (Figure 4). The presence of growth strata at the front of the westernmost anticlines in both study areas, over the erosional Choja Pediplain, suggests that some deformation proceeded after ~29 Ma, during deposition of the Altos de Pica Formation. However, the deformation recorded by folded Mesozoic layers appears of greater intensity than that of the Cenozoic growth layers (Figures 5c and 10c).

Given this, we propose that the timing of main folding of the Mesozoic layers forming the documented sections of the FTB at ~20–22ºS can be loosely bracketed to a maximum time span of ~40 Myr, sometime between ~68 Ma and ~29 Ma, with additional relatively minor deformation after ~29 Ma. Possibly, the main deformation period could be even shorter (~24 Myr), sometime between ~68 Ma and ~44 Ma, with minor shortening after the Eocene intrusions. In the case of the Pinchal Thrust, we can only propose from our observations that thrusting took place prior to ~29 Ma.

6.2 Further constraints on total shortening deduced from trishear modeling

Line-length-balancing only reveals a fraction of the shortening related to the folding of the Mesozoic series. Because the deduced underlying faults of the FTBs have not reached the surface (Figures 5c and 10c), we assume fault-propagation-folding to be the dominant mode of deformation in the studied FTBs. To further explore and quantify the associated deformation, we use kinematic trishear modeling (e.g. Allmendinger, 1998; Erslev, 1991) of the westernmost anticlines documented at the Quebrada Tambillo (Pinchal area) and Quebrada Blanca. This approach accounts for slip on propagating thrust-faults and models the deformation distributed at the tip of these evolving faults. The trishear formalism relies on a set of parameters that are adjusted here by trial and error so as to fit the deduced structural geometries of the modeled anticlines. The values of these parameters are within the range considered in previous studies (e.g. Allmendinger, 1998; Allmendinger & Shaw, 2000; Cristallini & Allmendinger, 2002; Hardy & Ford, 1997; Zehnder & Allmendinger, 2000). Here we present our best-fitting model, which allows for reproducing satisfactorily our structural results, acknowledging that it is most probably not unique. From there, we further discuss the kinematics of the investigated sites.

Further details are provided in supplementary material. Tables S1 to S3 provide the set of parameters used for our modeling.

The structural geometries of the westernmost anticlines of the two investigated sites are reproduced, and the evolution of deformation is modeled over time taking into account the Cenozoic growth strata. The final geometries of our best-fitting models are reported over our cross-sections, represented in Figure 13. The various stages of deformation are shown in Figures S13 and S14 in the supplementary material. We find that the geometries of the western anticlines can be reproduced with a cumulative shortening of 3.1 km for Quebrada Tambillo (Pinchal area), and of 6.6 km for Quebrada Blanca (Figure 13). These values account for both thrusting and folding across the western anticlines. They are however minimum shortening values as (1) the depth of the detachment considered for modeling is minimal and could be deeper than the base of the outcropping units, and (2) the model formalism does not account for small-scale internal deformation, especially within the forelimb of the anticlines where the ramps approach the surface.

The above shortening values deduced from trishear modeling only account for the deformation (folding and thrusting) absorbed across the westernmost anticlines of our two investigated sites. The synclinal folding accounts for a shortening of ~0.4 km as deduced by line-length-balancing in the Pinchal area, leading to a minimum amount of shortening of ~3.5 km across the whole Quebrada Tambillo section. This includes folding of the outcropping FTB, as well as slip on the detachment and western thrust ramp. When adding the minimum ~2.6 km of thrusting deduced on the Pinchal Thrust, we get a minimum shortening of ~6.1 km across the whole Pinchal area. Similarly, in the Quebrada Blanca area, the easternmost anticline and syncline take up ~2 km of shortening deduced by line-length-balancing, leading to a minimum amount of shortening of ~8.6 km across the whole Quebrada Blanca section, including folding of the outcropping FTB in addition to slip on the underlying detachment and western ramp.

The two investigated FTBs take up differing amounts of minimum shortening. These variations may relate to the disparate extents of outcropping structures, in particular because the scale of the two sections are significantly different, in terms of across-strike width (~7 km long section for the Quebrada Tambillo vs. ~17 km long section for the Quebrada Blanca). Indeed, the calculated shortenings similarly represent ~47% and ~34% of minimum shortening when scaled to the extent of the Quebradas Tambillo and Blanca sections, respectively. Differences between these sections may also relate to the depth of the underlying detachment (altitude of ~0.2 km for Quebrada Tambillo vs. depth of ~2 km for Quebrada Blanca, relative to sea level) (Figure 13). Lateral variations in deformation can also not be excluded.

6.3 Kinematics of shortening

Trishear modeling allows for simulating the evolution of thrust slip and folding in the case of the westernmost anticlines of the two investigated sites. By adding syntectonic layers while deformation proceeds, we also reproduce the overall geometry of the base of the Cenozoic Altos de Pica Formation deposits and of the subsequent growth strata (Figures S13 and S14). Syntectonic surfaces and layers are prescribed an initial 3–6° W dipping angle, similar to the present-day overall regional topographic slope (Figure 1). From there, we find that ~0.5 km and ~0.4 km of shortening are needed to reproduce to the first order the geometry of the base of the Altos de Pica Formation deposits at the front of the Quebrada Tambillo (Pinchal area) and Quebrada Blanca sections, respectively, using the trishear models adjusted to the final cross-sections. When compared to the minimum 3.1 km and 6.6 km of total shortening cumulated since ~68 Ma across the westernmost anticlines of these two sections, this indicates that the ~29 Ma old basal Cenozoic layers above the Choja surface only record at most 16% and 6% of this total shortening, respectively. We have tested the possibility of initial horizontal Cenozoic syntectonic layers. In this case, a post- ~29 Ma shortening of 0.8 km at most is needed to best adjust the observed geometry of the basal Altos de Pica Formation layers, even though a good fit to both the geometry of the growth strata and of the finite fold structure cannot be satisfactorily found.

These results are then used to quantitatively describe the evolution of shortening over time across the westernmost anticlines of the two investigated sections, with account on the timing of deformation discussed in section 6.1 (Figure 13d). We find that shortening rates were on average of ~0.07–0.16 km/Myr over the time span ~68–29 Ma. They could have been even as high as ~0.11–0.26 km/Myr if considering that the main deformation phase is confined to ~68–44 Ma. Subsequently, deformation rates decreased to an average value of ~0.015 km/Myr after ~29 Ma, starting possibly earlier.

It should be noted that these average values are most probably minimum values. Indeed, thrusting and folding are here only modeled for the westernmost anticlines of our study sites, and do not account for the shortening cumulated neither across the other structures of the FTB nor on the Pinchal Thrust. Also, the main phase of deformation prior to ~29 Ma could have lasted less than the ~68–29 Ma or ~68–44 Ma time intervals, respectively (Figure 13d).

Our results therefore quantitatively emphasize our former qualitative conclusion that the major phase of deformation recorded at the two investigated sites occurred sometime between ~68 and ~29 Ma, with a significant subsequent slowing down of deformation rates afterwards, possibly as soon as ~44 Ma or earlier (Figure 13d).

7. Discussion

7.1 The Andean Basement Thrust

7.1.1 Evidencing a large basement thrust system along the West Andean flank (~20–22°S)

We have further documented in the Pinchal zone the existence of a west-vergent basement thrust – the Pinchal Thrust along the western flank of the Andes, after its initial pointing out on earlier geological maps. Here, this thrust brings basement units of the Sierra de Moreno westward over folded Mesozoic units. Our study in the Pinchal area suggests that this thrust bears local complexities with several strands and minor splays, most probably related to the reactivation of structures in the initial pre-Andean back-arc basins. Laterally, the geological map of Skarmenta and Marinovic (1981), on which we based our investigations of the Pinchal Thrust, clearly documents this structure from ~21°15'S to 21°35'S, and possibly down to ~22°S with some structural complexities by ~21°35'S with the junction of two possible strands of this basement thrust.

Structurally similar basement thrust segments have been described along the Cordillera Domeyko between ~20°S and ~22°S. North of the map by Skarmenta and Marinovic (1981), the Quehuita (up to ~21°11'S) and Choja (between ~21°08'S–21°01'S) Faults are west-vergent thrusts similarly bringing basement units over folded Mesozoic sediments (Aguilef et al., 2019). North of ~21°S, intrusions, hydrothermalism and surface volcanics hamper any clear observation of similar basement thrusts. Such basement thrust, if existent, would however provide a reasonable mechanism for the exhumation and exposure of basement rocks east of the folded Mesozoic units and at higher elevations, at the latitude of Quebrada Blanca (~20°45'S) (Figure 1). For these reasons, we cannot tell with any certainty whether a thrust contact similar to that described in Pinchal (this study) and further north (Aguilef et al., 2019) exists at this latitude, but such structure is to be suspected.

South of the map by Skarmenta and Marinovic (1981), in the Sierra de Moreno at ~21°45'S, Haschke and Günther (2003)'s section report a basement thrust over folded Mesozoic units, in agreement with the style of deformation documented here, but with a relatively minor displacement on this thrust compared to our results in the Pinchal area. This thrust is here called the Sierra de Moreno Thrust. Together with the (1:1,000,000) Geological map of Chile (SERNAGEOMIN, 2003), Haschke and Günther (2003)'s map suggests that this basement thrust is cartographically continuous southward to the southern end of the Sierra de Moreno, at ~22°05'S. This possibly documents the lateral termination of this basement thrust.

As a conclusion, there exists a thrust system formed of various basement thrusts all along the Western Andean flank, bringing the basement of the Cordillera Domeyko westward over folded Mesozoic units – and therefore contributing to the uplift of the western margin of the Altiplano. This thrust system is segmented, with various strands mapped as local basement faults, as in our study (Figure 4) or in other maps (Aguilef et al., 2019; Haschke & Günther, 2003; SERNAGEOMIN, 2003; Skarmenta & Marinovic, 1981; Tomlinson et al., 2001). Altogether these various thrust segments document a much larger thrust system extending laterally over at least ~120 km (Figure 1), that we propose to name here the Andean Basement Thrust (hereafter ABT) system.

We interpret the ABT and the other thrusts west of it to root onto a low-angle, eastward dipping décollement, situated >2 km (Pinchal area) or >4 km (Quebrada Blanca area) beneath the present-day topographic surface. Deeper and eastward, this décollement probably steepens and forms a crustal-scale ramp, needed to sustain the uplift and topographic rise of the Western Andes, as proposed by Victor et al. (2004) and Armijo et al. (2015). Such crustal-scale structure has been termed the West Andean Thrust (or WAT) by Armijo et al. (2015).

7.1.2 Shortening and timing of deformation of the Andean Basement Thrust

From the likely minimum offset of the basement in the Pinchal area we estimated that the Pinchal Thrust (as part of the ABT system) alone accommodated locally a strict minimum of ~2.6 km of shortening on a horizontal distance of ~1 km. This multi-kilometric shortening would be associated with multi-kilometric basement exhumation, but only limited thermochronological data actually permit to evaluate the actual amount of exhumation. These data are presently absent locally in Pinchal, but sparsely exist at a regional scale when considering the ABT system over its whole extent. From apatite fission track dating in basement samples taken ~20 km east and south-east of our study sites of the Pinchal and Quebrada Blanca areas, Maksaev and Zentilli (1999) inferred at least 4–5 km of basement exhumation occurring between ~50–30 Ma. This is in good agreement with our results in terms of amount of uplift that would result from basement overthrusting on the ABT and above the WAT. Older thermochronological ages – (U-Th)/He zircon and apatite ages of ~91 Ma and ~57 Ma, respectively – were however found by Reiners et al. (2015) from the basement of the Quebrada Arcas, ~30 km south of our study site, in a structural setting equivalent to the basement of the Pinchal zone documented here. These ages do not contradict the previous estimates on total exhumation by Maksaev and Zentilli (1999), even though modeling would be needed here to precisely test this. However, they question the exact timing of basement exhumation, and, from there, of thrusting over the ABT. In the absence of properly analyzed and modeled samples closer to the ABT, it is difficult to assess more precisely its timing or amount of exhumation, uplift and shortening.

At a few places, the Pinchal segment of the ABT is covered by Cenozoic deposits. Given this observation and with existing thermochronological ages, we postulate that the ABT was most probably active sometime by Early Cenozoic to possibly Late Cretaceous – and that its activity had ceased by Early Miocene. This suggests it may have been coeval with deformation of the FTB documented immediately further west – or starting slightly before.

7.2 The West Andean Fold-and-Thrust-Belt at ~20–22ºS

7.2.1 Evidencing a west-vergent fold-and-thrust belt along the West Andean flank (~20–22°S)

The series of west-vergent folds described in this study at ~20–22ºS as deforming Mesozoic units are interpreted to form above thrusts that root at depth onto a common east-dipping decollement, as proposed classically in FTBs. A similar system of folds and faults affecting Mesozoic units is expected to extend laterally further north and south than just the two sites described here, most probably over our entire study zone of ~20–22ºS (Figure 1), even though a large part north of the Quebrada Blanca area is covered by Cenozoic strata. This is deduced from existing maps and previous works (e.g. Aguilef et al., 2019; Haschke & Günther, 2003; SERNAGEOMIN, 2003; Skarmenta & Marinovic, 1981). It therefore probably spreads out over a north-south distance of at least ~200 km – and possibly more as folded Mesozoic sediments are mapped on the (1:1,000,000) Geological map of Chile (SERNAGEOMIN, 2003) in the north- and south-ward continuation of the two zones investigated here.

Further west, structures at depth are covered by Cenozoic deposits. Seismic profiles from the Chilean Empresa Nacional del Petroleo (ENAP), as re-interpreted by Victor et al. (2004), Jordan et al. (2010), Fuentes et al. (2018), Labbé et al. (2019) or Martínez et al. (2021), show a series of several blind mostly west-verging thrust-faults affecting both the Cenozoic and the underlying Mesozoic units. Nonetheless, deformation is mostly well-imaged for post ~29 Ma growth strata within the Cenozoic series deposited above the Choja erosional surface, and remains less well-resolved for underlying Mesozoic units. These observations may reflect the fact that Mesozoic units are much more deformed than Cenozoic layers, a deduction in line with our own field observations in the Pinchal and Quebrada Blanca areas (Figures 4 and 9). As proposed by Victor et al. (2004), these blind west-vergent thrust-faults at ~20–22°S can reasonably be interpreted as connecting onto an east-dipping detachment, deepening towards the mountain range, again in line with our interpretation of the structures in our field study areas (Figures 5c and 10c).

Altogether, these data suggest that all these thrust faults, either blind or deduced from outcropping folds, pertain to the same FTB system. By analogy to what has been proposed at the latitude of Santiago de Chile (~33.5°S) (Armijo et al., 2010; Rault, 2011; Riesner et al., 2017;

Riesner et al., 2018), we propose to name this FTB hereafter as the West Andean Fold-and-Thrust-Belt (WAFTB). The WAFTB at ~20–22°S therefore extends laterally over at least ~200 km, and across-strike over a much wider region (~50 km, maybe locally more) than the two ~7–17 km wide sites investigated in this study (Figure 1), as most of the FTB is hidden beneath the less deformed Cenozoic cover (Figure 1).

7.2.2 Shortening across the Western Andean Fold-and-Thrust Belt (~20-22°S)

The WAFTB of northern Chile (~20–22°S) accommodates a minimum shortening of ~3–9 km, as quantified from the ~7–17 km wide cross-sections representative of the two investigated areas (not including the contribution of the ABT in the case of the Pinchal area). Few authors attempted to quantify the shortening in this part of the Andes. At 20°30'S, Victor et al. (2004) only evaluated the deformation affecting the post ~29 Ma deposits and not the total shortening as could be derived from folded Mesozoic series. At ~21°45'S, ~30 km south of the Pinchal area, Haschke and Günther (2003) reported a minimum shortening of >9 km from a ~50 km wide cross-section, but without providing nor discussing the data used to make this estimate. Their section encompasses an equivalent of the WAFTB and ABT investigated in this study in the Sierra de Moreno area, but also extends further east. Within the ~8–10 km wide Sierra de Moreno area itself, they estimate a minimum shortening of ~4 km (i.e. a minimum of ~30% of shortening), a value consistent with our results. This study of Haschke and Günther (2003) is to our knowledge the only other work attempting to estimate the minimum total shortening absorbed by the WAFTB at 20–22°S. It becomes obvious that the various structures of the WAFTB in northern Chile, wherever they are (Quebrada Blanca, Pinchal or Sierra Moreno areas), all absorb multi-kilometric shortening, at the scale of only one to three major folds and thrusts.

This conclusion further emphasizes that the minimum ~3–9 km of shortening proposed here from the folds of the Quebrada Blanca and Pinchal areas (when excluding the contribution of the ABT in the Pinchal area) are under-estimates of the total shortening across the whole WAFTB at this latitude. When applying the minimum ~34–47% shortening estimated across our two investigated sites to the ~50 km across-strike extent of the whole WAFTB, we find a minimum crustal shortening of ~26–44 km, a value consistent – even though in the high range – with the ~20–30 km qualitatively estimated by Armijo et al. (2015) by scaling with structural relief and crustal thickness. A precise quantification of the deformation recorded by buried folded Mesozoic units west of our study sites is at the moment not possible from available seismic profiles (Victor et al., 2004; Jordan et al., 2010; Labbé et al., 2019).

7.3 Temporal evolution of deformation along the western Andes (~20–22°S)

Our investigations underline that the deformation of the Quebrada Blanca and Pinchal areas is not linearly distributed over time, and can be assigned to two main periods: (1) a period of major deformation sometime between ~68–29 Ma (possibly ~68–44 Ma) at a minimum average shortening rate of ~0.1–0.3 km/Myr; and (2) a subsequent period of moderate deformation from ~29–0 Ma (starting possibly earlier) at an average rate of <0.1 km/Myr (Figure 13d). These deductions and rates hold for the westernmost anticline of the study sites, but the reduction in deformation rates is expected at the scale of both whole investigated sites. Indeed, the difference in the deformation cumulated by Mesozoic units and by post ~29 Ma Cenozoic layers can be qualitatively – but clearly – intuited from our cross-sections (Figures 5, 10 and 13). Westward, it may also be inferred but with less certainty from the ENAP seismic profiles (see discussion above). This deformation slow-down, starting by ~29 Ma at latest and possibly earlier by ~44 Ma, could therefore be regional across the entire WAFTB.

This reasoning essentially applies to the WAFTB but may also hold for the ABT. If the age of basement thrusting is not precisely known, it most probably occurred by Early Cenozoic (Maksaev & Zentilli, 1999) or even Late Cretaceous - Early Cenozoic (deduced after Reiners et al., 2015), and had ceased by ~29 Ma (see discussion in section 7.1).

This proposed time window for major folding and possibly for thrusting over the ABT is generally consistent with the main Incaic phase of deformation inferred by various authors as the main period of Andean mountain-building *stricto sensu* (e.g. Charrier et al., 2007; Cornejo et al., 2003; Pardo-Casas & Molnar, 1987; Steinmann, 1929).

Based on the ENAP seismic profiles in the westward prolongation of our study areas, Victor et al. (2004) investigated the folding and thrusting recorded by the growth strata of the Cenozoic Altos de Pica Formation. They determined a post ~29 Ma shortening of ~3 km, accommodated by several west-vergent thrusts within the ~40 km wide Atacama Bench. In both our study areas, we were able to reproduce with trishear modeling the first-order pattern of the slightly deformed Cenozoic growth strata over and in front of the western anticlines. We found ~0.4–0.5 km of post ~29 Ma shortening on one single most frontal fault and fold in the case of our two investigated sections (Figures S12, S13), that is over a distance of ~5–8 km. These values are in overall good agreement with the results of Victor et al. (2004) when setting them to the same spatial scale, as they together consistently represent ~6–8% of shortening. Compared to the minimum ~3–6 km of ante- ~29 Ma shortening (or ~34–47% of shortening) quantified on one single structure from each study section (Figures S12, S13), the post ~29 Ma shortening is clearly of limited importance.

The simplest interpretation would be that this post ~29 Ma decline of the shortening rate results from the slow-down of the same protracted regional compressional event which caused the formation of the west-vergent WAFTB and ABT. With the presently available data at 20–22°S, we cannot exclude that this slow-down may have started before ~29 Ma – possibly as soon as ~44 Ma, or even before (section 6.3) – but definitely not afterwards. Anyhow, in the absence of sedimentary markers that would provide further quantitative details on the incremental deformation between ~68 Ma and ~29 Ma, the evolution of shortening cannot be quantified more precisely over time, and only average rates can be proposed over the large time spans of the phases of major and moderate deformation.

7.4 Regional implications

Even though multi-kilometric, the shortening accommodated by the west-vergent structures of the western Andes outlined in this study represents a modest contribution to the total crustal shortening of >300 km across the entire Central Andes at ~20ºS (e.g. Anderson et al., 2017; Barnes & Ehlers, 2009; Eichelberger et al., 2013; Elger et al., 2005; Faccenna et al., 2017; Kley & Monaldi, 1998; McQuarrie et al., 2005; Oncken et al., 2012; Sheffels, 1990). It should however be recalled that the deformation absorbed across the western Andes took place mostly in the early stages of the Andean orogeny, sometime between ~68–29 Ma (possibly ~68–44 Ma) in the case of the WAFTB, starting possibly earlier for the ABT – in any case during the Incaic phase. In fact, when replaced within the temporal evolution of Andean mountain-building at these latitudes (e.g. Armijo et al., 2015; Charrier et al., 2007; McQuarrie et al., 2005; Oncken et al., 2006), the early multi-kilometric shortening evidenced here represents in fact a major contribution to initial Andean deformation, which has been most often neglected in orogen-wide studies. The slowing down of deformation across the western Andean flank by ~29 Ma – and possibly starting after ~44 Ma – may have accompanied the jumping and transfer of deformation towards the East (i.e. towards the eastern Altiplano and further east, e.g. Isacks et al., 1988; McQuarrie et al., 2005; Oncken et al., 2006).

Conclusion

In this study, we investigate and explore two major structural features within the western flank of the Andes at ~20–22°S: (1) the Andean Basement Thrust (ABT), which stands as a west-vergent, >120 km long system of ~north-south trending thrusts bringing Paleozoic basement over folded Mesozoic series; (2) the West Andean Fold-and-Thrust-Belt (WAFTB), which is a west-vergent FTB deforming Mesozoic and Cenozoic sediments, mostly covered by the Cenozoic Altos de Pica Formation, but cropping out in few (up to ~10–20 km wide) places along the mountain flank. The WAFTB extends over at least ~200 km north-south and ~50 km across-strike. Even though our investigations only rely on two limited outcropping sites, our deductions have regional implications when compared and up-scaled with previous results.

Using field and satellite observations, we build structural cross-sections and quantify the recorded shortening at two key sites along the western mountain flank. We find a minimum shortening of ≥2.6 km on the ABT and of ≥3–9 km on the few exposed structures of the WAFTB. This strict minimum shortening – derived from outcrop areas of limited extent – corresponds only to a fraction of the entire deformation at the scale of the whole Western Cordillera at ~20–22°S. When set on scale with the extent of the investigated structures, it clearly implies the possibility of multi-kilometric shortening across the western flank of the Andes, possibly up to 26–44 km or more.

We further exploit the differential deformation recorded by folded Mesozoic layers and Cenozoic growth strata of the post ~29 Ma Altos de Pica Formation. We show that the outcropping WAFTB was mainly active between ~68–29 Ma (possibly ~68–44 Ma), and that its deformation rates significantly decreased after ~29 Ma (a decrease that may have started sometime earlier, e.g. by ~44 Ma). By comparison to previous studies of the blind portions of the WAFTB west of our study sites, we propose that such slowing-down of deformation rates was regional rather than local. In addition, field observations and published thermochronological results of basement exhumation suggest that this temporal evolution of deformation rates may also hold for the ABT. We therefore propose that the post ~29 Ma (or post ~44Ma) decline in shortening rates resulted from the regional slowing-down of the same protracted compressional event that caused the formation of the west-vergent WAFTB and ABT, most probably accompanying the transfer of Andean deformation towards the Altiplano Plateau, Eastern Cordillera, and further eastward.

Acknowledgements

This study was supported by grants from CNRS-INSU (program TELLUS-SYSTER) and from the Institut de physique du globe de Paris (IPGP). Field work was also funded by the Andean Tectonics Laboratory of the Advanced Mining Technology Center, University of Chile. Earlier work on this zone by RL and DC was supported by ANR project MegaChile (grant ANR-12-BS06-0004-02) and LABEX UnivEarthS project. TH benefited from a PhD grant attributed by the French Ministry of Higher Education and Research. Pleiades satellite imagery was obtained through the ISIS program of the CNES under an academic license and is not for open distribution. The authors thank A. Delorme for his technical assistance in producing the DEMs. Numerical computations for the DEMs were performed on the S-CAPAD platform, Institut de physique du globe de Paris (IPGP). The kinematic modeling was made using FoldFault Forward version 6, freely available from http://www.geo.cornell.edu/geology/faculty/RWA/programs/faultfoldforward.html (Allmendinger, 1998). R. Armijo and the late R. Thiele are warmly thanked for the fruitful discussions that led over the years to this work and manuscript. We also benefited from discussions with C. Creixell, N. Blanco, A. Tomlinson and F. Sepulveda (SERNAGEOMIN), from the valuable help of M. Riesner for the 3D mapping, and that of L. Barrier for facies and polarity identifications. L. Barrier and N. Bellhasen are also thanked for discussions that inspired and led to trishear modeling. L. Giambiagi, C. Mpodozis and an anonymous reviewer are acknowledged for their thorough and detailed reviews. This study was partly supported by IdEx Université de Paris ANR-18-IDEX-0001. This is IPGP contribution number XXX.

References

Aguilef, S., Franco, C., Tomlinson, A., Blanco, N., Alvarez, J., Montecino, D., et al. (2019).

Geología del área Quehuita-Chela, Regiones de Tarapacá y Antofagasta. Santiago, Chile: SERNAGEOMIN.

Allmendinger, R. W., Figueroa, D., Snyder, D., Beer, J., Mpodozis, C., & Isacks, B. L. (1990). Foreland shortening and crustal balancing in the Andes at 30°S latitude. Tectonics, 9(4), 789–809. https://doi.org/10.1029/TC009i004p00789

Allmendinger, R. W. (1998). Inverse and forward numerical modeling of trishear fault-propagation folds. *Tectonics*, *17*(4), 640–656. https://doi.org/10.1029/98TC01907

Allmendinger, R. W., & Shaw, J. H. (2000). Estimation of fault propagation distance from fold shape: Implications for earthquake hazard assessment. *Geology*, *28*(12), 1099–1102.

Amilibia, A., Sàbat, F., McClay, K. R., Muñoz, J. A., Roca, E., & Chong, G. (2008). The role of inherited tectono-sedimentary architecture in the development of the central Andean mountain belt: Insights from the Cordillera de Domeyko. Journal of Structural Geology, 30(12), 1520–1539. https://doi.org/10.1016/j.jsg.2008.08.005

Anderson, R. B., Long, S. P., Horton, B. K., Calle, A. Z., & Ramirez, V. (2017). Shortening and structural architecture of the Andean fold-thrust belt of southern Bolivia (21°S): Implications for kinematic development and crustal thickening of the central Andes. *Geosphere*, *13*(2), 538–558. https://doi.org/10.1130/GES01433.1

Andriessen, P. A. M., & Reutter, K.-J. (1994). K-Ar and Fission Track Mineral Age Determination of Igneous Rocks Related to Multiple Magmatic Arc Systems Along the 23°S Latitude of Chile and NW Argentina. In Klaus-Joachim Reutter, E. Scheuber, & P. J. Wigger (Eds.), Tectonics of the Southern Central Andes (pp. 141–153). Berlin, Heidelberg: Springer Berlin Heidelberg. https://doi.org/10.1007/978-3-642-77353-2_10

Armijo, R., Rauld, R., Thiele, R., Vargas, G., Campos, J., Lacassin, R., & Kausel, E. (2010). The West Andean Thrust, the San Ramón Fault, and the seismic hazard for Santiago, Chile. *Tectonics*, *29*(TC2007). https://doi.org/10.1029/2008TC002427

Armijo, R., Lacassin, R., Coudurier-Curveur, A., & Carrizo, D. (2015). Coupled tectonic evolution of Andean orogeny and global climate. *Earth-Science Reviews*, *143*, 1–35. https://doi.org/10.1016/j.earscirev.2015.01.005

Arriagada, C., Cobbold, P. R., & Roperch, P. (2006). Salar de Atacama basin: A record of compressional tectonics in the central Andes since the mid-Cretaceous. Tectonics, 25(1). https://doi.org/10.1029/2004TC001770

Astini, R. A., & Dávila, F. M. (2010). Comment on "The West Andean Thrust, the San Ramón Fault, and the seismic hazard for Santiago, Chile" by Rolando Armijo et al.: COMMENTARY. Tectonics, 29(4). https://doi.org/10.1029/2009TC002647

Baker, M. C. W. (1977). Geochronology of upper Tertiary volcanic activity in the Andes of north Chile. *Geologische Rundschau*, *66*(1), 455–465. https://doi.org/10.1007/BF01989588

Barnes, J., Ehlers, T., McQuarrie, N., O'Sullivan, P., & Tawackoli, S. (2008). Thermochronometer record of Central Andean Plateau growth, Bolivia (19.5°S). *Tectonics*, *27*(TC3003). https://doi.org/10.1029/2007TC002174

Barnes, J. B., & Ehlers, T. A. (2009). End member models for Andean Plateau uplift. *Earth-Science Reviews*, *97*(1–4), 105–132. https://doi.org/10.1016/j.earscirev.2009.08.003

Barrionuevo, M., Liu, S., Mescua, J., Yagupsky, D., Quinteros, J., Giambiagi, L., et al. (2021). The influence of variations in crustal composition and lithospheric strength on the evolution of deformation processes in the southern Central Andes: insights from geodynamic models. International Journal of Earth Sciences, 110. https://doi.org/10.1007/s00531-021-01982-5

Bascuñán, S., Arriagada, C., Le Roux, J., & Deckart, K. (2016). Unraveling the Peruvian Phase of the Central Andes: stratigraphy, sedimentology and geochronology of the Salar de Atacama Basin (22°30-23°S), northern Chile. Basin Research, 28(3), 365– 392. https://doi.org/10.1111/bre.12114

Blanco, N., & Tomlinson, A. J. (2013). Carta Guatacondo, Region de Tarapaca. Santiago, Chile: SERNAGEOMIN.

Blanco, N., Tomlinson, A. J., Moreno, K., & Rubilar, D. (2000). *Importancia estratigráfica de icnitas de dinosaurios en la Fm. Chacarilla (Jurásico Superior - Cretácico Inferior), I Región, Chile*. Presented at the IX Congreso Geológico Chileno. Servicio Nacional de Geología y Minería, Puerto Varas, Chile.

Blanco, N., Vásquez, P., Sepúlveda, F., Tomlinson, A. J., Quezada, A., & Ladino, M. (2012). Geológico para el Fomento de la Exploración de Recursos Minerales e Hídricos de la

Cordillera de la Costa, Depresión Central y Precordillera de la Región de Tarapacá (20°–21°S). Santiago, Chile: SERNAGEOMIN.

Brooks, B. A., Bevis, M., Whipple, K., Ramon Arrowsmith, J., Foster, J., Zapata, T., et al. (2011). Orogenic-wedge deformation and potential for great earthquakes in the central Andean backarc. *Nature Geoscience*, *4*(6), 380–383. https://doi.org/10.1038/ngeo1143

Buchelt, M., & Tellez, C. (1988). The Jurassic La Negra Formation in the area of Antofagasta, northern Chile (lithology, petrography, geochemistry). In *The Southern Central Andes* (Springer-Verlag Berlin Heidelberg, Vol. 17, pp. 169–182). https://doi.org/10.1007/BFb0045181

Charrier, R., Pinto, L., & Rodríguez, M. P. (2007). Tectonostratigraphic evolution of the Andean Orogen in Chile. In T. Moreno & W. Gibbons (Eds.), *The Geology of Chile* (First, pp. 21–114). The Geological Society of London. https://doi.org/10.1144/GOCH.3

Cornejo, P., Matthews, S., & Pérez de Arce, C. (2003). *The "K-T" compressive deformation event in northern Chile (24°–27°S)*.

Cristallini, E. O., & Allmendinger, R. W. (2002). Backlimb trishear: a kinematic model for curved folds developed over angular fault bends. *Journal of Structural Geology*, *24*(2), 289–295. https://doi.org/10.1016/S0191-8141(01)00063-3

DeCelles, P. G., Zandt, G., Beck, S. L., Currie, C. A., Ducea, M. N., Kapp, P., et al. (2015). Cyclical orogenic processes in the Cenozoic central Andes. In Peter G. DeCelles, M. N. Ducea, B. Carrapa, & P. A. Kapp, *Geodynamics of a Cordilleran Orogenic System: The Central Andes of Argentina and Northern Chile*. Geological Society of America. https://doi.org/10.1130/2015.1212(22)

DeMets, C., Gordon, R., Argus, D., & Stein, S. (1994). Effect of recent revisions to the geomagnetic reversal time scale on estimates of current plate motions. *Geophysical Research Letters*, *21*. https://doi.org/10.1029/94GL02118

Dingman, R. J., & Galli, C. O. (1965). *Geology and Ground-Water Resources of the Pica Area, Tarapaca Province, Chile*. Geological Survey Bulletin 1189. US Dept of Interior.

Eichelberger, N., McQuarrie, N., Ehlers, T. A., Enkelmann, E., Barnes, J. B., & Lease, R. O. (2013). New constraints on the chronology, magnitude, and distribution of deformation within the central Andean orocline: CENTRAL ANDEAN OROCLINE DEFORMATION. Tectonics, 32(5), 1432–1453. https://doi.org/10.1002/tect.20073

Elger, K., Oncken, O., & Glodny, J. (2005). Plateau-style accumulation of deformation: Southern Altiplano. *Tectonics*, *24*(4). https://doi.org/10.1029/2004TC001675

Erslev, E. A. (1991). Trishear fault-propagation folding. *Geology*, *19*, 617–620. https://doi.org/10.1130/0091-7613(1991)019<0617:TFPF>2.3.CO;2

Faccenna, C., Becker, T. W., Conrad, C. P., & Husson, L. (2013). Mountain building and mantle dynamics. *Tectonics*, *32*(1), 80–93. https://doi.org/10.1029/2012TC003176

Faccenna, C., Oncken, O., Holt, A. F., & Becker, T. W. (2017). Initiation of the Andean orogeny by lower mantle subduction. *Earth and Planetary Science Letters*, *463*, 189–201. https://doi.org/10.1016/j.epsl.2017.01.041

Farías, M., Charrier, R., Comte, D., Martinod, J., & Hérail, G. (2005). Late Cenozoic deformation and uplift of the western flank of the Altiplano: Evidence from the depositional, tectonic, and geomorphologic evolution and shallow seismic activity (northern Chile at 19°30′S): WESTERN ALTIPLANO UPLIFT. *Tectonics*, *24*(4), n/a-n/a. https://doi.org/10.1029/2004TC001667

Fuentes, G., Martínez, F., Bascuñan, S., Arriagada, C., & Muñoz, R. (2018). Tectonic architecture of the Tarapacá Basin in the northern Central Andes: New constraints from field and 2D seismic data. Geosphere, 14(6), 2430–2446. https://doi.org/10.1130/GES01697.1

Galli, C., & Dingman, R. J. (1962). Cuadrángulos Pica, Alca, Matilla y Chacarilla: Con un estudio sobre los recursos de agua subterránea, Provincia de Tarapacá.

Galli-Olivier, C. (1967). Pediplain in Northern Chile and the Andean Uplift. *Science*, *158*(3801), 653–655. https://doi.org/10.1126/science.158.3801.653

Garcia, M., & Hérail, G. (2005). Fault-related folding, drainage network evolution and valley incision during the Neogene in the Andean Precordillera of Northern Chile. *Geomorphology*, *65*(3–4), 279–300. https://doi.org/10.1016/j.geomorph.2004.09.007

Garzione, C. N., McQuarrie, N., Perez, N. D., Ehlers, T. A., Beck, S. L., Kar, N., et al. (2017).

Tectonic Evolution of the Central Andean Plateau and Implications for the Growth of Plateaus. Annual Review of Earth and Planetary Sciences, 45(1), 529–559. https://doi.org/10.1146/annurev-earth-063016-020612

Hardy, S., & Ford, M. (1997). Numerical modeling of trishear fault propagation folding. *Tectonics*, *16*(5), 841–854. https://doi.org/10.1029/97TC01171

Haschke, M., & Günther, A. (2003). Balancing crustal thickening in arcs by tectonic vs. magmatic means. *Geology*, *31*(11), 933. https://doi.org/10.1130/G19945.1

Heit, B., Sodoudi, F., Yuan, X., Bianchi, M., & Kind, R. (2007). An S receiver function analysis of the lithospheric structure in South America. *Geophysical Research Letters*, *34*(14). https://doi.org/10.1029/2007GL030317

Henriquez, S., DeCelles, P. G., & Carrapa, B. (2019). Cretaceous to Middle Cenozoic Exhumation History of the Cordillera de Domeyko and Salar de Atacama Basin, Northern Chile. Tectonics, 38(2), 395–416. https://doi.org/10.1029/2018TC005203

Homewood, P., & Lateltin, O. (1988). Classic Swiss Clastics (Flysch and Molasse) - The Alpine connection. *Geodinamica Acta*, *2*(1), 1–11. https://doi.org/10.1080/09853111.1988.11105150

Horton, B. K. (2018). Sedimentary record of Andean mountain building. Earth-Science Reviews, 178, 279–309. https://doi.org/10.1016/j.earscirev.2017.11.025

Introcaso, A., Pacino, M. C., & Fraga, H. (1992). Gravity, isostasy and Andean crustal shortening between latitudes 30º and 35ºS. Tectonophysics, 205, 31–48. https://doi.org/10.1016/0040-1951(92)90416-4

Isacks, B. L. (1988). Uplift of the Central Andean Plateau and bending of the Bolivian Orocline. *Journal of Geophysical Research*, *93*(B4), 3211–3231. https://doi.org/10.1029/JB093iB04p03211

Kley, J., & Monaldi, C. R. (1998). Tectonic shortening and crustal thickness in the Central Andes: How good is the correlation? *Geology*, *26*(8), 723–726. https://doi.org/10.1130/0091-7613(1998)026<0723:TSACTI>2.3.CO;2

Labbé, N., García, M., Simicic, Y., Contreras-Reyes, E., Charrier, R., De Pascale, G., &

Arriagada, C. (2019). Sediment fill geometry and structural control of the Pampa del Tamarugal basin, northern Chile. GSA Bulletin, 131(1–2), 155–174. https://doi.org/10.1130/B31722.1

Lamb, S. (2011). Did shortening in thick crust cause rapid Late Cenozoic uplift in the northern Bolivian Andes? *Journal of the Geological Society*, *168*(5), 1079–1092. https://doi.org/10.1144/0016-76492011-008

Lamb, S. (2016). Cenozoic uplift of the Central Andes in northern Chile and Bolivia—reconciling paleoaltimetry with the geological evolution. *Canadian Journal of Earth Sciences*, *53*(11), 1227–1245. https://doi.org/10.1139/cjes-2015-0071

Lossada, A. C., Hoke, G. D., Giambiagi, L. B., Fitzgerald, P. G., Mescua, J. F., Suriano, J., & Aguilar, A. (2020). Detrital Thermochronology Reveals Major Middle Miocene Exhumation of the Eastern Flank ofthe Andes That Predates the PampeanFlat Slab (33°–33.5°S). Tectonics, 39(4), e2019TC005764. https://doi.org/10.1029/2019TC005764

Lucassen, F., Becchio, R., Wilke, H. G., Franz, G., Thirlwall, M. F., Viramonte, J., & Wemmer, K. (2000). Proterozoic–Paleozoic development of the basement of the Central Andes (18–26°S) — a mobile belt of the South American craton. *Journal of South American Earth Sciences*, *13*(8), 697–715. https://doi.org/10.1016/S0895-9811(00)00057-2

Martínez, F., Fuentes, G., Perroud, S., & Bascuñan, S. (2021). Buried thrust belt front of the western Central Andes of northern Chile: Style, age, and relationship with basement heterogeneities. Journal of Structural Geology, 147, 104337. https://doi.org/10.1016/j.jsg.2021.10433

Martinod, J., Gérault, M., Husson, L., & Regard, V. (2020). Widening of the Andes: An interplay between subduction dynamics and crustal wedge tectonics. *Earth-Science Reviews*, *204*, 103170. https://doi.org/10.1016/j.earscirev.2020.103170

McQuarrie, N. (2002). The kinematic history of the central Andean fold-thrust belt, Bolivia: Implications for building a high plateau. Geological Society of America Bulletin, 114(8), 950-963. https://doi.org/10.1130/0016-7606(2002)114<0950:TKHOTC>2.0.CO;2

McQuarrie, N., Horton, B. K., Zandt, G., Beck, S., & DeCelles, P. G. (2005). Lithospheric evolution of the Andean fold–thrust belt, Bolivia, and the origin of the central Andean plateau. *Tectonophysics*, *399*(1–4), 15–37. https://doi.org/10.1016/j.tecto.2004.12.013

Mpodozis, C., & Ramos, V. A. (1989). The Andes of Chile and Argentina. In G. E. Ericksen, M. T. Canas Pinochet, & J. A. Reinemund (Eds.), *Geology of the Andes and its Relation to Hydrocarbon and Mineral Resources* (pp. 59–90). Circum-Pacific Council for Energy and Mineral Resources Earth Sciences Series, Houston, Texas.

Mpodozis, C., Arriagada, C., Basso, M., Roperch, P., Cobbold, P., & Reich, M. (2005). Late Mesozoic to Paleogene stratigraphy of the Salar de Atacama Basin, Antofagasta, Northern Chile: Implications for the tectonic evolution of the Central Andes. Tectonophysics, 399(1–4), 125–154. https://doi.org/10.1016/j.tecto.2004.12.019

Muñoz, N., & Charrier, R. (1996). Uplift of the western border of the Altiplano on a west-vergent thrust system, Northern Chile. *Journal of South American Earth Sciences*, *9*(3–4), 171–181. https://doi.org/10.1016/0895-9811(96)00004-1

Norabuena, E., Leffler-Griffin, L., Mao, A., Dixon, T., Stein, S., Sacks, I. S., et al. (1998). Space geodetic observations of nazca-south america convergence across the central andes. *Science (New York, N.Y.)*, *279*(5349), 358–362. https://doi.org/10.1126/science.279.5349.358

Oncken, O., Boutelier, D., Dresen, G., & Schemmann, K. (2012). Strain accumulation controls failure of a plate boundary zone: Linking deformation of the Central Andes and lithosphere mechanics. *Geochemistry, Geophysics, Geosystems*, *13*(Q12007). https://doi.org/10.1029/2012GC004280

Oncken, Onno, Chong, G., Franz, G., Giese, P., Götze, H.-J., Ramos, V. A., et al. (Eds.). (2006). *The Andes: Active Subduction Orogeny*. Berlin, Heidelberg: Springer. Retrieved from https://doi.org/10.1007/978-3-540-48684-8

Pardo‐Casas, F., & Molnar, P. (1987). Relative motion of the Nazca (Farallon) and South American Plates since Late Cretaceous time. *Tectonics*, *6*(3), 233–248. https://doi.org/10.1029/TC006i003p00233

Puigdomenech, C., Somoza, R., Tomlinson, A., & Renda, E. M. (2020). Paleomagnetic data from the Precordillera of northern Chile: A multiphase rotation history related to a multiphase deformational history. Tectonophysics, 791, 228569.

https://doi.org/10.1016/j.tecto.2020.228569

Ramos, V. A. (1988). Late Proterozoic - Early Paleozoic of South America – a Colisional History. *Episodes*, *11*(3), 7.

Ramos, V. A. (2008). The Basement of the Central Andes: The Arequipa and Related Terranes. *Annual Review of Earth and Planetary Sciences*, *36*(1), 289–324. https://doi.org/10.1146/annurev.earth.36.031207.124304

Rapela, C. W., Pankhurst, R. J., Casquet, C., Baldo, E., Saavedra, J., & Galindo, C. (1998). Early evolution of the Proto-Andean margin of South America. *Geology*, *26*(8), 707–710.

Rauld, R. A. (2011). *Deformación cortical y peligro sísmico asociado a la falla San Ramón en el frente cordillerano de Santiago, Chile Central (33^{o}S)*. Retrieved from http://www.tesis.uchile.cl/tesis/uchile/2011/cf-rauld_rp/html/index.html

Reiners, P.W., Thomson, S. N., Vernon, A., Willett, S. D., Zattin, M., Einhorn, J., et al. (2015). Low-temperature thermochronologic trends across the central Andes, 21°S–28°S. In P. G. DeCelles, M. N. Ducea, B. Carrapa, & P. A. Kapp, Geodynamics of a Cordilleran Orogenic System: The Central Andes of Argentina and Northern Chile. Geological Society of America. https://doi.org/10.1130/2015.1212(12)

Reutter, Klaus-J., Scheuber, E., & Chong, G. (1996). The Precordilleran fault system of Chuquicamata, Northern Chile: evidence for reversals along arc-parallel strike-slip faults. Tectonophysics, 259(1–3), 213–228. https://doi.org/10.1016/0040- 1951(95)00109-3

Riesner, M., Lacassin, R., Simoes, M., Armijo, R., Rauld, R., & Vargas, G. (2017). Kinematics of the active West Andean fold-and-thrust belt (central Chile): Structure and long-term shortening rate. *Tectonics*, *36*(2), 287–303. https://doi.org/10.1002/2016TC004269

Riesner, Magali, Lacassin, R., Simoes, M., Carrizo, D., & Armijo, R. (2018). Revisiting the Crustal Structure and Kinematics of the Central Andes at 33.5°S: Implications for the Mechanics of Andean Mountain Building. *Tectonics*, *37*(5), 1347–1375. https://doi.org/10.1002/2017TC004513

Riesner, Magali, Simoes, M., Carrizo, D., & Lacassin, R. (2019). Early exhumation of the Frontal Cordillera (Southern Central Andes) and implications for Andean mountain-building at ~33.5°S. *Scientific Reports*, *9*(7972). https://doi.org/10.1038/s41598-019-

44320-1

Rosu, A.-M., Deseilligny, M., Delorme, A., Binet, R., & Klinger, Y. (2014). Measurement of ground displacement from optical satellite image correlation using the free open-source software MicMac. *ISPRS Journal of Photogrammetry and Remote Sensing*, *100*. https://doi.org/10.1016/j.isprsjprs.2014.03.002

Rupnik, E., Deseilligny, M., Delorme, A., & Klinger, Y. (2016). Refined satellite image orientation in the free open-source photogrammetric tools Apero/Micmac. *ISPRS Annals of Photogrammetry, Remote Sensing and Spatial Information Sciences*, *III–1*, 83–90. https://doi.org/10.5194/isprs-annals-III-1-83-2016

SERNAGEOMIN. (2003). Mapa Geológico de Chile: versión digital. Servicio Nacional de Geología y Minería, Publicación Geológica Digital, No. 4 (CD-ROM, versión 1.0, 2003). Santiago.

Sheffels, B. M. (1990). Lower bound on the amount of crustal shortening, in the central Bolivian Andes. *Geology*, *18*(9), 812–815. https://doi.org/10.1130/0091-7613(1990)018<0812:LBOTAO>2.3.CO;2

Skarmenta, J., & Marinovic, N. (1981). Hoja Quillagua.

Steinmann, G. (1929). Geologie von Peru. *The Journal of Geology*. https://doi.org/10.1086/623704

Tassara, A., Götze, H.-J., Schmidt, S., & Hackney, R. (2006). Three-dimensional density model of the Nazca plate and the Andean continental margin. *Journal of Geophysical Research: Solid Earth*, *111*(B09404). https://doi.org/10.1029/2005JB003976

Tomlinson, A. J., & Blanco, N. (1997a). Structural evolution and displacement history of the West Fault system, Precordillera, Chile: part 1, synmineral history. In: Proccedings 8th Congreso Geológico Chileno. Antofagasta, pp. 1873–1877.

Tomlinson, A. J., & Blanco, N. P. (1997b). Structural evolution and displacement history of the west fault system, precordillera, Chile: part 2, postmineral history. In: VIII Congreso Geológico Chileno, pp. 1873–1882.

Tomlinson, A., Blanco, N., Maksaev, V., Dilles, J., Grunder, A., & Ladino, M. (2001). Geología de la Precordillera Andina de Quebrada Blanca-Chuquicamata, Regiones I y II (20°30’-22°30’S). *Informe Registrado IR-01-20*.

Tomlinson, A. J., Blanco, N., & Ladino, M. (2015). Carta Mamina, Región de Tarapacá. SERNAGEOMIN.

Vergara, H., & Thomas, A. (1984). Hoja Collacagua, Región de Tarapacá. Santiago, Chile: SERNAGEOMIN.

Victor, P., Oncken, O., & Glodny, J. (2004). Uplift of the western Altiplano plateau: Evidence from the Precordillera between 20° and 21°S (northern Chile): ALTIPLANO WEST FLANK. *Tectonics*, *23*(4). https://doi.org/10.1029/2003TC001519

Wölbern, I., Heit, B., Yuan, X., Asch, G., Kind, R., Viramonte, J., et al. (2009). Receiver function images from the Moho and the slab beneath the Altiplano and Puna plateaus in the Central Andes. *Geophysical Journal International*, *177*(1), 296–308. https://doi.org/10.1111/j.1365-246X.2008.04075.x

Yuan, X., Sobolev, S. V., Kind, R., Oncken, O., Bock, G., Asch, G., et al. (2000). Subduction and collision processes in the Central Andes constrained by converted seismic phases. *Nature*, *408*(6815), 958–961. https://doi.org/10.1038/35050073

Zandt, G., Velasco, A. A., & Beck, S. L. (1994). Composition and thickness of the southern Altiplano crust, Bolivia. *Geology*, *22*(11), 1003–1006. https://doi.org/10.1130/0091-7613(1994)022<1003:CATOTS>2.3.CO;2

Zehnder, A. T., & Allmendinger, R. W. (2000). Velocity field for the trishear model. *Journal of Structural Geology*, *22*, 1009–1014.

Figures

Figure 1. Simplified geological and structural map of the western Central Andes at ~20–22ºS, Northern Chile (modified from Armijo et al., 2015), and average topographic profile (top; ve: vertical exaggeration). The two main structural ensembles are here the Marginal Block and the Western Cordillera. The Marginal Block encompasses the Coastal Cordillera and the longitudinal valley of the Atacama Bench (or Central Depression). The Western Cordillera includes the West Andean Fold-and-Thrust-Belt (WAFTB), a basement high (Cordillera Domeyko), and the modern volcanic arc. A large part of the WAFTB is hidden beneath blanketing Cenozoic deposits and only outcrops in few places. The Andean Basement Thrust (ABT) separates the WAFTB and the basement high of the Western Cordillera. The location of Figures 4 (Pinchal area) and 9 (Quebrada Blanca area) is given by black boxes. Inset*:* Location of the map (red box) within the Central Andes along the South American Continent. WAT: West Andean Thrust (after Armijo et al., 2015); FTB: Fold-and-Thrust-Belt; Cz: Cenozoic; Mz: Mesozoic; Pz-Pc: Paleozoic and Precambrian.

Figure 2. Landscape field overviews of the Pinchal area depicting the main tectono-stratigraphic units. The Paleozoic (Pz) basement stands clearly out in the background, characterized by its darker color and higher altitudes. The Mesozoic (Mz) series in the central part and in the foreground bear a marine part and a volcano-detrital part, delimited by an outstanding calcareous (Calc.) crest. Unconformable Cenozoic erosional surfaces, with limited fluvial deposits can also be observed. View points of both pictures are located on Figure 4.

Figure 3. First-order stratigraphic column of the Pinchal area derived from field observations obtained mainly along Quebrada Tania (Figures 4 and 5a) where the Mesozoic series seems to be most complete. Thicknesses of the stratigraphic units are not at scale on the figure, but are given in the main text (section 4.1.1). By analogy to regional descriptions, these layers are suspected to be Triassic at the base, and Jurassic in the case of the marine fossiliferous levels (see section 4.1.3 for additional details). The description of Cenozoic units is here completed based on the work of Victor et al. (2004). Color-code in line with maps (Figures 1, 4 and S13) and cross-sections (Figure 5). In the Pinchal area, Paleozoic basement overthrusts folded Mesozoic series

along the Pinchal Thrust, so that part of the deeper and older Mesozoic series may be missing here (as depicted by "?"). See Figures S1–S12 and corresponding captions (in supplementary material) for detailed sedimentologic descriptions.

Figure 4. Structural map of the Pinchal area (at ~21°30'S) derived from mapping in the field and on satellite imagery (location on Figure 1). White thin lines highlight Mesozoic layers mappable on satellite images. Thick blue line depicts the calcareous crest, which is used as a marker bed (Figure 2). A–A' and B–B' sections locate the topographic profiles used for the surface cross-sections of Quebrada Tania and Quebrada Martine, respectively (Figures 5a-b). In the case of the Quebrada Tambillo cross-section, a topographic swath profile was used along C–C'. The fold axes are relatively well defined for the synclinal fold, but less well constrained for the anticlinal fold because only observable along Quebrada Tambillo. Black dots refer to the location of field photographs, and are numbered according to the figures where these pictures are reported. PT: Pinchal Thrust; Q: Quebrada.

Figure 5. Cross-sections along **(a)** the Quebrada Tania (A–A' on Figure 4), **(b)** the Quebrada Martine (B–B' on Figure 4), and **(c)** the Quebrada Tambillo (C–C' on Figure 4). Reported dip angles have been measured in the field. Faults are outlined in black, and dashed when they are only observable at a local spatial scale. Only larger faults (continuous lines) are mapped on Figure 4. Fold axes are depicted above their surface trace, based on our field observations, and their orientation illustrates the deduced orientation of the corresponding axial planes. Grey numbers with arrows point out to field pictures and indicate the associated figure. In the case of the Quebrada Tania section **(a)**, the sedimentary polarity criterion (β) indicated to the west of the section has been observed ~1 km further downstream than reported here. For the Quebrada Martine section **(b),** note the stripe of continental Mesozoic rocks trapped in between two strands of the Pinchal Thrust. Sub-surface interpretation from surface observations is reported with transparent colors in the case of the Quebrada Tambillo section **(c)**. Note the different spatial scales of the three sections. PT: Pinchal Thrust.

Figure 6. Field view of the Pinchal Thrust (PT), thrusting the dark-grayish Paleozoic basement over the greenish folded Mesozoic units. Reddish rocks on the hanging wall to the east-northeast correspond to the thrust shear zone (hatched area in picture). Location on Figure 4. Non-interpreted photograph can be found in the supporting information (Figure S15).

Figure 7. Field pictures of small-scale structural features characteristic of the deformation within the Pinchal zone (Location on Figures 4 and 5). Non-interpreted photographs for (b) and (c) can be found in the supporting information (Figures S16).

(a) Shear band with characteristic C/S-fabric (for "Cisaillement/Schistosité") indicative of top-to-the-west thrusting. Observation within the metamorphic basement in the hanging wall of the Pinchal Thrust.

(b) Example of a small-scale fold within the marine Mesozoic units (blue line) in Quebrada Tania, within the inverted limb of the mapped syncline, nearby the fold axis. Note also the erosional surface (yellow) forming the unconformable contact between the Cenozoic deposits over the deformed Mesozoic.

(c) Small-scale thrusts (steep red line to the right) and décollements (flat red line to the left) observed within the marine Mesozoic strata (blue) of the inverted synclinal limb along Quebrada Tania. The limestone-dominated cm–dm beds are characteristic of the lower part of the marine Mesozoic units (Figure 3).

Figure 8. Field pictures of the two major folds within the Pinchal area (location on Figure 4). Non-interpreted photos can be found in the supporting information (Figures S17).

(a) Panoramic view over the north-eastern part of the Pinchal area. The Paleozoic basement (red crosses) overthrusts the Mesozoic units (blue and violet horizons) along the Pinchal Thrust (red line with triangles). The topographic low locates the synclinal axis. The calcareous crest on both sides is highlighted by the thick blue lines. For better visibility, Cenozoic erosional surfaces covered by thin deposits are not highlighted.

(b) Panoramic view along Quebrada Tambillo, in the southern part of the Pinchal area. The ~200 m deep incised canyon reveals the geometry of the large western anticline affecting Mesozoic layers (violet) underneath the unconformable Cenozoic strata (yellow). The fold axis (black line) probably coincides with an approximately vertical fault, also well observable on satellite imagery. Note also the repetition of smaller folds with westward decreasing amplitude and wavelength discernable beneath the westward thickening Cenozoic growth strata to the right of the picture. The Mesozoic calcareous crest (blue) and the Paleozoic basement (red crosses) over the Pinchal Thrust (red) appear in the far eastern background.

Figure 9. Structural map of the Quebrada Blanca zone (at ~20°45'S), refined from Armijo et al. (2015) (location on Figure 1). Colored lines report mappable layers. For visibility, only major, well-correlated layer traces are represented here. Black boxes locate the swath profiles from which layers were projected for the construction of the structural east–west cross-section (Figure 10). The A–B section corresponds to the topographic profile used for this same cross-section. Strike and dip measurements are extracted from 3D-mapping (see section 3.3) or observed in the field. Strike symbols without dip magnitude are derived from satellite imagery. Thick black lines correspond to major fold axes. Field pictures are located (with view direction), and numbered according to the associated figure. Ages from uranium-lead (U/Pb) radioisotope dating on zircon are taken from the Guatacondo geological map (Blanco & Tomlinson, 2013). Letters C, D, E, F, G and H to the north-east (within the folded Chacarilla and Majala Formations) report the layers illustrated on Figure 12. Cz: Cenozoic; K: Cretaceous; Jr: Jurassic; Q: Quebrada.

Figure 10. East–west cross-section of the Quebrada Blanca site, established from the projection of selected, well-expressed layers mapped on satellite imagery. APF: Altos de Pica Formation.
(a) Observations, reporting the geometry of projected layers and associated dip angles, together with their stratigraphic ages (color-code).
(b) Sub-surface interpretation and extrapolation of observations.
(c) East–west cross-section based on (a) and (b). Interpretation at depth is indicated with transparent colors, in contrast with sub-surface observations. Extrapolation above the topographic surface is drawn with dashed lines. Ages from uranium-lead (U/Pb) radioisotope dating on zircon are taken from the Guatacondo geological map (Blanco & Tomlinson, 2012). The ~27–29 Ma age of the basal deposits of the Altos de Pica formation is derived from regional considerations (Victor et al., 2004).

Figure 11. Field picture of the western limb of the western anticline in the Quebrada Blanca area. Non-interpreted photographs are provided in supplementary material (Figure S18). Location on Figures 9 and 10.

(a) Series of folds with westward decreasing amplitude and wavelength (hundreds to tens of meters) observed at the front of the western anticline.

(b) Detailed view of the westernmost outcropping small-scale anticlines, located on (a) by the black box.

Figure 12. Landscape view on the western limb of the eastern large-scale anticline in the Quebrada Blanca area (Location on Figures 9 and 10). Here, steeply inclined Mesozoic horizons are very well discernible in the landscape. Bedding traces C, D, E, F, G and H underlined here are also georeferenced on the structural map (Figure 9) from mapping on satellite imagery. Note the thrust-affected small-scale fold (red dashed line) emphasizing the west-vergence of tectonic structures. The non-interpreted picture is provided in supplementary material (Figure S19).

Figure 13. Kinematics of folding of the western anticlines of the Quebrada Blanca and Pinchal zones as deduced from field observations and trishear modeling. Modeling was performed with FaultFold Forward v.6 (Allmendinger, 1998).

(a-c) Final stages of the best-fit models in the case of **(a)** the Quebrada Blanca area; **(b)** the Quebrada Tambillo (Pinchal area), shown here at the same scale as (a). **(c)** Detailed and enlarged view of our results for the Quebrada Tambillo (Pinchal area). Note the large scale-difference between the sections of the two investigated sites (a,b). Thicker lines outline model results, while transparent lines and colors refer to the cross-sections of Figures 10c and 5c. These lines are color-coded according to the stratigraphic level they represent, as in the original cross-sections. Black lines report the modeled thrusts and horizontal arrows report the model total shortening. PT: Pinchal Thrust.

(d) Shortening vs. time, as deduced from trishear modeling of the western anticlines of the Quebrada Blanca and Pinchal areas, and the ages of deformed layers. The three temporal benchmarks correspond to the age of the youngest folded Cretaceous (Kr) unit (~68 Ma), to the age of magmatic intrusions (~44 Ma) that are cartographically discordant, both derived from the Guatacondo geological map (Blanco & Tomlinson, 2013 – see also Figures 9 and 10c), and to the ~29 Ma age of the oldest Cenozoic layer of the Altos de Pica Formation (APF) (Victor et al., 2004) above the Choja erosional surface. It is possible that most deformation occurred prior to

~44 Ma, as deduced from the age of the intrusions cartographically seemingly post-dating folding (Figure 9), even though this argument is to be taken with caution. Our results underline two phases of deformation, with a slowing down of deformation since ~29 Ma at least, possibly even before. Intermediate stages of the trishear modeling are reported on Figures S20 and S21 (supplementary material) for the cross-sections of Quebrada Tambillo and Quebrada Blanca, respectively. Model parameters are indicated in Tables S1–S3 in supplementary material.

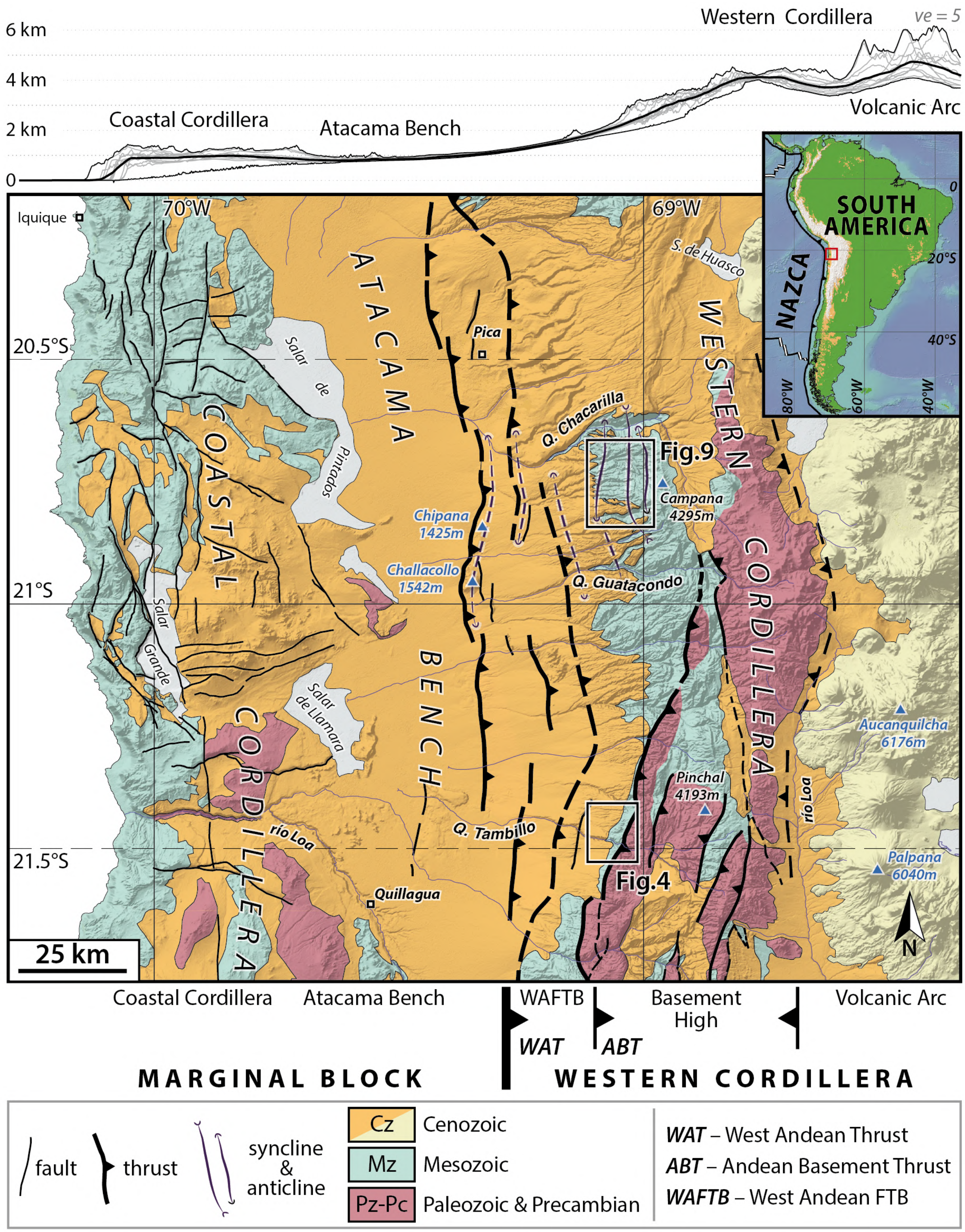

Western Cordillera
ve = 5
6 km
4 km
2 km
0
Volcanic Arc
Coastal Cordillera
Atacama Bench
SOUTH AMERICA
NAZCA
0
20°S
40°S
80°W
60°W
40°W
Iquique
70°W
69°W
S. de Huasco
ATACAMA
Pica
WESTERN
20.5°S
Salar de Pintados
COASTAL
Q. Chacarilla
Fig.9
Campana 4295m
Chipana 1425m
Challacollo 1542m
21°S
Salar Grande
Q. Guatacondo
CORDILLERA
BENCH
Salar de Llamara
Aucanquilcha 6176m
Pinchal 4193m
Q. Tambillo
río Loa
21.5°S
Fig.4
Palpana 6040m
Quillagua
25 km
N
Coastal Cordillera
Atacama Bench
WAFTB
Basement High
Volcanic Arc
WAT
ABT
MARGINAL BLOCK
WESTERN CORDILLERA
fault
thrust
syncline & anticline
Cz
Cenozoic
Mz
Mesozoic
Pz-Pc
Paleozoic & Precambian
WAT – West Andean Thrust
ABT – Andean Basement Thrust
WAFTB – West Andean FTB

Figure 1.

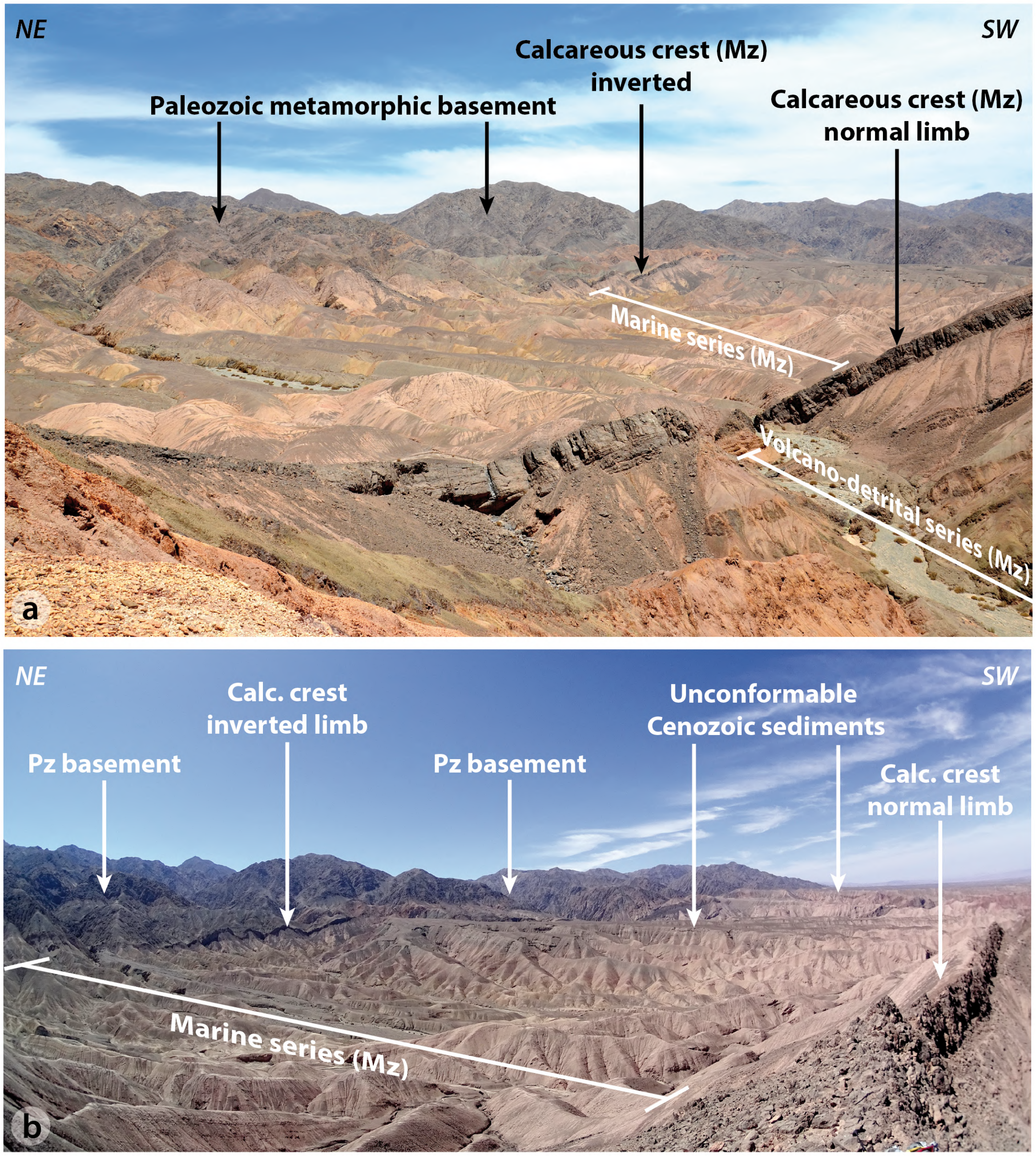
NE
SW
Calcareous crest (Mz)
inverted
Paleozoic metamorphic basement
Calcareous crest (Mz)
normal limb
Marine series (Mz)
Volcano-detrital series (Mz)
a
NE
SW
Calc. crest
inverted limb
Unconformable
Cenozoic sediments
Pz basement
Pz basement
Calc. crest
normal limb
Marine series (Mz)
b

Figure 2.

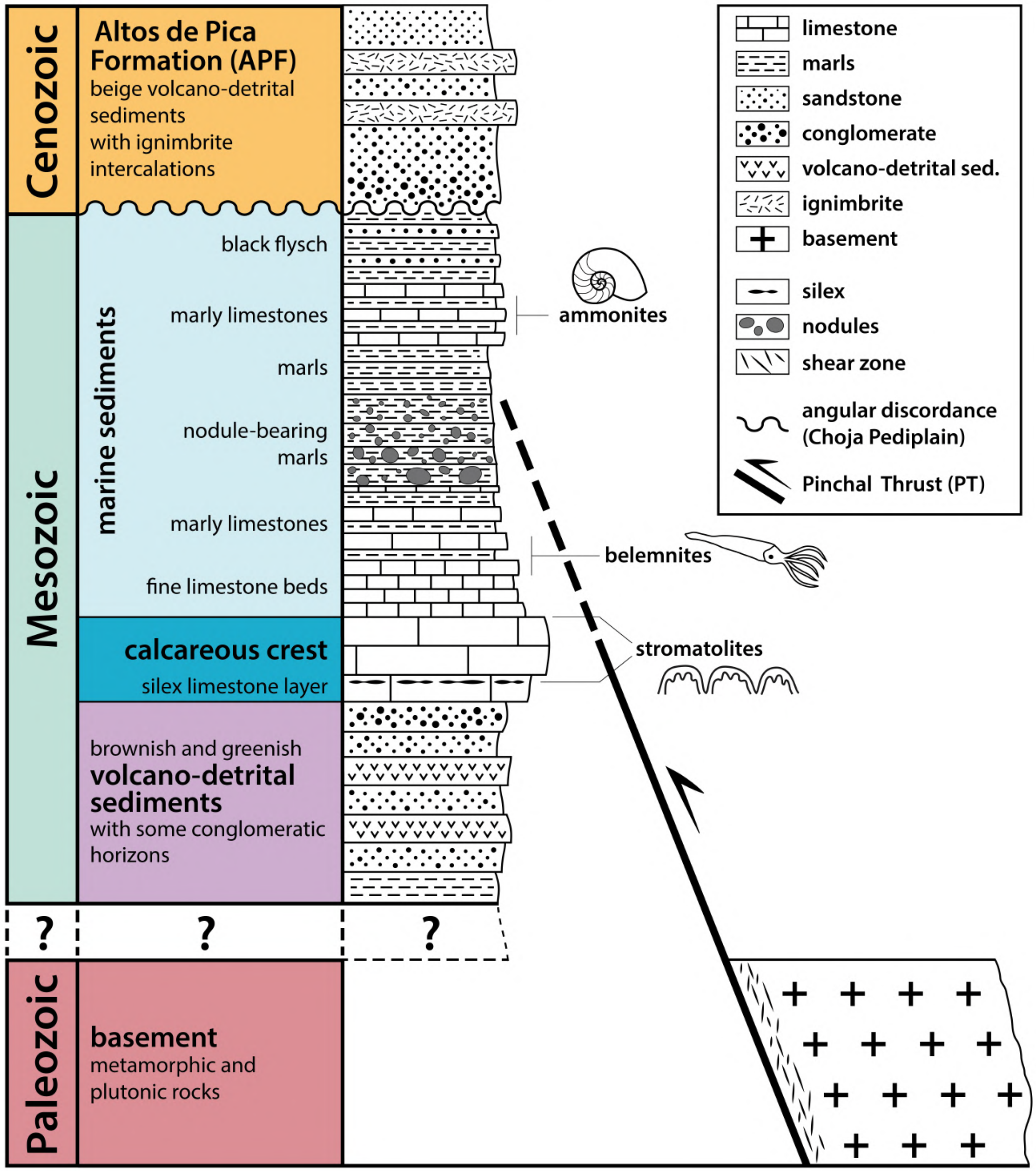
Cenozoic
Altos de Pica Formation (APF)
beige volcano-detrital sediments with ignimbrite intercalations
Mesozoic
marine sediments
black flysch
marly limestones
marls
nodule-bearing marls
marly limestones
fine limestone beds
calcareous crest
silex limestone layer
brownish and greenish
volcano-detrital sediments
with some conglomeratic horizons
?
?
?
Paleozoic
basement
metamorphic and plutonic rocks
ammonites
belemnites
stromatolites
limestone
marls
sandstone
conglomerate
volcano-detrital sed.
ignimbrite
basement
silex
nodules
shear zone
angular discordance (Choja Pediplain)
Pinchal Thrust (PT)

Figure 3.

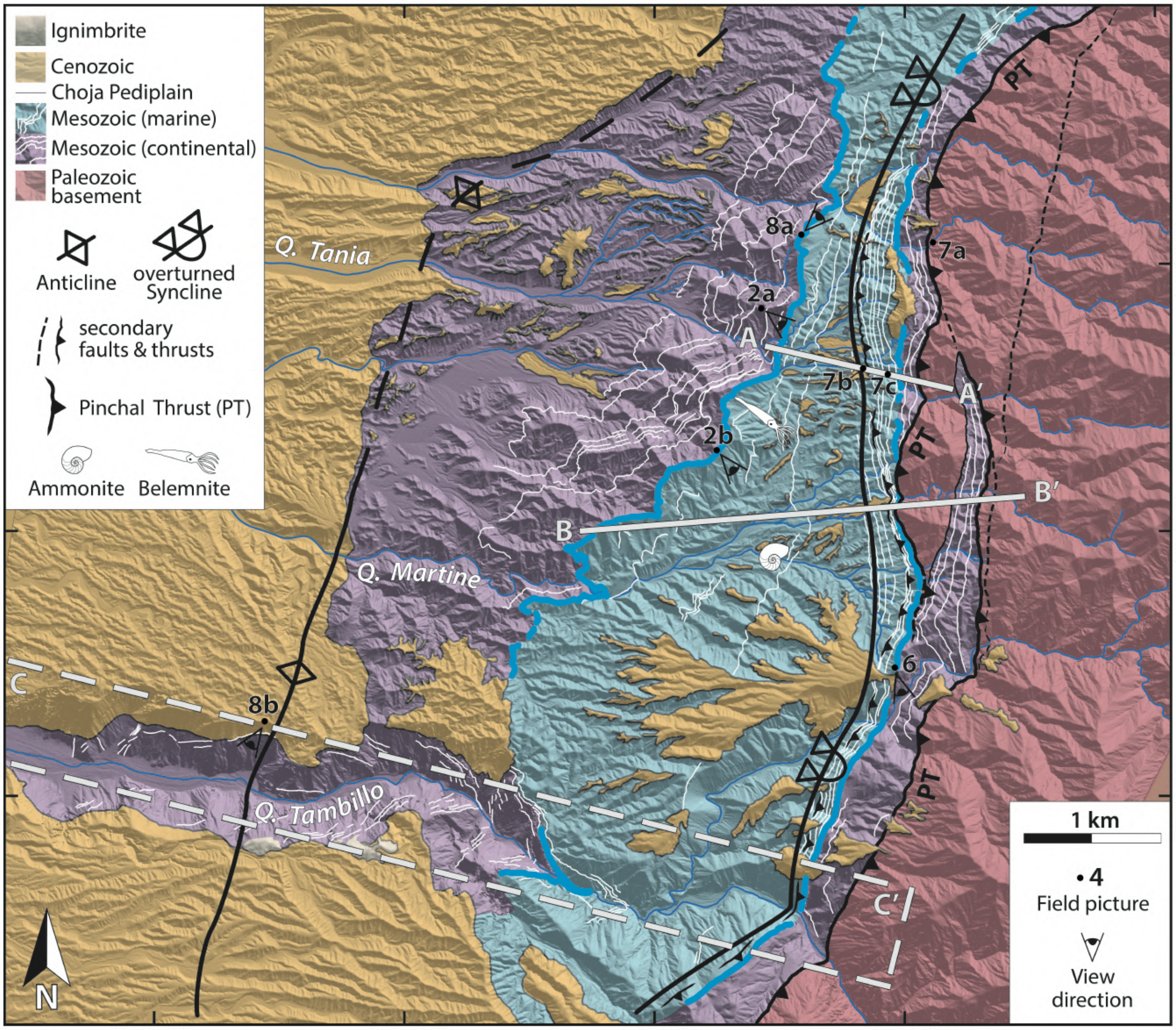

Ignimbrite
Cenozoic
Choja Pediplain
Mesozoic (marine)
Mesozoic (continental)
Paleozoic basement
Anticline
overturned Syncline
secondary faults & thrusts
Pinchal Thrust (PT)
Ammonite
Belemnite
Q. Tania
Q. Martine
Q. Tambillo
PT
A
A′
B
B′
C
C′
2a
2b
6
7a
7b
7c
8a
8b
1 km
4 Field picture
View direction
N
69°05′W
69°04′W
69°03′W
69°02′W
21°27′S
21°28′S
21°29′S

Figure 4.

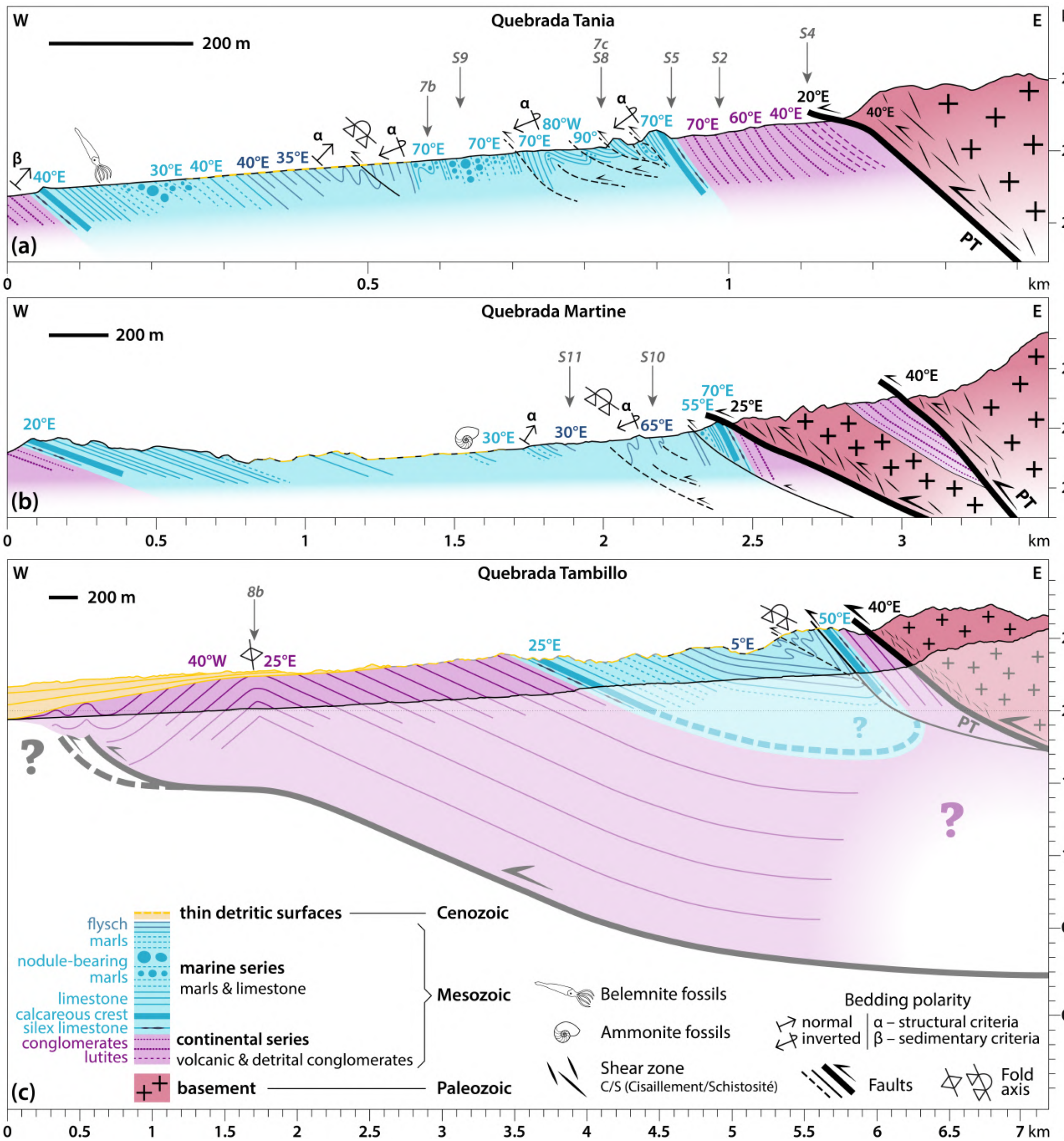

Quebrada Tania
W
E
200 m
(a)
km
PT
Quebrada Martine
(b)
Quebrada Tambillo
(c)
thin detritic surfaces
Cenozoic
flysch
marls
nodule-bearing marls
limestone
calcareous crest
silex limestone
marine series
marls & limestone
Mesozoic
conglomerates
lutites
continental series
volcanic & detrital conglomerates
basement
Paleozoic
Belemnite fossils
Ammonite fossils
Shear zone
C/S (Cisaillement/Schistosité)
Faults
Bedding polarity
normal
inverted
α – structural criteria
β – sedimentary criteria
Fold axis

Figure 5.

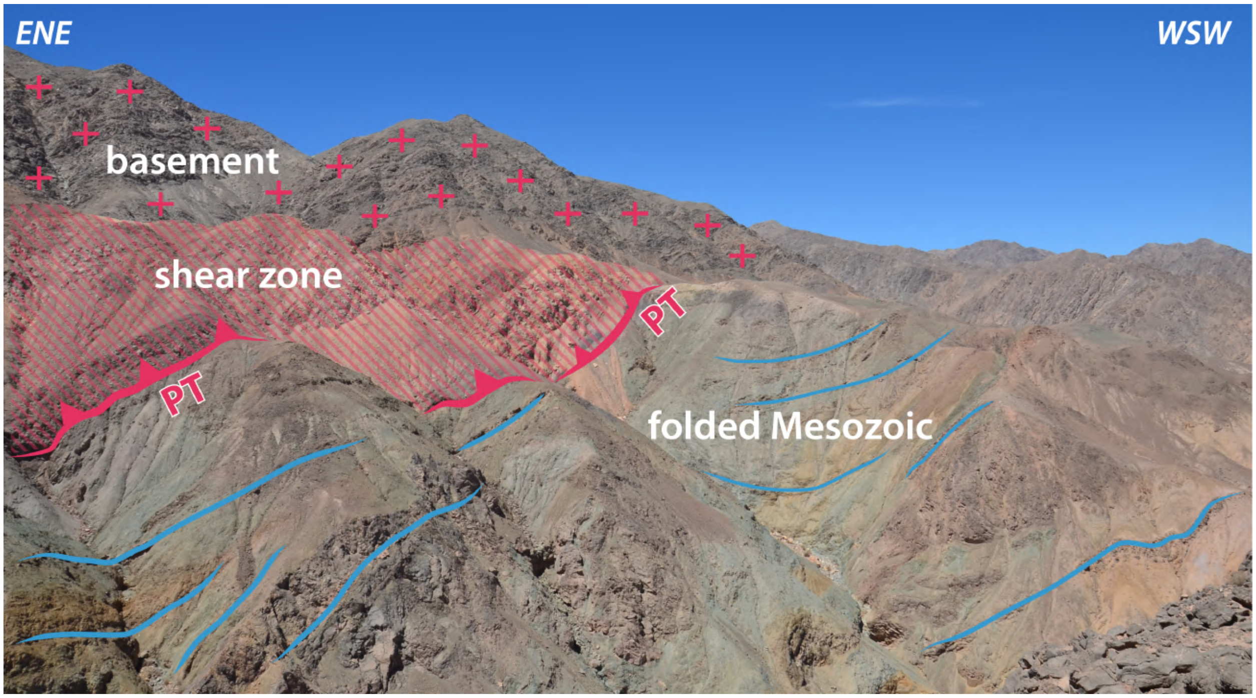

Figure 6.

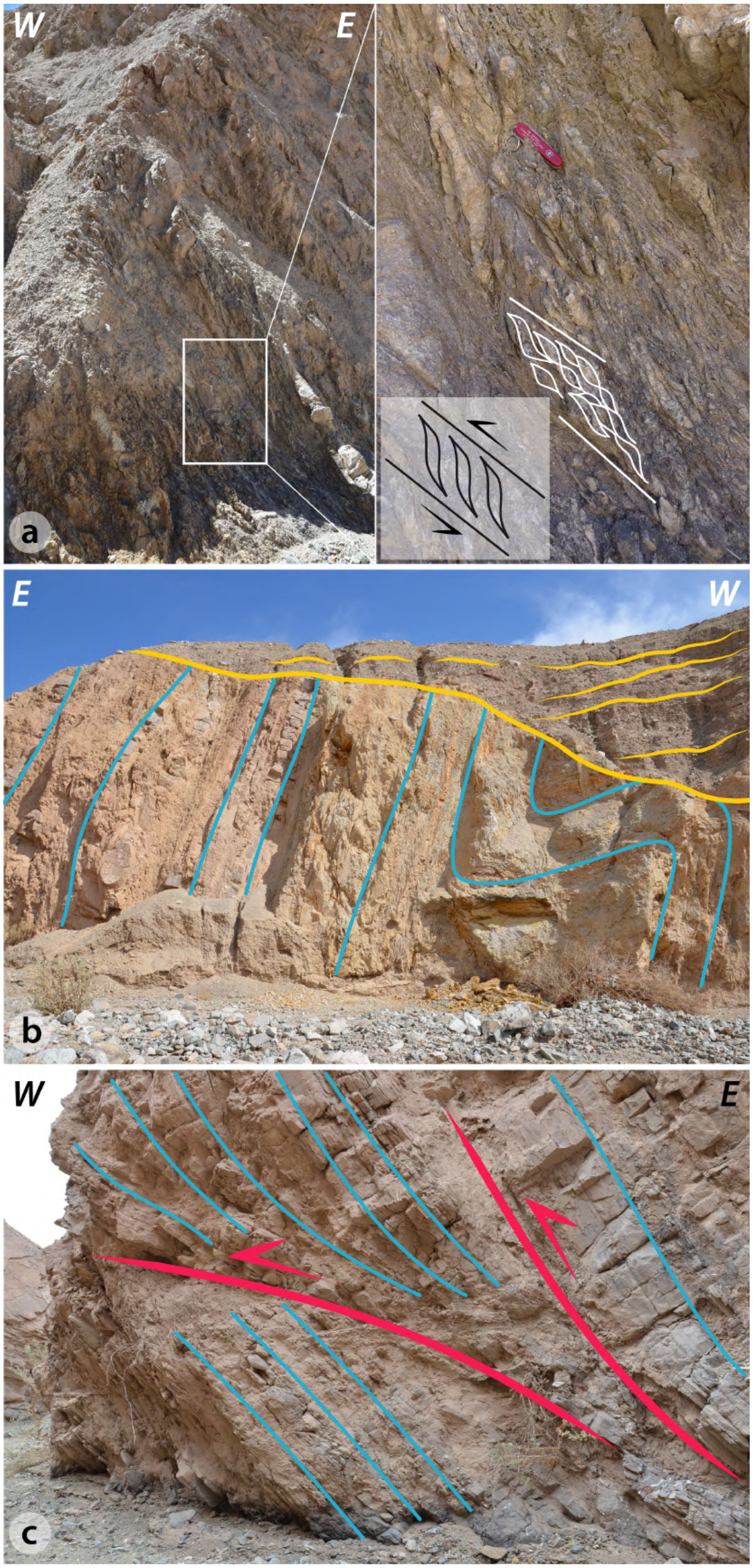

Figure 7.

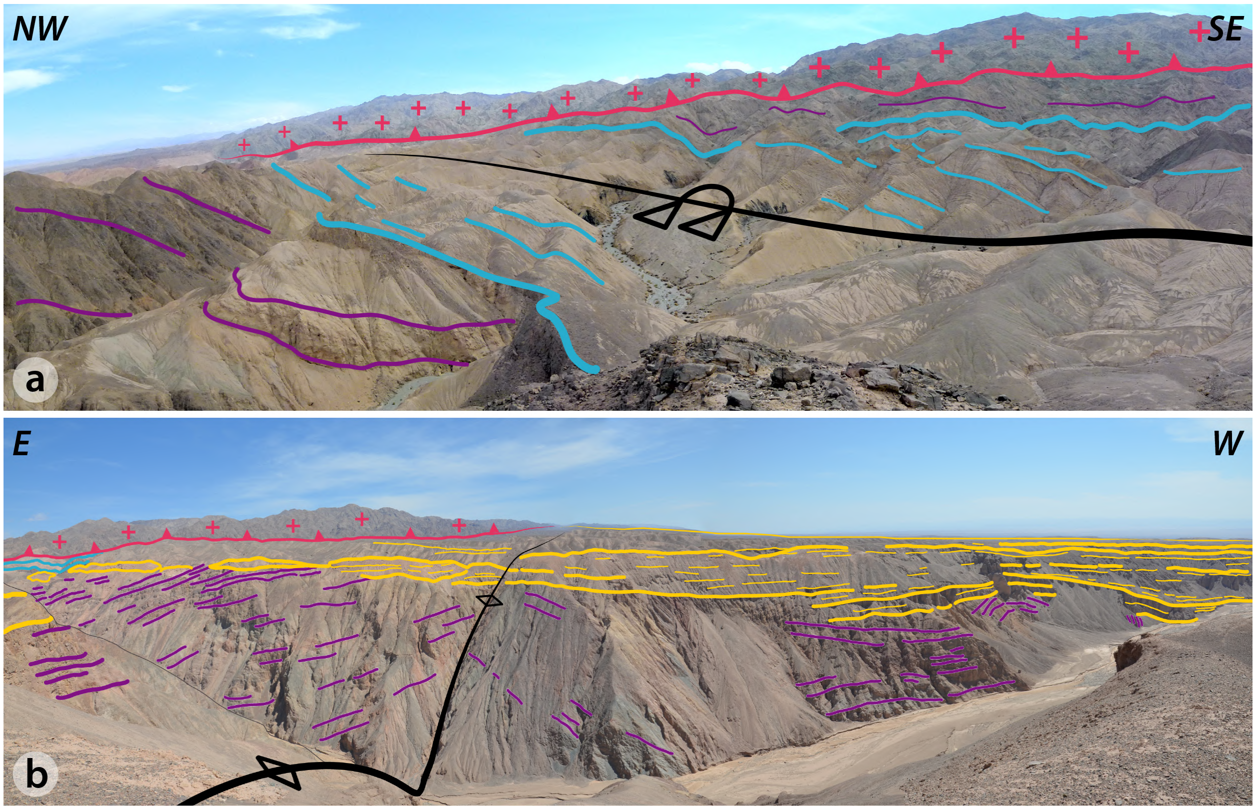

Figure 8.
.

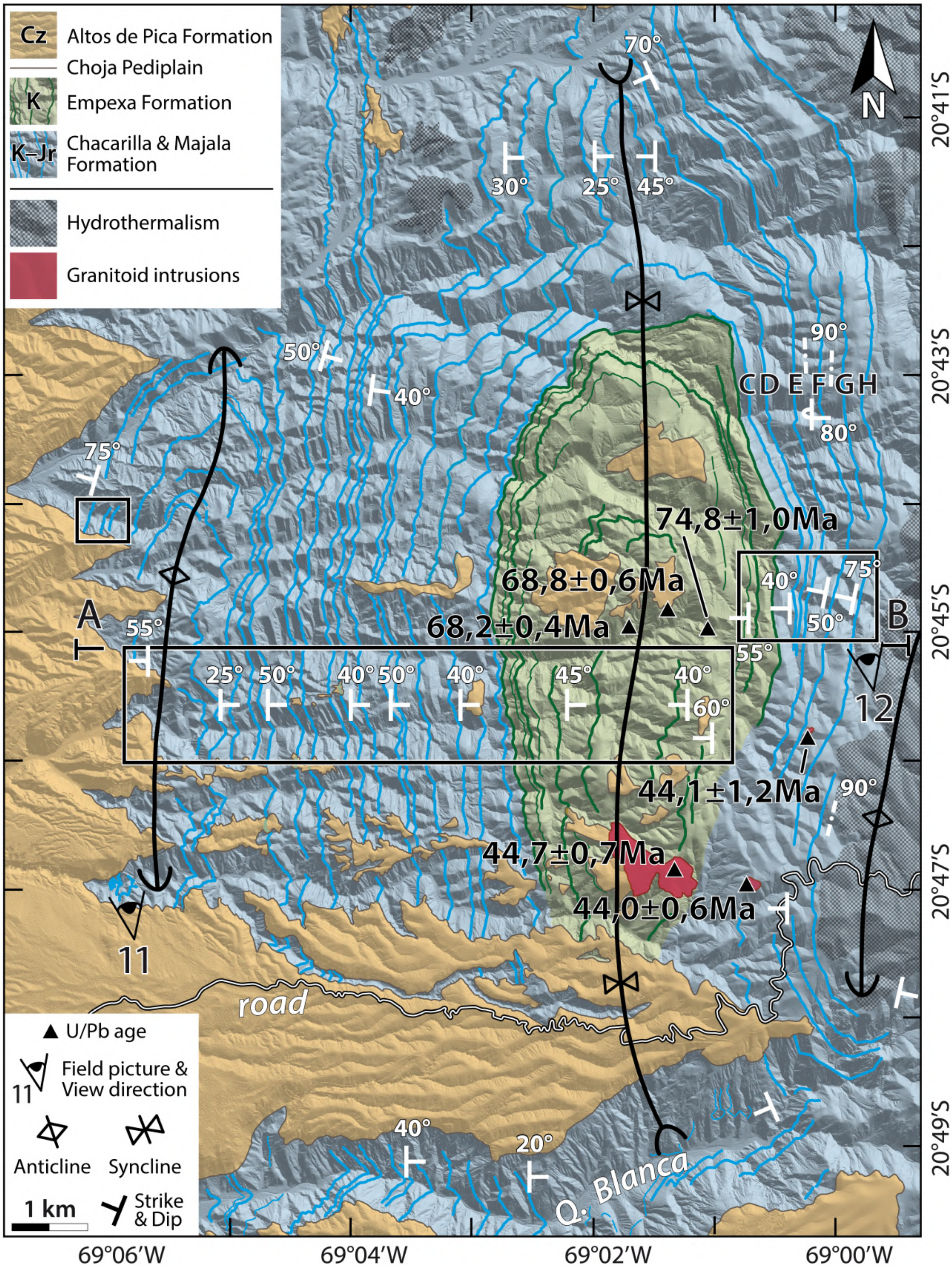

Cz Altos de Pica Formation
Choja Pediplain
K Empexa Formation
K–Jr Chacarilla & Majala Formation
Hydrothermalism
Granitoid intrusions
U/Pb age
11 Field picture & View direction
Anticline
Syncline
1 km
Strike & Dip
74,8±1,0Ma
68,8±0,6Ma
68,2±0,4Ma
44,1±1,2Ma
44,7±0,7Ma
44,0±0,6Ma
A
B
12
11
C D E F G H
road
Q. Blanca
N
20°41'S
20°43'S
20°45'S
20°47'S
20°49'S
69°06'W
69°04'W
69°02'W
69°00'W

Figure 9.

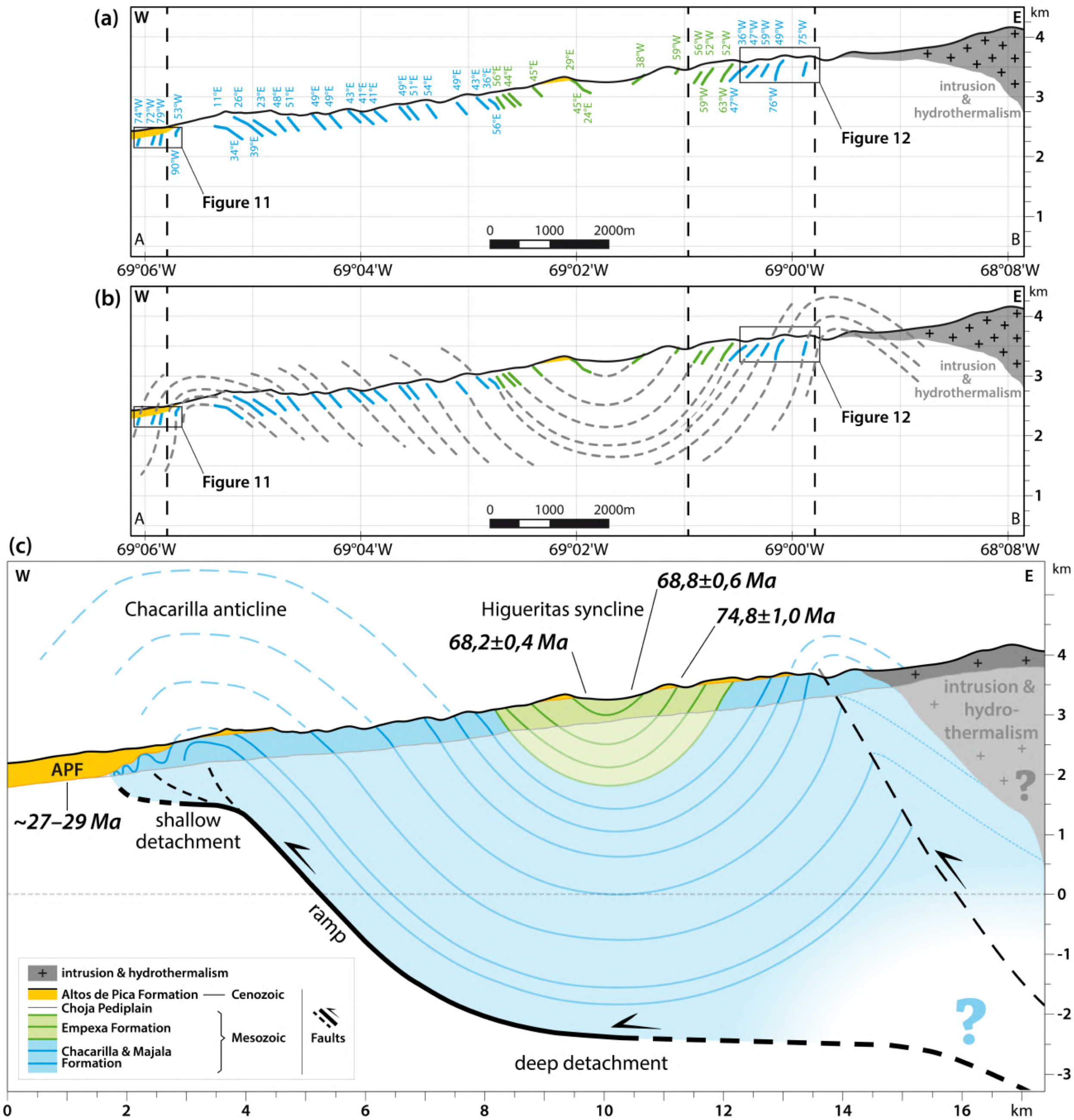
(a)
W
E
km
Figure 11
Figure 12
intrusion & hydrothermalism
0 1000 2000m
A
B
69°06'W
69°04'W
69°02'W
69°00'W
68°08'W
(b)
(c)
Chacarilla anticline
Higueritas syncline
68,8±0,6 Ma
74,8±1,0 Ma
68,2±0,4 Ma
APF
~27–29 Ma
shallow detachment
ramp
deep detachment
intrusion & hydro-thermalism
intrusion & hydrothermalism
Altos de Pica Formation
Choja Pediplain
Cenozoic
Empexa Formation
Mesozoic
Chacarilla & Majala Formation
Faults

Figure 10.

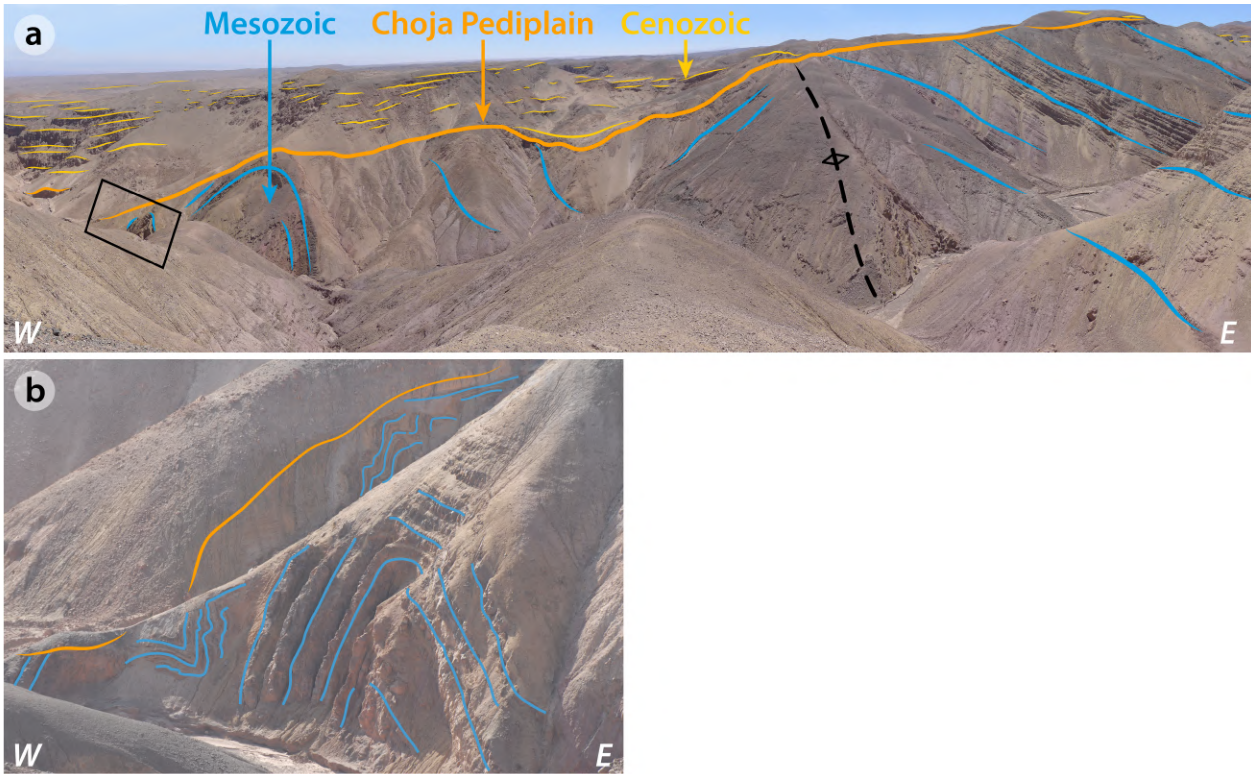

Figure 11.

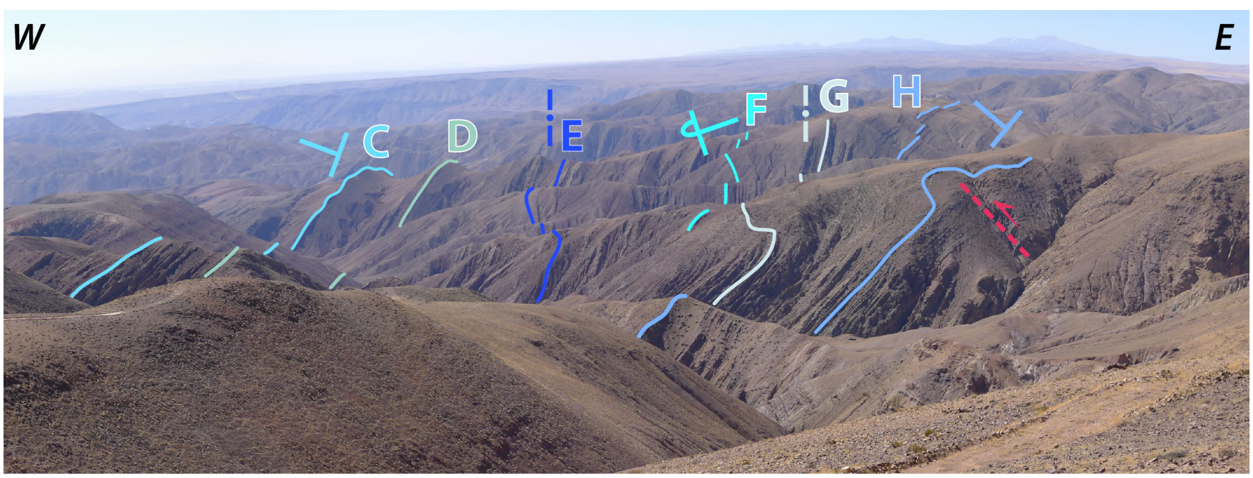

Figure 12.

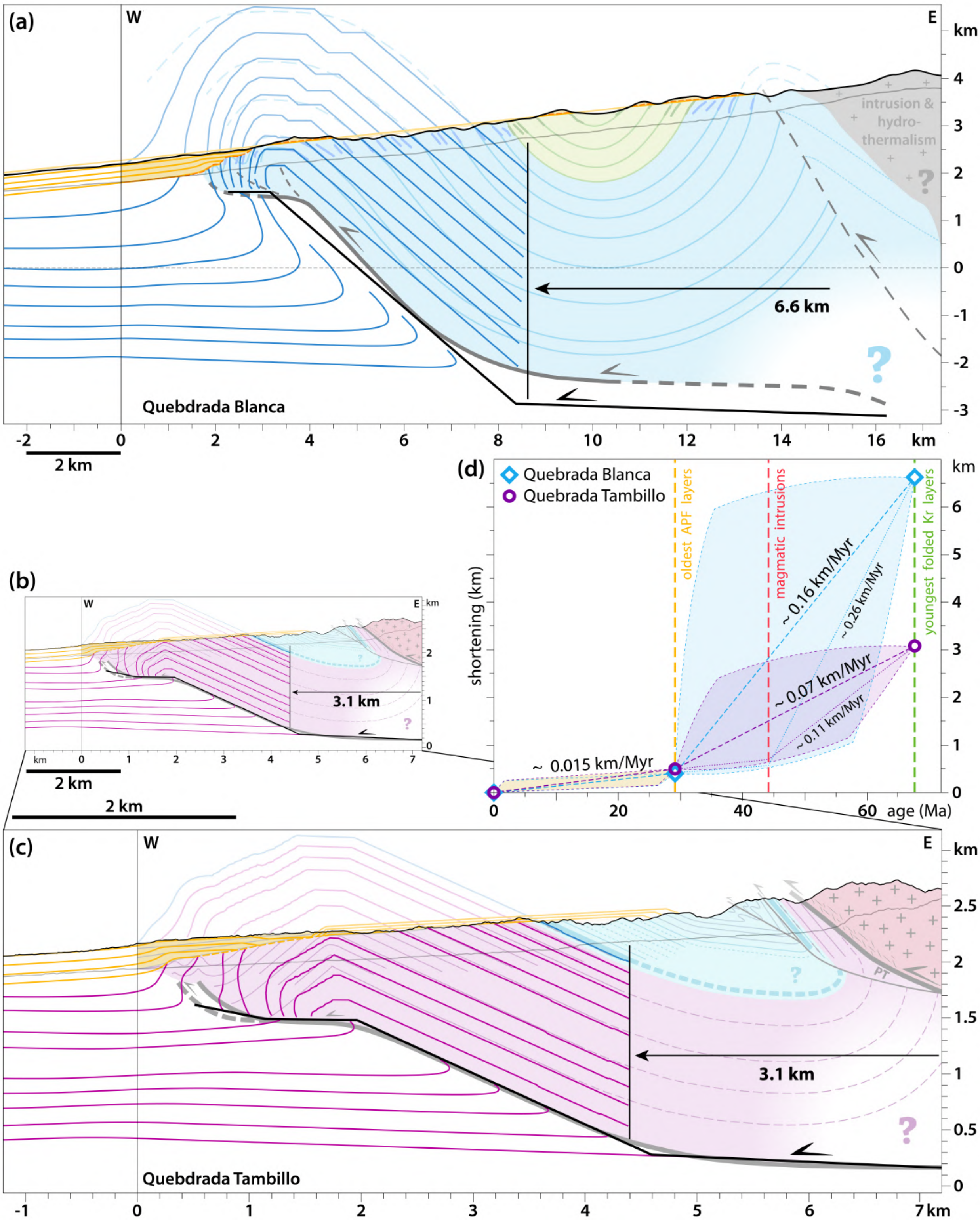
(a)
W
E
km
intrusion & hydro- thermalism
6.6 km
Quebdrada Blanca
2 km
(d)
Quebrada Blanca
Quebrada Tambillo
oldest APF layers
magmatic intrusions
youngest folded Kr layers
shortening (km)
~ 0.16 km/Myr
~ 0.26 km/Myr
~ 0.07 km/Myr
~ 0.11 km/Myr
~ 0.015 km/Myr
age (Ma)
(b)
3.1 km
2 km
2 km
(c)
3.1 km
PT
Quebdrada Tambillo

Figure 13.

AGU PUBLICATIONS

Tectonics

Supporting Information for

The western Andes at ~20–22°S: A contribution to the quantification of crustal shortening and kinematics of deformation.

Tania Habel (1), Martine Simoes (1), Robin Lacassin (1), Daniel Carrizo (2)(3), German Aguilar (2)

(1) Université de Paris, Institut de physique du globe de Paris, CNRS, F-75005 Paris, France
(2) Advanced Mining Technology Center, Facultad de Ciencias Físicas y Matemáticas, Universidad de Chile, Avenida Tupper 2007, Santiago, Chile
(3) now at GeoEkun SpA, Santiago 7500593, Chile

Contents of this file

Additional Supporting Information (Files uploaded separately)

Introduction

This supporting information document is subdivided into three sections:
(1) A sedimentary description of the units encountered at the Pinchal zone, and further illustrating section 4.1.1. Field photographs are provided (Figures S1–S12) and their position is pointed out on the corresponding structural map (Figure S13) and within the stratigraphic column (Figure S14).
(2) Non-interpreted and interpreted field photographs (Figures S15–S19), to be compared to their interpreted version in the main text (Figures 6, 7b-c, 8a-b, 11a-b, 12).
(3) Additional information on trishear modeling. Here, we present further details on the trishear modeling method and on our results (Text S1), complementary to section 3.4 and 6.2 in the main text. This text is accompanied by figures illustrating six key stages of our best-fitting trishear model for Quebrada Tambillo (Figure S20) and Quebrada Blanca (Figure S21); by a table showing the range of tested parameters during modeling (Table S1); as well as tables with the parameters for each of the six stages of our preferred model for Quebrada Tambillo (Table S2) and Quebrada Blanca (Table S3).
All the photographs (presented in the supporting information and in the main text) were taken by us during our field missions in March 2018 and January 2019 in the Western Cordillera of Northern Chile.

In addition to this document, we provide our georeferenced field-logistics dataset (field-logistics.kmz). Therewith one can visualize (e.g. on Google Earth) the off-road track we used to reach the extremely remote Pinchal area, the localisation of our Pinchal base-camp, and the GPS positions of field photographs for both study sites. In hyper-arid environments such as here, tracks may be preserved for several years, in between two rare rain episodes. We therefore recall that the off-road track and base-camp indicated here were those of March 2018 and January 2019, and cannot guarantee their state and usability after that period.

(1) Sedimentary description (Pinchal area)

Figure S1. Migmatitic gneisses, a common metamorphic facies found in the Paleozoic basement rocks to the east of the Pinchal area. Hiking stick given for scale. Location #S1 on Figures S13 and S14.

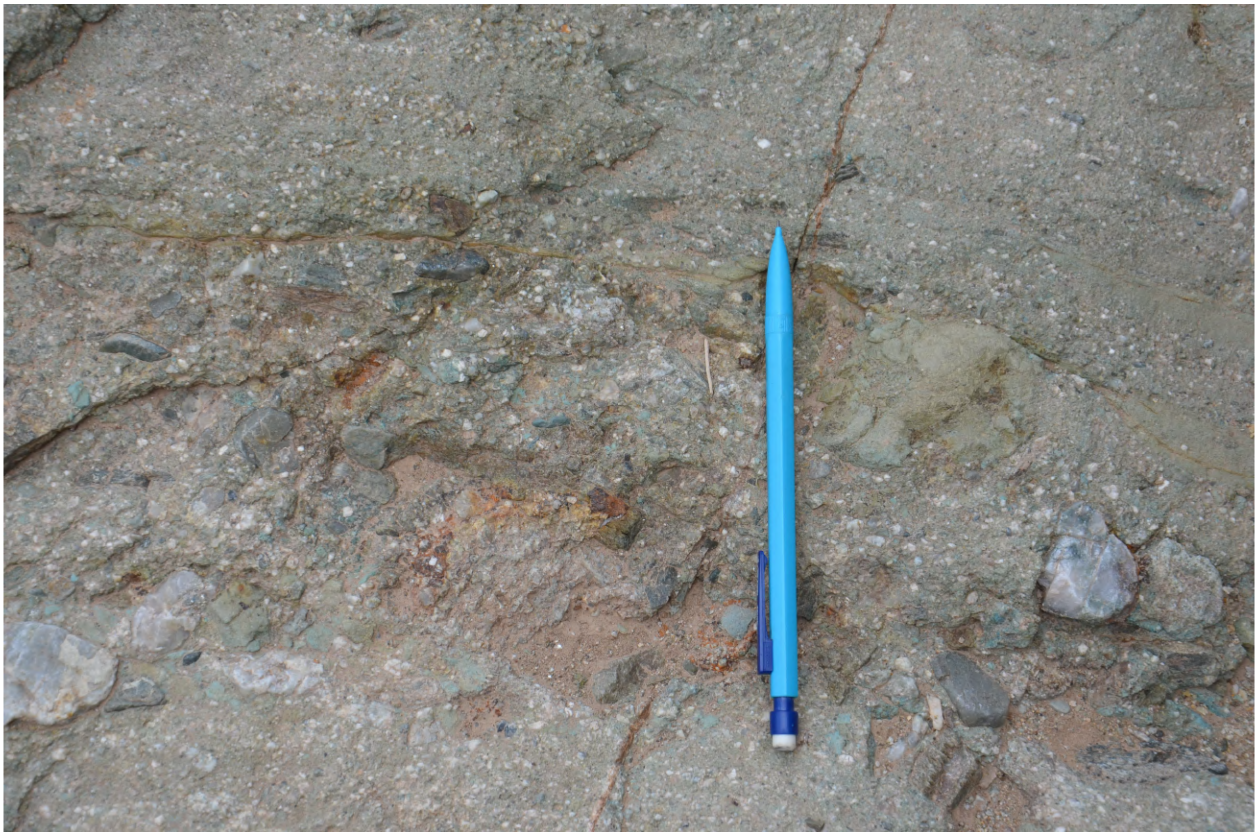

Figure S2. Volcano-detrital conglomerates, here of greenish color, belonging to the continental Mesozoic series, with millimetric to centimetric clasts. Location #S2 on Figures 5a, S13 and S14.

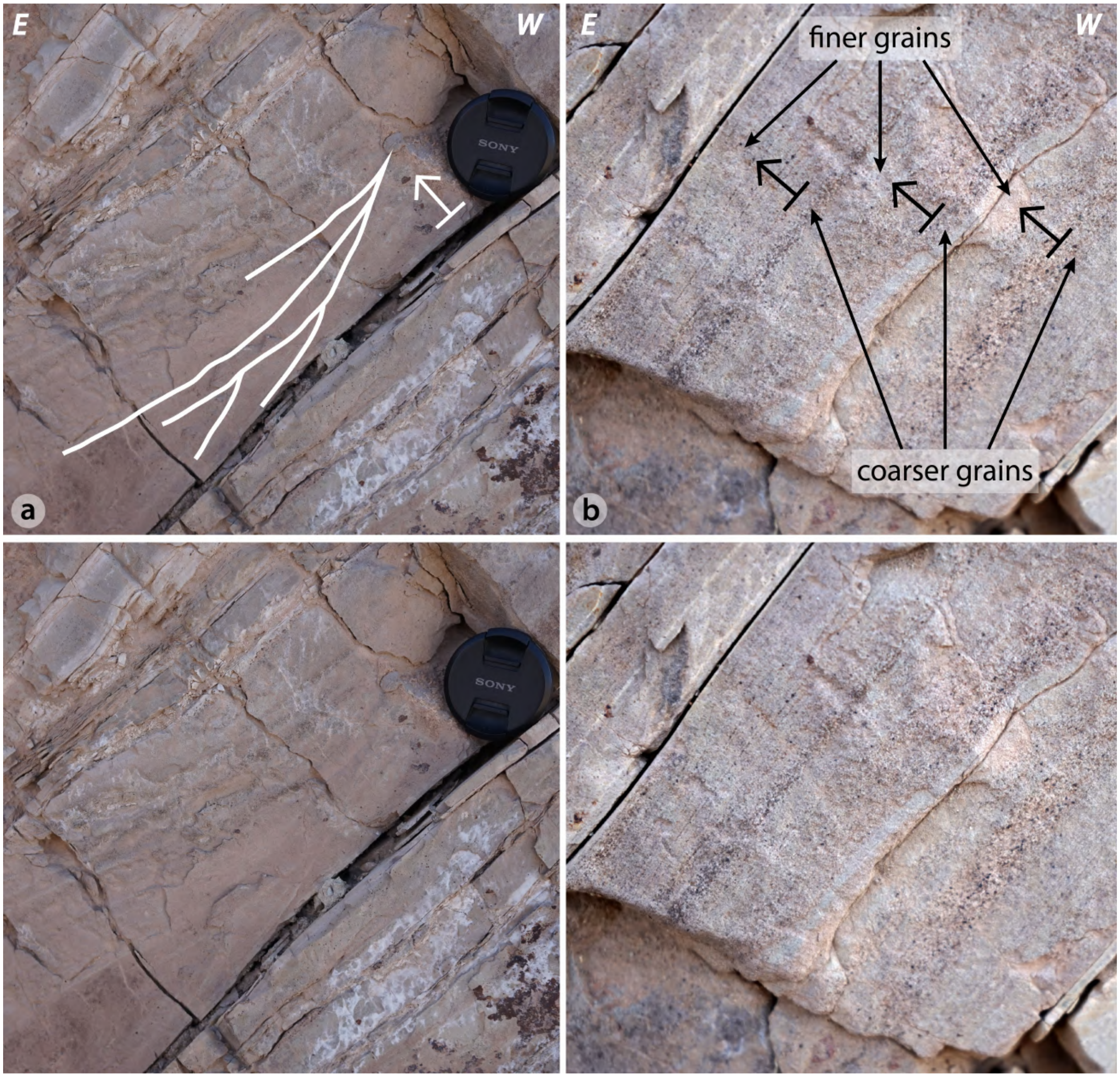

Figure S3. Detrital layers within the Mesozoic units, characterized by **(a)** tangential beds, indicative of normal polarity with top-to-the-east; **(b)** grain-size grading (finer at the top, coarser at the base of the layer) indicating top-to-the-east bedding polarity. Note also the erosive base contrasting with the sharp top of the layer. Top: interpreted field pictures; bottom: non-interpreted pictures. Location #S3 on Figures S13 and S14.

Figure S4. Dark green detrital pelites (lutites). This unit resembles sediments given a Triassic age (Aguilef et al., 2019) immediately north of the Pinchal area. Note the strong deformation as these lutites are located next to the Pinchal Thrust. Location #S4 on Figures 5a, S13 and S14.

Figure S5. Silex nodules at the base of the calcareous crest (blue pencil for scale). Location #S5 on Figures 5a, S13 and S14.

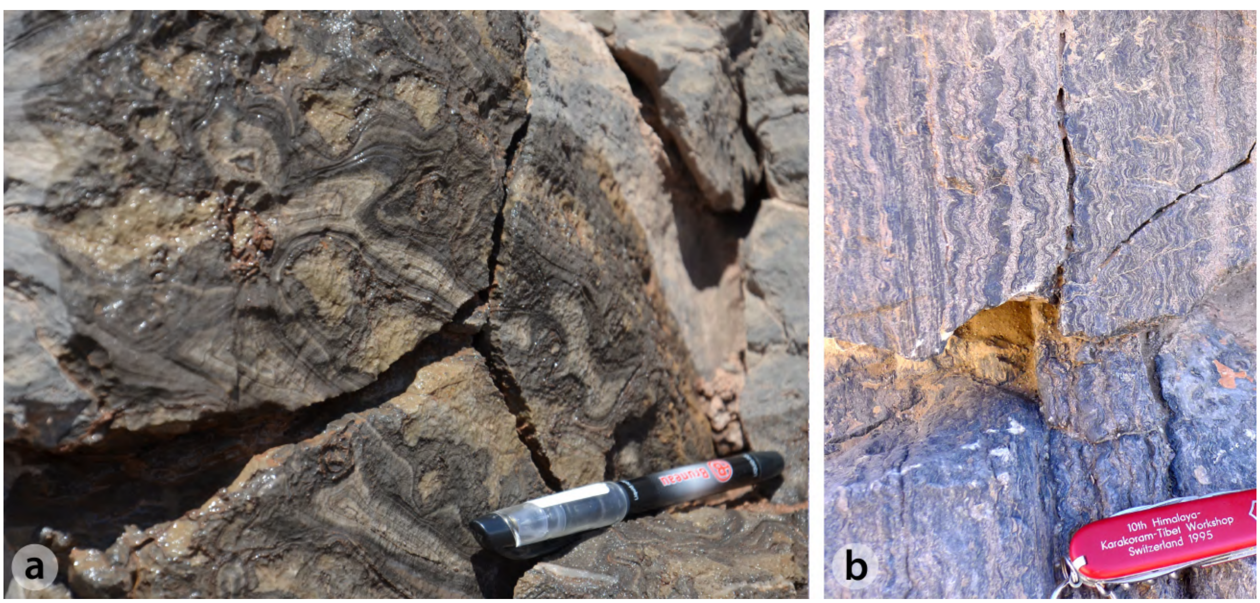

Figure S6. Stromatolite fossils from the Mesozoic (marine) series, located within **(a)** the western normal synclinal fold limb; and **(b)** the eastern inverted synclinal fold limb. Location #S6a and S6b, respectively, on Figures S13 and S14.

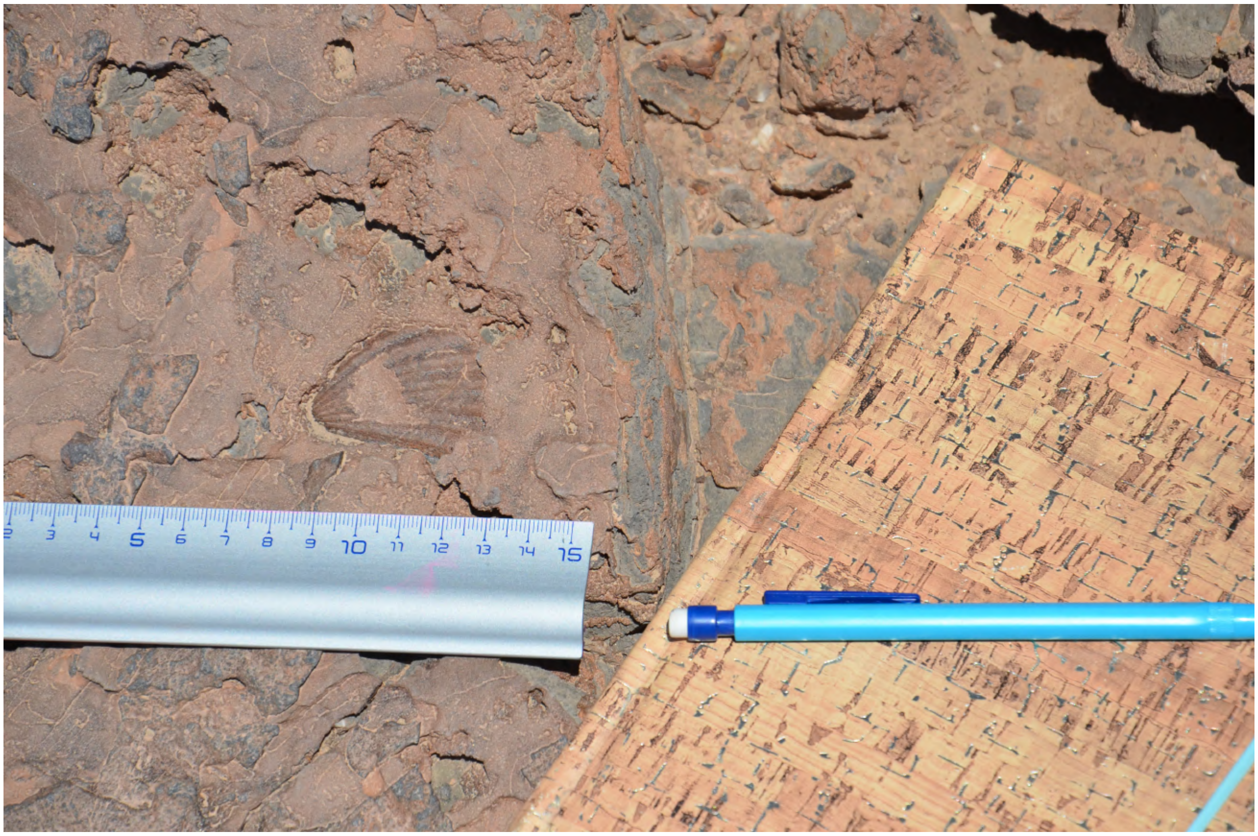

Figure S7. Bivalve fossils from the Mesozoic (marine) series, located within the western normal synclinal fold limb. Location #S7 on Figures S13 and S14.

Figure S8. Fine limestone layers within the Mesozoic (marine) series, characterized by a rose-beige color and an alternance of thin-bedded (cm–dm), regular beds. Location #S8 on Figures 5a, S13 and S14.

Figure S9. Nodule bearing marls from the Mesozoic (marine) series. The nodules vary in size from centimeters to few meters, as in the case of the large ones illustrated in this field photo. Location #S9 on Figures 5a, S13 and S14.

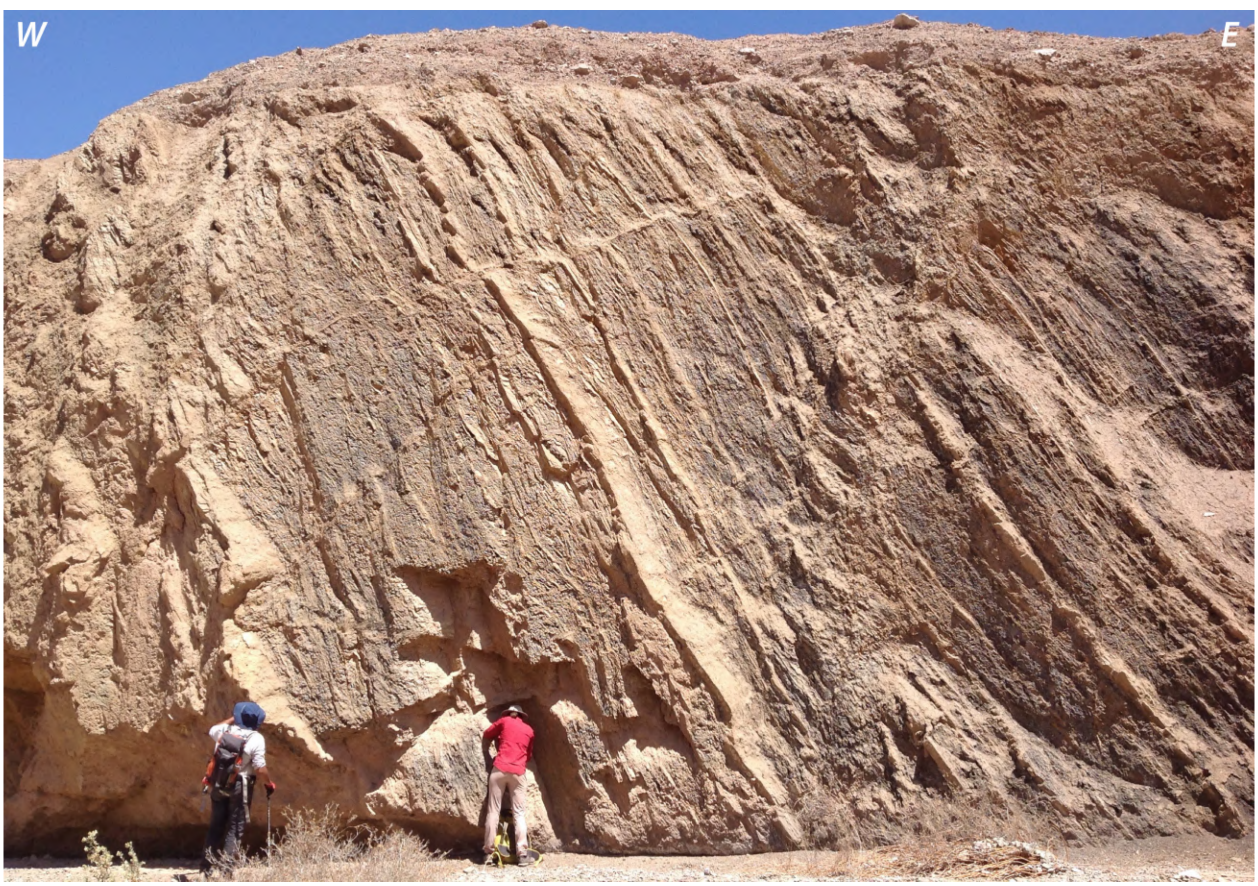

Figure S10. Thin-layered limestone series within marls. Location #S10 on Figures 5b, S13 and S14.

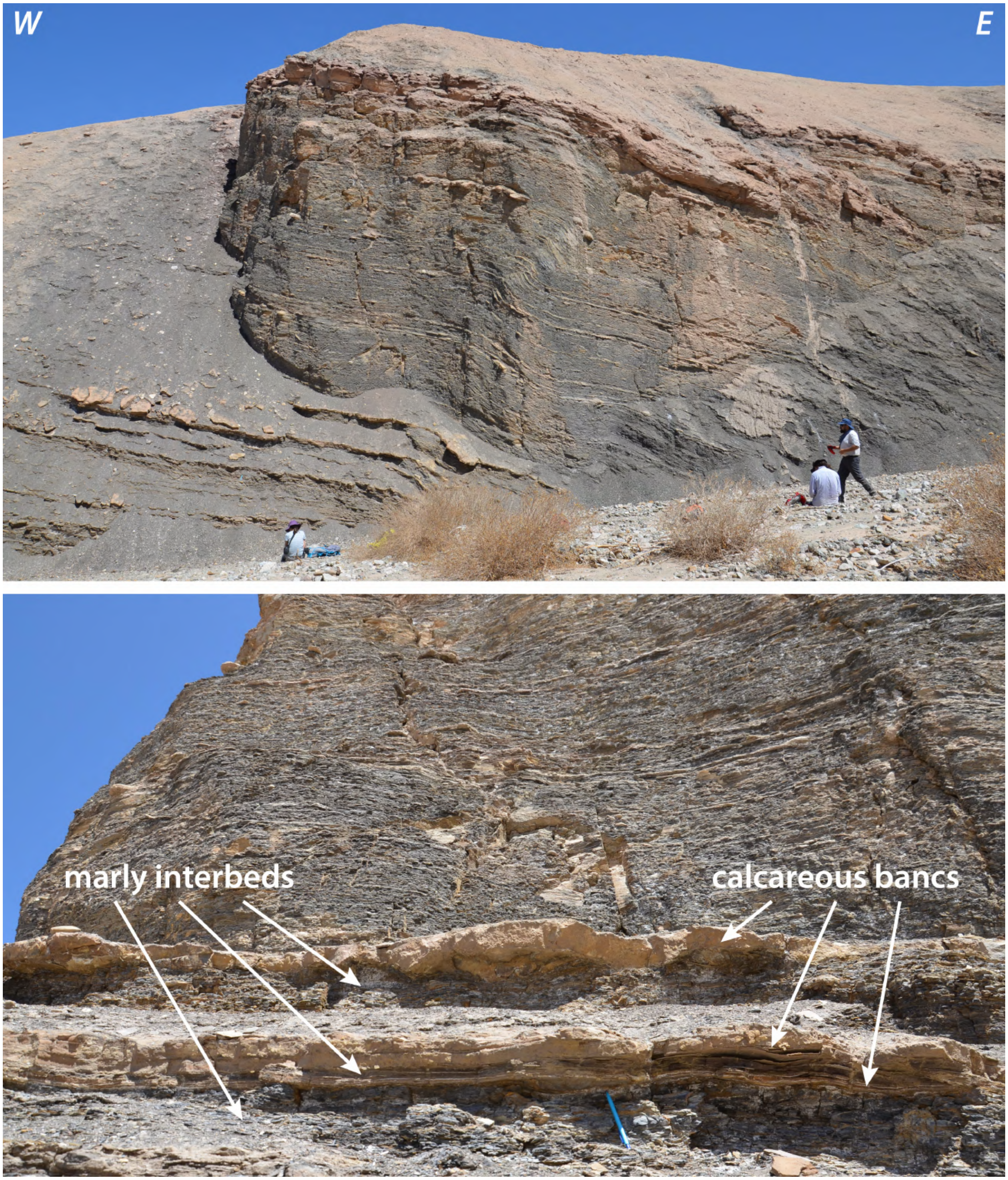

Figure S11. Flysch formation characterized by beige, resistant calcareous beds of millimetric to decimetric thickness, within dark-grey, more friable, marls. Top: landscape view; bottom: detailed outcrop view (blue pencil for scale). Location #S11 on Figures 5b, S13 and S14.

Figure S12. Red arenites at the base of the Cenozoic series bearing detrital and volcanic clasts of millimetric to pluri-centimetric size. Location #S12 on Figures S13 and S14.

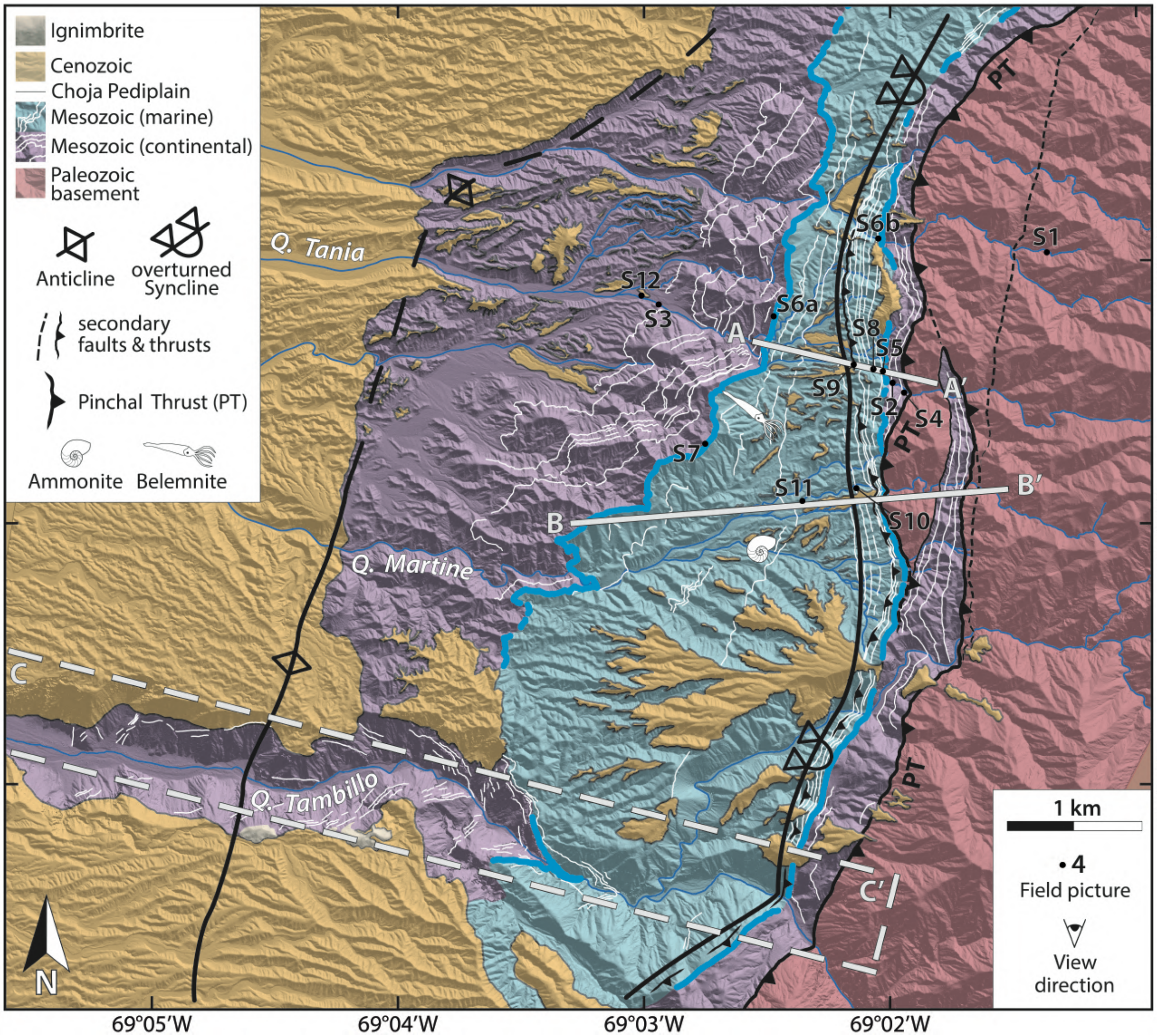

Figure S13. Structural map of the Pinchal area (~21°30′S), as Figure 4 in main text, but here with locations of supplementary field references (S1–S12). Black dots refer to the location of field photographs, and are numbered according to the figures where these pictures are reported. Location of this map is the same as that of Figure 4, reported on Figure 1. White thin lines highlight Mesozoic layers mappable on satellite images. Thick blue line depicts the calcareous crest, which is used as a marker bed (Figure 2). A–A′ and B–B′ sections locate the topographic profiles used for the cross-sections of Quebrada Tania and Quebrada Martine, respectively (Figures 5a-b). In the case of the Quebrada Tambillo cross-section, a topographic swath profile was used along C–C′. The fold axes are relatively well defined for the synclinal fold, but less well constrained for the anticlinal fold because only observable along Quebrada Tambillo. PT: Pinchal Thrust; Q: Quebrada.

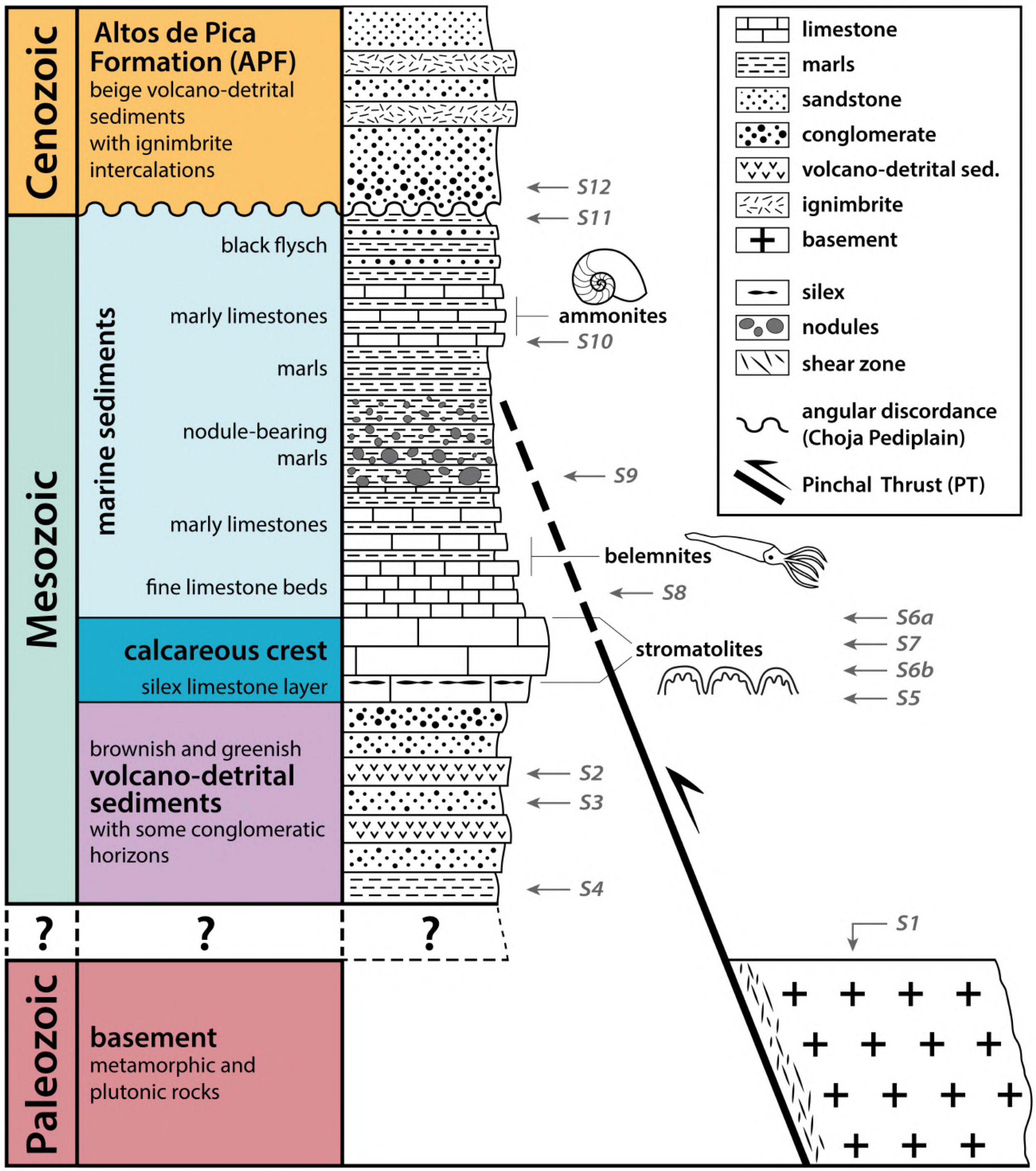

Figure 14. First-order stratigraphic column of the Pinchal area derived from field observations obtained mainly along Quebrada Tania (Figures 4 and S13) where the Mesozoic series seems to be most complete. Thicknesses of the stratigraphic units are not at scale on the figure, but are given in the main text (section 4.1.1). This column is also reported on Figure 3 (main text), but here with the addition of the stratigraphic locations of field observations illustrated on Figures S1 to S12. In the Pinchal area, Paleozoic basement overthrusts folded Mesozoic series along the Pinchal Thrust (PT), so that part of the deeper and older Mesozoic series may be missing here (as depicted by "?"). Abbreviation "sed." for sediments. See Figures S1–S12 and corresponding captions (in supplementary material) for detailed sedimentologic descriptions.

(2) Non-interpreted field photographs

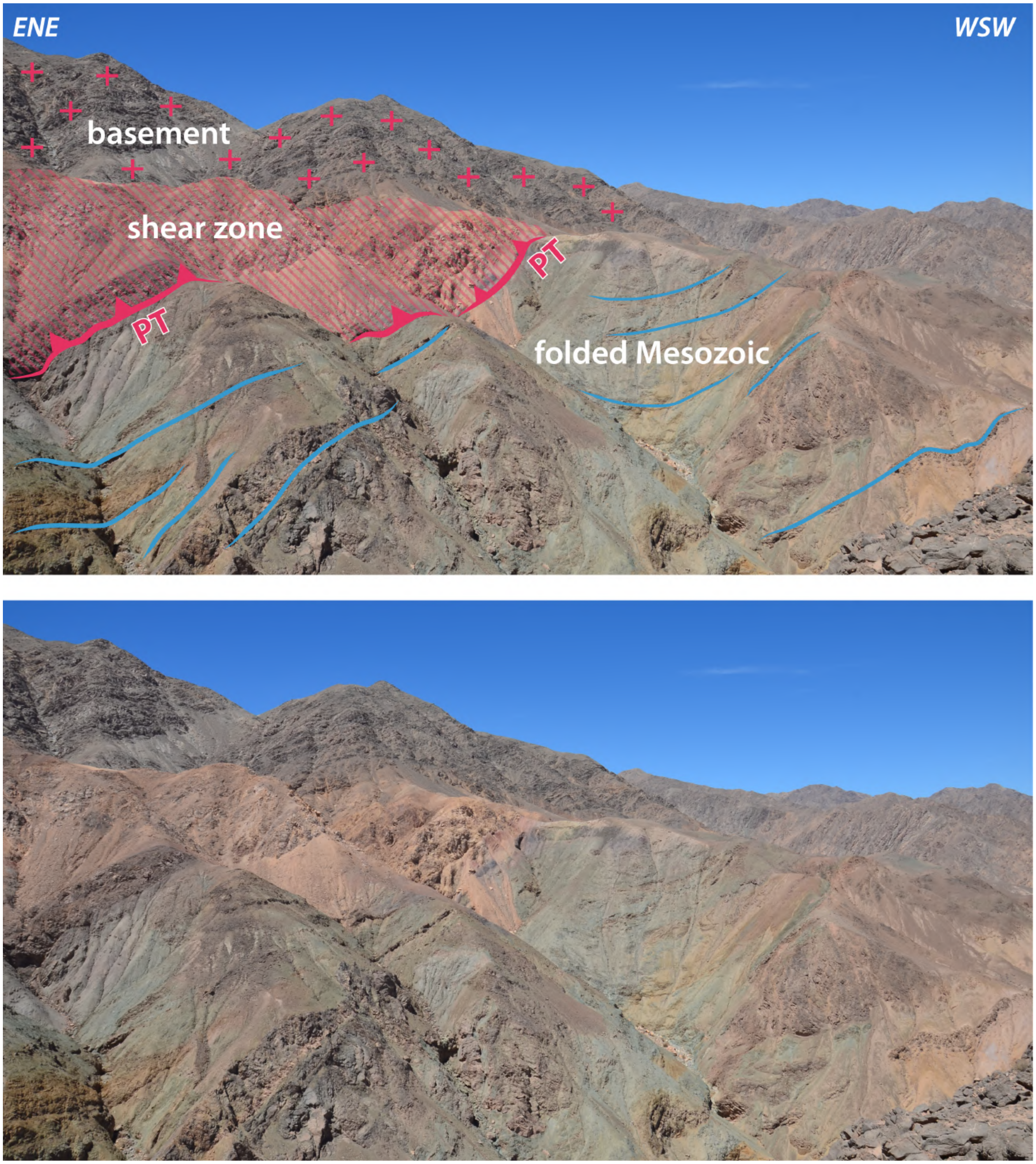

Figure 15. Field view of the Pinchal Thrust (PT), overthrusting the dark-grayish Paleozoic basement over the greenish folded Mesozoic units. Reddish rocks on the hanging wall to the East-Northeast correspond to the thrust shear zone (hatched area in picture). Same as Figure 6 (Top), but with non-interpreted field picture (bottom). Location #6 on Figure 4.

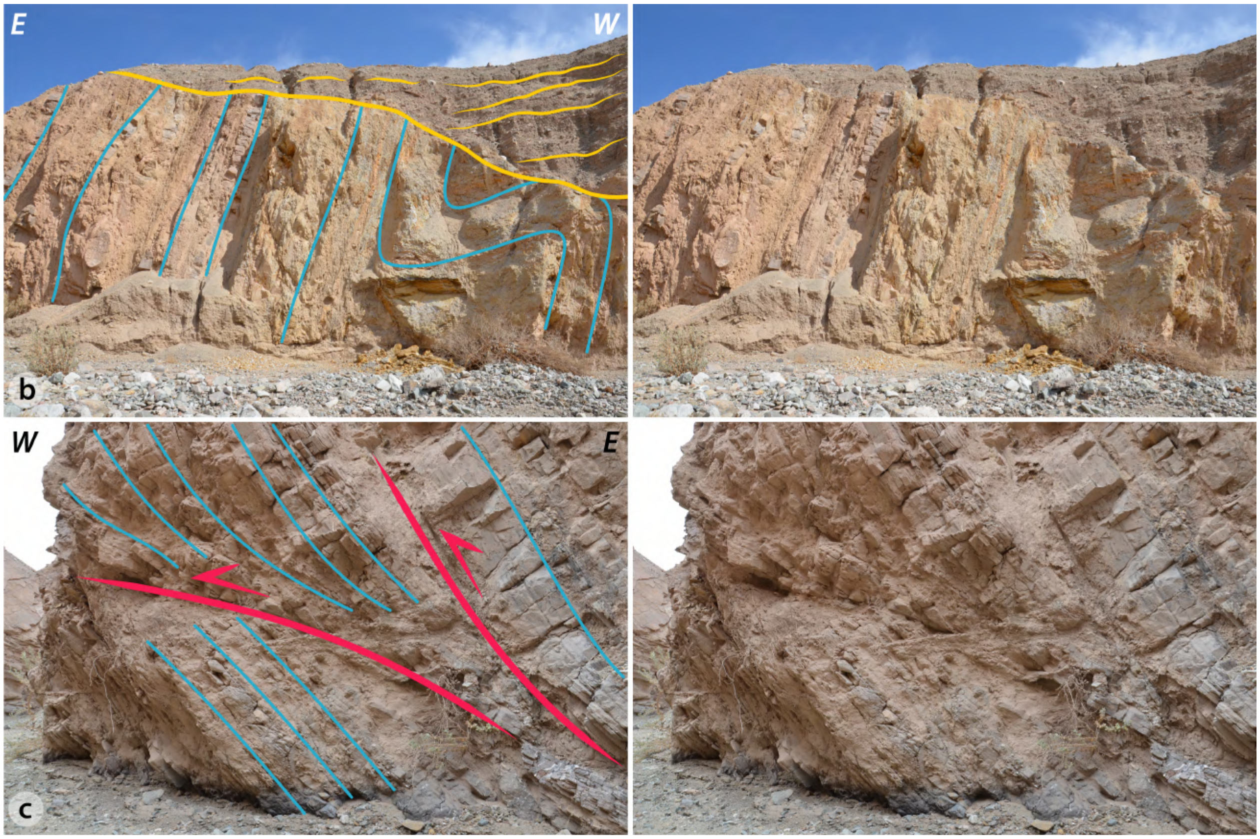

Figure S16. Field pictures of small-scale structural features characteristic of the deformation within the Pinchal zone, as in Figures 7b-c in main text. Locations #7b and 7c in Figure 4, respectively. Left: interpreted picture as in main text; right: non-interpreted picture.

(b) Example of a small-scale fold within the marine Mesozoic units (blue lines) in Quebrada Tania, within the inverted limb of the mapped syncline, nearby the fold axis. Note also the erosional surface (yellow) forming the unconformable contact between the Cenozoic deposits over the deformed Mesozoic.

(c) Small-scale thrusts (steep red line to the right) and décollements (flat red line to the left) observed within the marine Mesozoic strata (blue) of the inverted synclinal limb along Quebrada Tania.

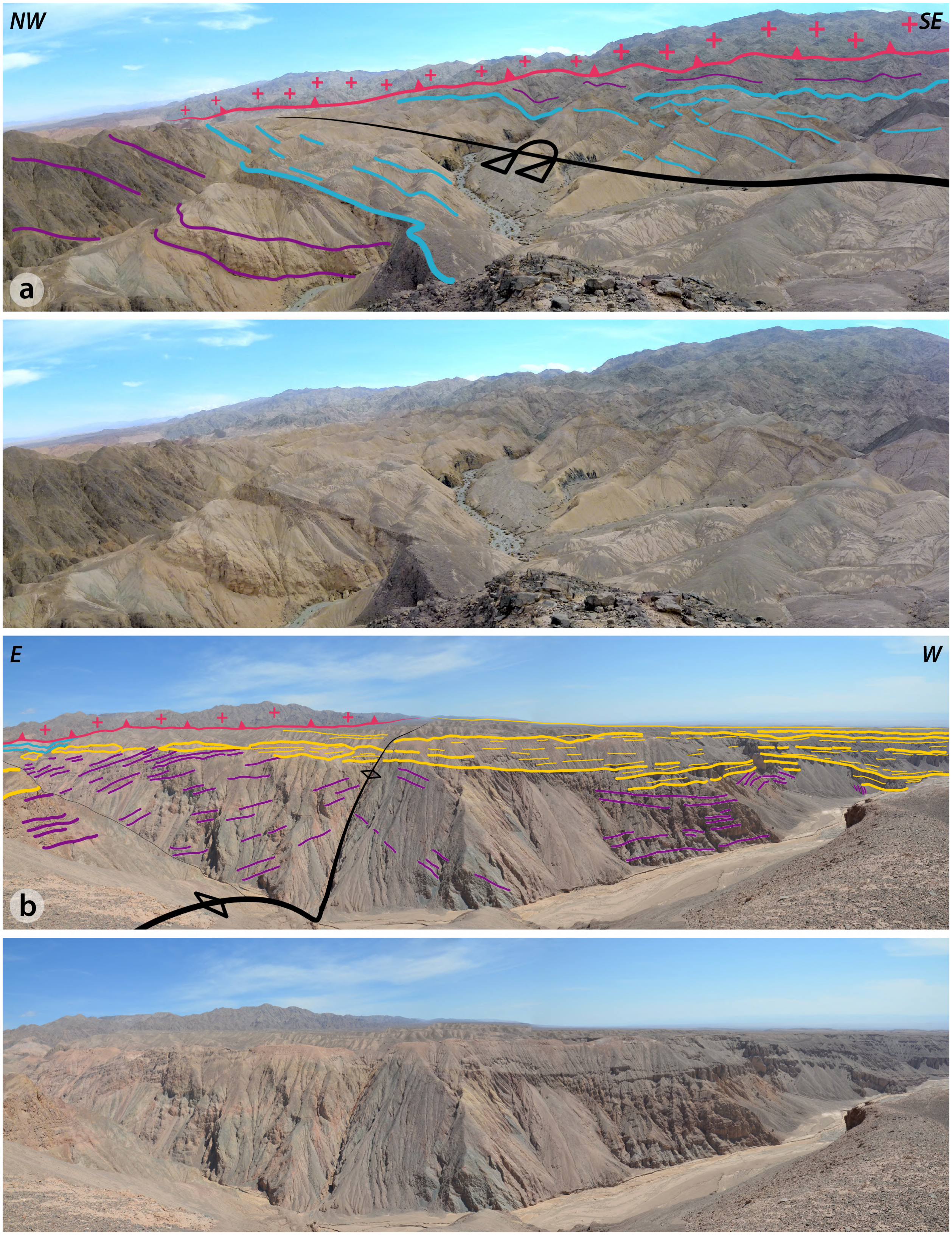

Figure S17. Field pictures of the two major folds within the Pinchal zone, as in Figure 8 in main text. Location #8a and 8b in Figure 4. **(a)** Panoramic view over the north-eastern part of the Pinchal area. **(b)** Panoramic view along Quebrada Tambillo, in the southern part of the Pinchal area. Top: interpreted picture; bottom: non-interpreted picture, for (a) and (b) respectively. For complete figure descriptions see main text.

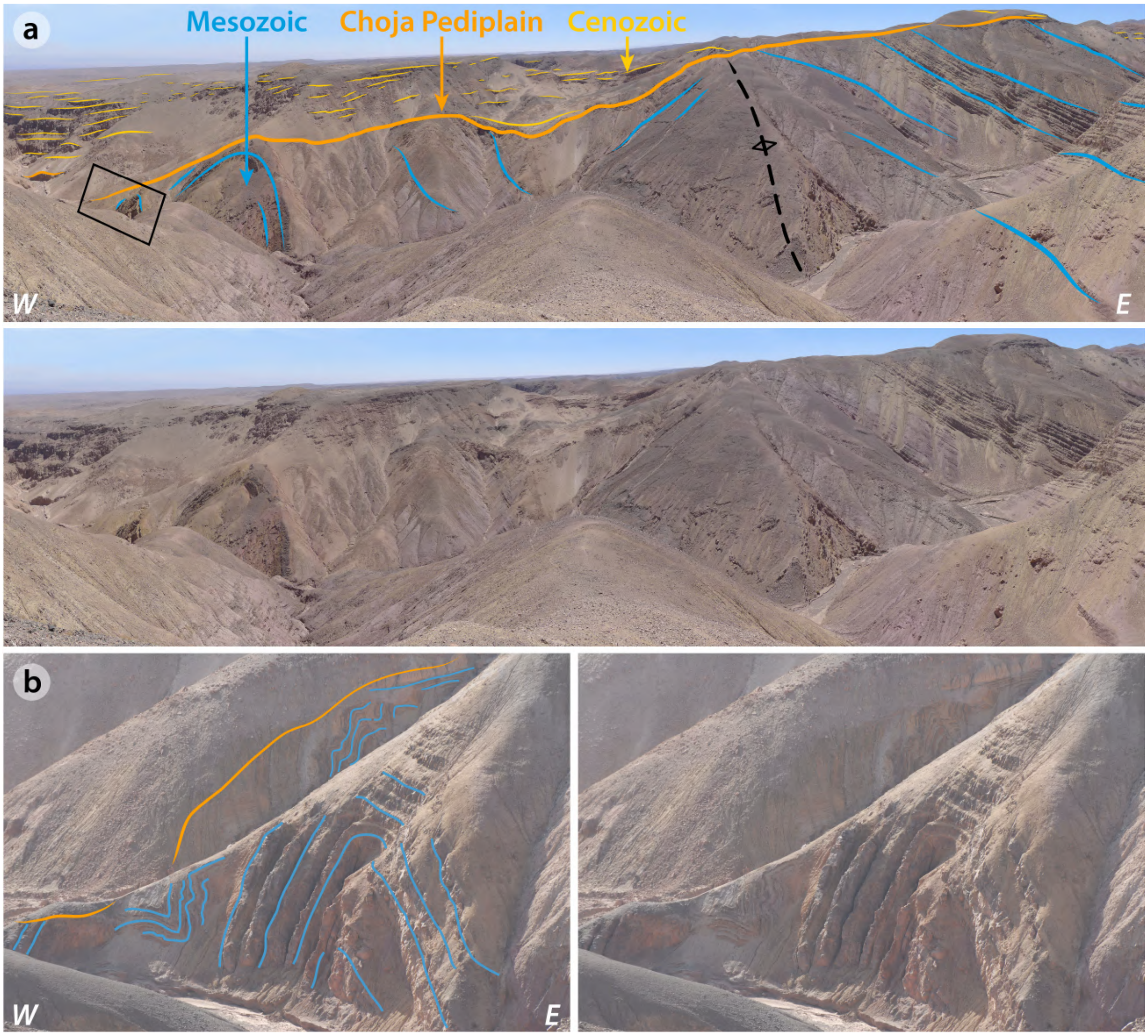

Figure S18. Field picture of the western limb of the western anticline in the Quebrada Blanca area. Same as Figure 11 in main text. Location #11 in Figure 9.

(a) Series of folds with westward decreasing amplitude and wavelength (hundreds to tens of meters) observed at the front of the western anticline. Top: interpreted picture; bottom: non-interpreted picture.

(b) Detailed view of the westernmost outcropping small-scale anticlines, located on (a) by the black box. Left: interpreted picture; right: non-interpreted picture.

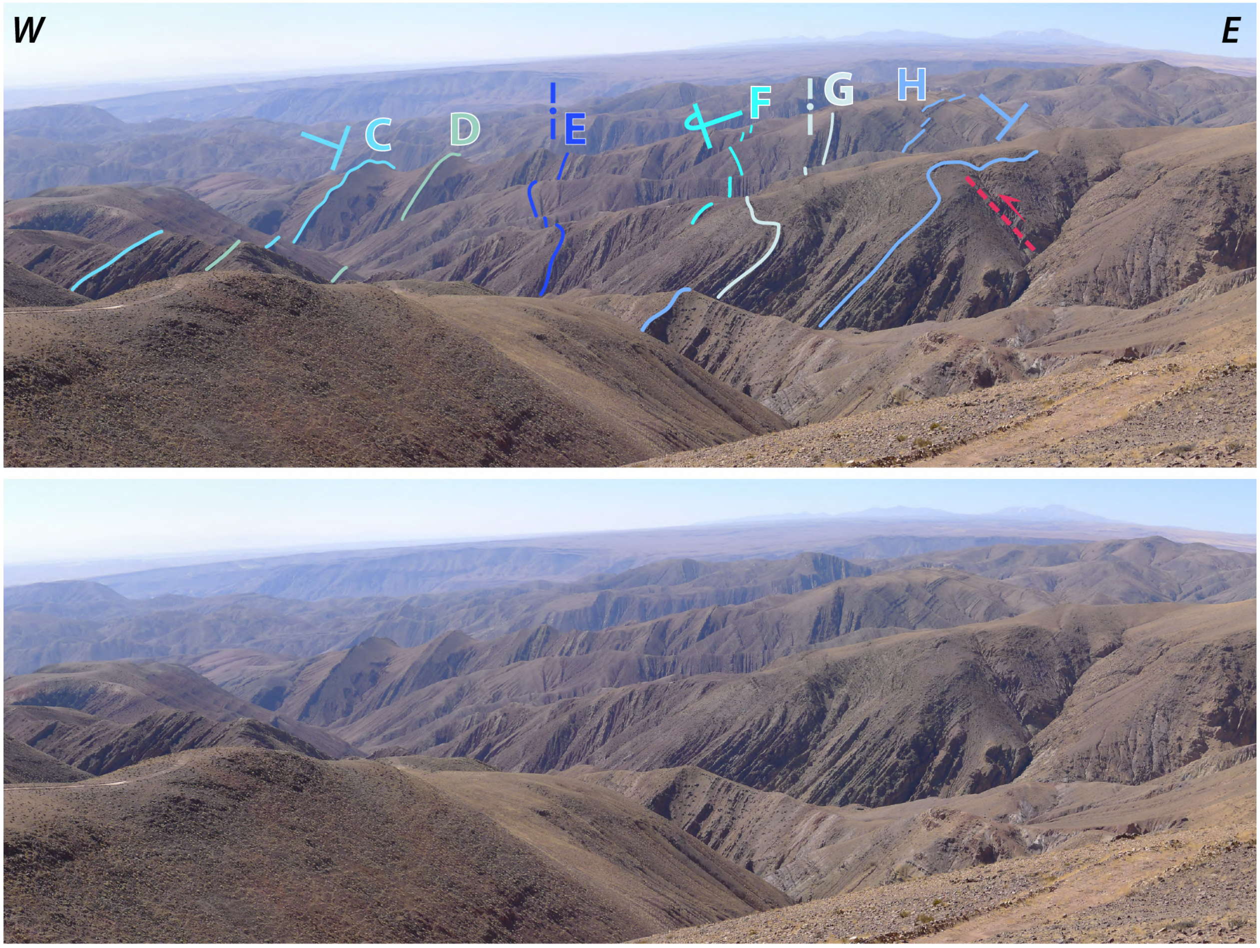

Figure S19. Landscape view on the western limb of the eastern large-scale anticline in the Quebrada Blanca area. Same as Figure 12 in main text; location #12 in Figure 9. Here, steeply inclined Mesozoic horizons are very well discernible in the landscape. Bedding traces C, D, E, F, G and H underlined here are also georeferenced on the structural map (Figure 9) by mapping on satellite imagery. Note the thrust-affected small-scale fold (red dashed line) emphasizing the west-vergence of tectonic structures. Top: interpreted picture; bottom: non-interpreted picture.

(3) Trishear modeling

Text S1. Additional information on trishear modeling (method and results)

As briefly resumed in sections 3.4 and 6.2, we used the trishear folding approach (e.g. Allmendinger, 1998; Erslev, 1991) to better constrain the amount of shortening across our study areas. We further detail the trishear method and results here.

Method

We assume fault-propagation folding to be the dominant mode of deformation in the studied fold-and-thrust-belt, and in particular in the case of the western anticlines of the cross-sections along Quebrada Tambillo (Pinchal area) and Quebrada Blanca.

We use the code FaultFold Forward version 6 (freely available from http://www.geo.cornell.edu/geology/faculty/RWA/programs/faultfoldforward.html (Allmendinger, 1998) that models the distributed deformation in triangular zones at the tip of propagating faults. The formalism relies on the following parameters: the coordinates of the fault tip, the angle of the propagating fault ramp, the slip on the fault, the propagation-to-slip-ratio (P/S) of the fault, the trishear angle (i.e. the angle of the triangular zone at the tip of the fault where distributed deformation occurs), and the inclined shear angle (either parallel or similar folding) controlling the backlimb kinematics. We assume here the case of linear symmetric trishear to keep models as simple as possible, meaning that folding of the backlimb occurs parallel to the fault. We tested non-linear trishear but these trials lead to unsatisfying results when compared to our cross-sections.

For the initial conditions of the models, we assume slightly sub-horizontal layers, with a slight eastward tilt (3°E at Quebrada Tambillo, 2°E at Quebrada Blanca) as expected in the initial Andean basin. The final geometry of the fold and sedimentary cover, the fault ramp angles and bends are constrained to fit our geological cross-sections.

By adding sedimentary layers step by step during progressing deformation, we model syntectonic deposition of the Cenozoic series and reproduce the angular unconformity of the Cenozoic over Mesozoic units. The syntectonic deposits are also assumed to be initially slightly sub-horizontal, here with a slight westward tilt (3°W at Quebrada Tambillo, 6°W at Quebrada Blanca), following the approximate angle of the present-day average topography in the corresponding study areas. In fact, the basal Choja Pediplain may be comparable to the first order to the present-day average rising topography; subsequent deposition along the western mountain flank had most certainly a slight westward tilt as observed today within the eastern Atacama Bench (Figure 1). We tested the addition of horizontal syn-tectonic Cenozoic layers, but the outcoming modeled fold-forms were much less consistent with our field and map observations. We tested different dipping angles (between 1–7°W) and chose the values that allowed us to best fit our data.

The trishear modeling confirms the necessity of a fault ramp propagating from a deep décollement towards the surface to fit the observed folds, as classically observed in fold-and-thrust-belts. We simplify the fault geometry into a few fault segments: 4 segments for Quebrada Tambillo, and 3 segments for Quebrada Blanca (Figures 13, S20 and S21). Segment 1 corresponds to the flat deep detachment which is parallel to the initial Mesozoic bedding. The second fault segment ramps-up from this regional décollement with an eastward dipping angle of 24°E for Quebrada Tambillo, 40.6°E for Quebrada Blanca. These geometries are needed to fit the dip angles observed in the hanging wall of the faults (i.e. within the backlimb of the modeled folds). A shallow flat detachment is needed at both study sites to reproduce the large-scale tilt of the Cenozoic cover and the geometry of fold forelimbs. For Quebrada Tambillo, an 11.3° eastward-dipping fourth segment is necessary to best fit the surface observations in the western part of the cross-section.

Neither the trishear angle, nor the P/S ratio are deductible from geological observations (Allmendinger & Shaw, 2000), while their effect on folding is crucial as pointed out by various studies (e.g. Hardy & Ford, 1997; Allmendinger, 1998; Zehnder & Allmendinger, 2000). With the aim to satisfactorily reproduce the geometry of the folded Mesozoic units and the tilt of the Cenozoic strata cover (Figures 5 and 10), we tested numerous combinations of parameters, in the range of values considered as reasonable in the cited studies, and regarding our geological constraints. By trial and error, we thus establish a set of best-fitting parameters for Quebrada Tambillo and Quebrada Blanca respectively, indicated in Tables S1 to S3. We recognize here that these may not be unique but only represent possible geologically viable solutions.

Results

The final stages (i.e. present-day deformation pattern) of our best fitting models are represented in Figure 13 (main text), together with the corresponding structural cross-section. The cumulative shortening, as constrained by the trishear modeling, in agreement with our geological cross-sections, is of 3.1 km for Quebrada Tambillo, and of 6.6 km for Quebrada Blanca (Figure 13). We recall here that these values account for folding and fault slip, but only for the westernmost anticlines and the two study sites.

Figures S20 and S21 illustrate the various stages of folding and fault propagation of our models, and complement the findings and discussion of section 6.3 in the main text. Some chronological constraints can be added to these various stages using geological observations, from the initial conditions prior to folding (~68 Ma), the first Cenozoic syn-tectonic deposits (~29 Ma) and to the present-day situation (0 Ma). Considering this, we find that most folding occurred prior to the first Cenozoic deposits of the Altos de Pica Formation at ~29 Ma (stage 3 on Figures S20-S21): before ~29 Ma, 2.6 km (out of the total 3.1 km) and 6.2 km (out of the total 6.6 km) of shortening had been completed for Quebrada Tambillo and for Quebrada Blanca, respectively. After ~29 Ma, the amount of additional shortening is only of 0.5 km and 0.4 km for Quebrada Tambillo and Quebrada Blanca, respectively, and corresponds to less than 20% (16% and 6%, respectively) of the total shortening, even though the duration of both time spans (~68–29 Ma and ~29–0 Ma periods) is of the same order. These findings are further represented on the graph of Figure 13d in the main text).

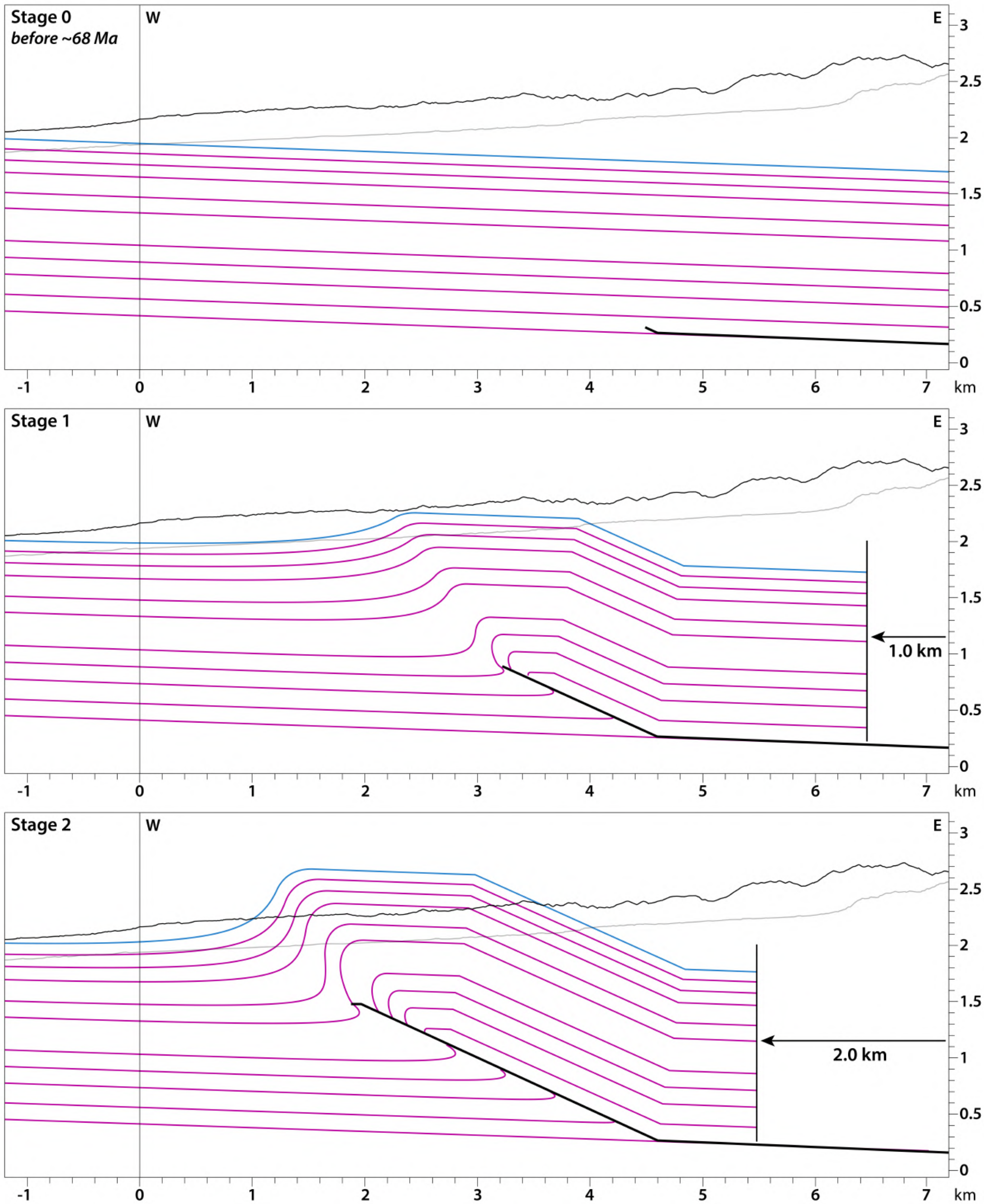

Figure S20. See second part of the figure and description next page.

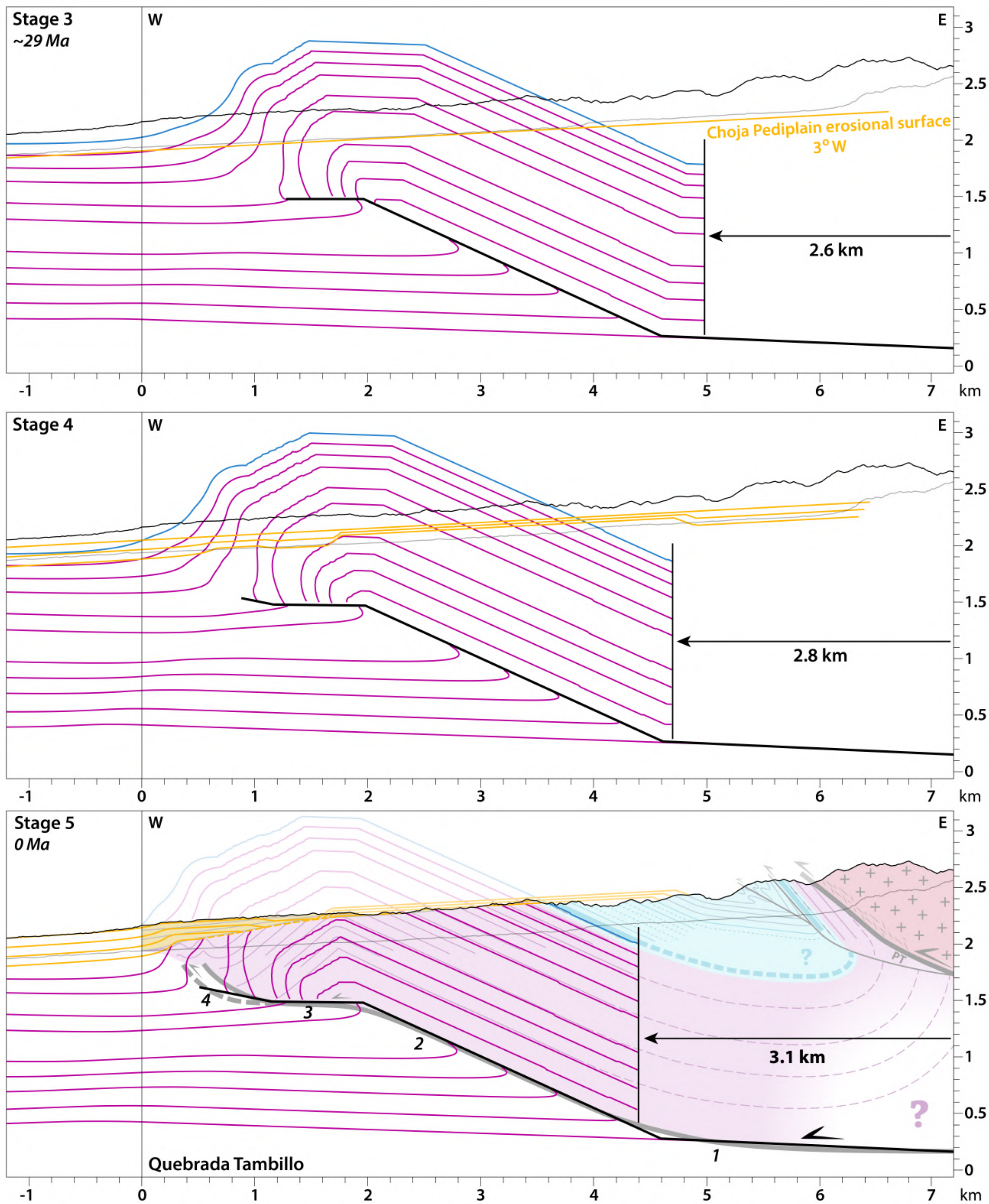

Figure S20. Outcomes from trishear modeling performed with FaultFold Forward v.6 (Allmendinger, 1998) in the case of the Quebrada Tambillo section, with chronological constraints provided from geological observations and data (see section 6.1 in main text). The black horizontal arrows underline the cumulated shortening at each stage. The final stage (present-day situation) is overlapped with our structural cross-section. Model parameters are provided in Table S2. In final stage, fault segments are numbered as in Table S1.

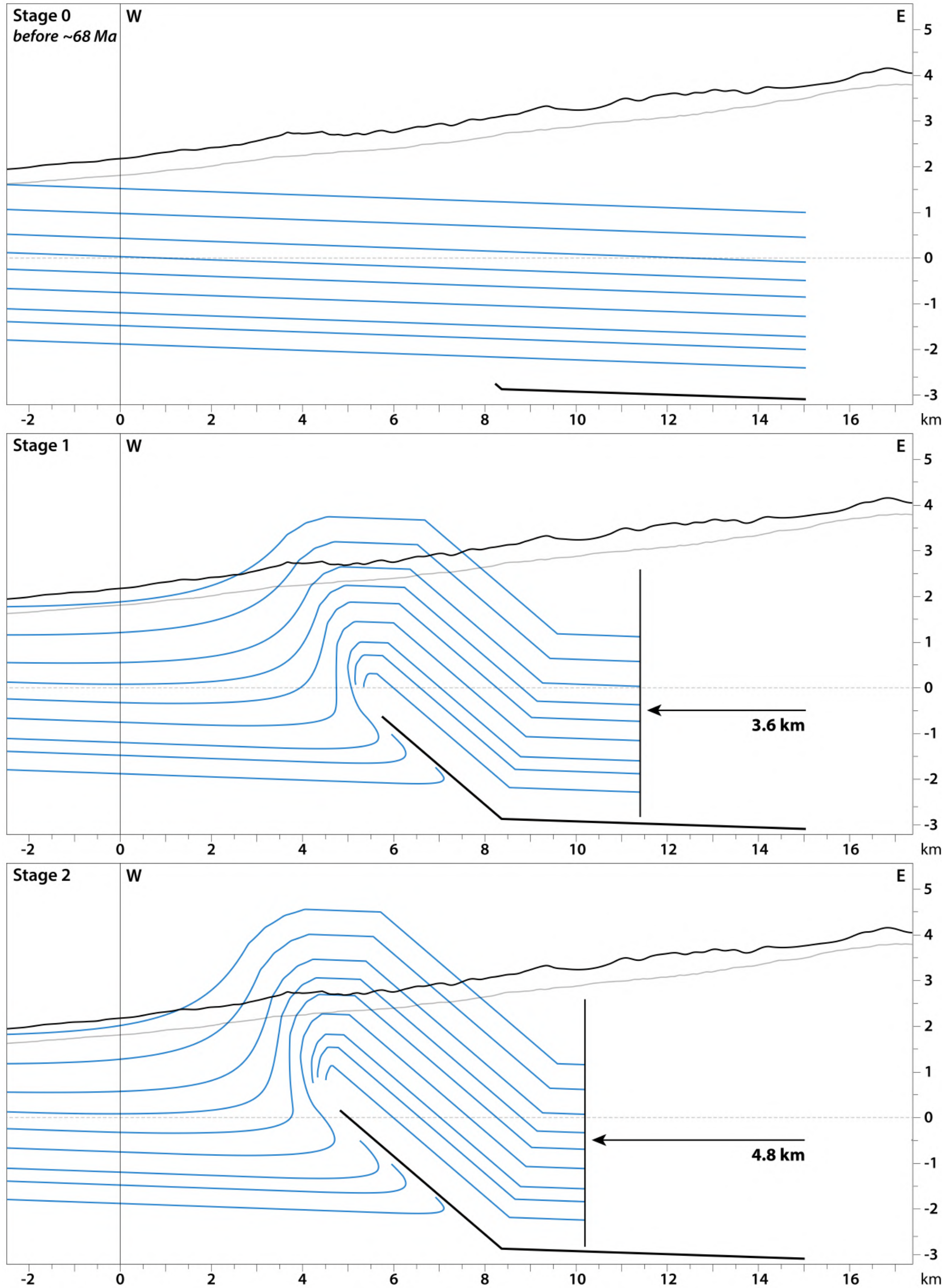

Figure S21. See second part of the figure and description next page.

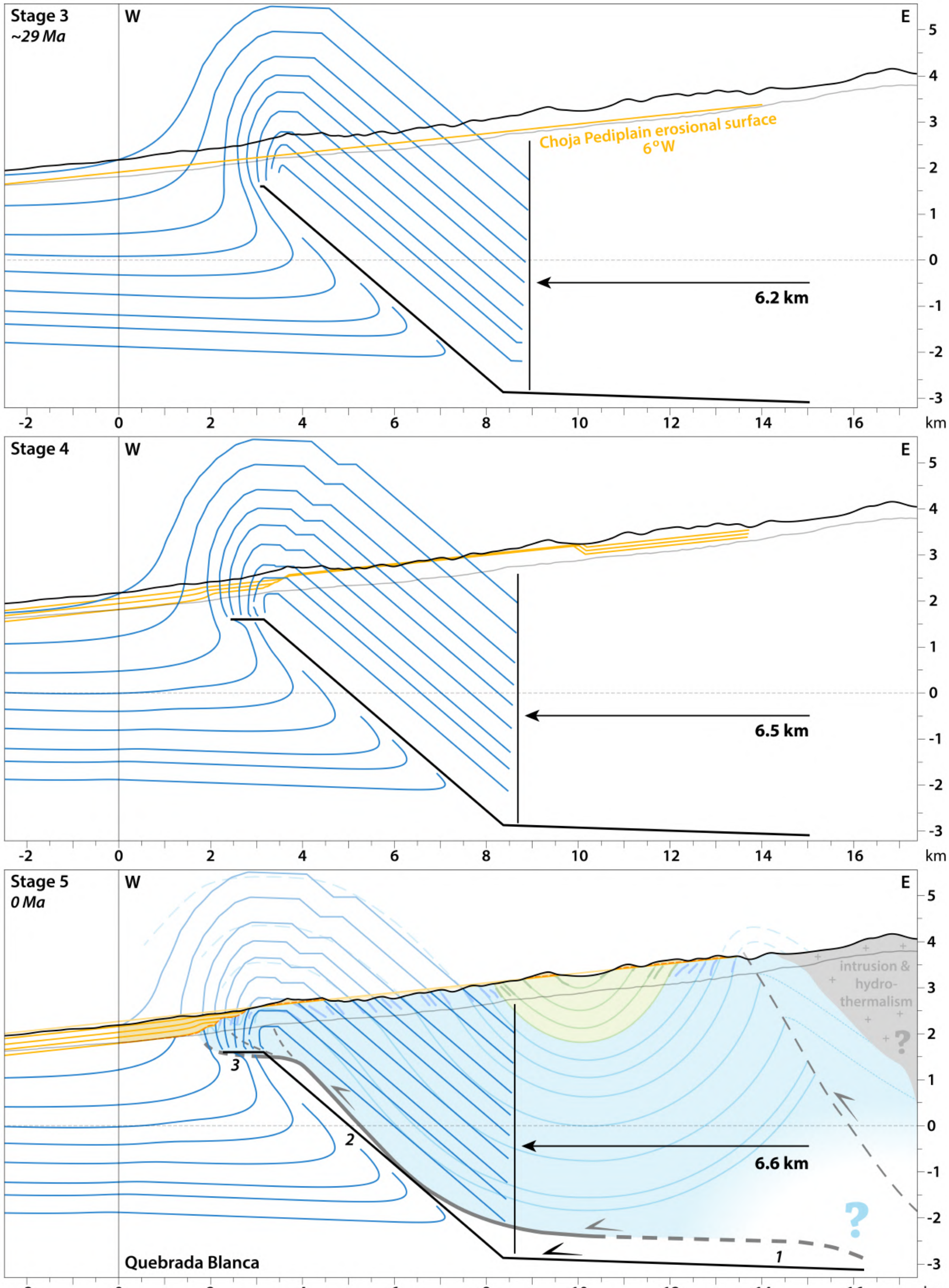

Figure S21. Outcomes from trishear modeling performed with FaultFold Forward v.6 (Allmendinger, 1998) in the case of the Quebrada Blanca section, with chronological constraints provided from geological observations and data (see section 6.1 in main text). The black horizontal arrows underline the cumulated shortening at each stage. The final stage (present-day situation) is overlapped with our structural cross-section. Model parameters are provided in Table S3. In final stage, fault segments are numbered as in Table S1.

	Fault angle	Trishear angle	P/S	Inclined shear angle	Initial bedding dip
Quebrada Tambillo	Segment 1: 0–4°E Segment 2: 20–30°E Segment 3: 0–10°E Segment 4: 5–20°E	50–110°	0.8–3.0	Parallel and similar folding tested	Mesozoic: 0–5°E Cenozoic: 0–4°W
Quebrada Blanca	Segment 1: 0–4°E Segment 2: 30–40°E Segment 3: 0–10°E	50–120°	0.7–3.0	Parallel and similar folding tested	Mesozoic: 0–4°E Cenozoic: 0–7°W

Table S1. Range of tested parameters for the trishear modeling performed with FaultFold Forward v.6 (Allmendinger, 1998). Trial and error forward modeling lead to ~65 tested models for Quebrada Tambillo and ~100 models for Quebrada Blanca. Best results came out with a fault-ramp composed of 4 segments for Quebrada Tambillo, and 3 segments for Quebrada Blanca; segments are here numbered from the deepest to the shallowest. Fault position (tips and bends) and slip on the fault are derived from our geological cross-sections. Initial layer dip angles are chosen in view of the current topography in a range of reasonable initial geometries, which allow to correctly reproduce the sections. The trishear angle controls the size of the deformed area, the P/S (propagation/slip) ratio controls the degree of folding accommodated in the trishear zone. Values for both parameters were tested based on values described as common in the literature. Concerning the inclined shear angle, best fit is obtained with parallel folding for all stages. The inclined shear angle controls the shape of the fold backlimb (Cristallini & Allmendinger, 2002).

Stage	Fault angle	Trishear angle	P/S	Slip (km)	Initial bedding dip
0	3°E	60°	1.4	0	Mesozoic: 3°E
1	24.0°E	60°	1.4	1.0	
2	0°	60°	1.2	2.0	
3	0°	60°	1.2	2.5	
4	11.3°E	90°	1.2	2.6	Cenozoic: 3°W
5	11.3°E	90°	1.2	3.1	

Table S2. Best-fit parameters for the trishear modeling performed with FaultFold Forward v.6 (Allmendinger, 1998) at Quebrada Tambillo. Model results are illustrated on Figure S20.

Stage	Fault angle	Trishear angle	P/S	Slip (km)	Initial bedding dip
0	2°E	50°	0.9	0	Mesozoic: 2°E
1	40.6°E	70°	0.9	3.6	
2	40.6°E	80°	1.0	4.8	
3	0°	90°	0.9	6.2	Cenozoic: 6°W
4	0°	90°	0.9	6.5	
5	0°	90°	0.9	6.6	

Table S3. Best-fit parameters for the trishear modeling performed with FaultFold Forward v.6 (Allmendinger, 1998) at Quebrada Blanca. Model results are illustrated on Figure S21.

Additional Supporting Information (Files uploaded separately)

Data Set S1. Georeferenced dataset (field-logistics.kmz) for visualization (e.g. on Google Earth) of strategic points and paths for the realization of our field missions (in 2018 and 2019). Data points are organized in self-explaining folders:

The folders "major roads" and "dirt tracks" contain lines showing the main paths we followed. Pink, red and orange lines are practicable by (4W drive) cars. White lines are practicable by foot only. Pay attention that we followed the "dirt tracks" for the last time in January 2019. In the case of subsequent rain, even moderate, part of the tracks may have become impracticable by car since then.

The folder "guiding points" comprises strategic (turning-) points on the road, towns and the position of our base-camp in the Pinchal area. Please leave the base-camp always clean and tidy, in the same way as you wish to find it. There, we enjoyed the moon and the stars while cooking excellent French-German-Chilean dishes.

The folder "GPS positions photos" includes two sub-folders for the two investigated areas with the localisations of the field photographs equivalent to those depicted on the structural schemes (Figures 4, 9 and S13). Color and symbol of the point-markers give additional information: Paddle symbol stands for view points, pushpin symbol for pictures illustrating stratigraphic and sedimentary observations. Red for Paleozoic basement, blue for Mesozoic units, yellow for Cenozoic deposits.

References

Allmendinger, R. W. (1998). Inverse and forward numerical modeling of trishear fault-propagation folds. Tectonics, 17(4), 640–656. https://doi.org/10.1029/98TC01907

Allmendinger, R. W. & Shaw, J. H. (2000). Estimation of fault propagation distance from fold shape: Implications for earthquake hazard assessment. Geology, 28(12), 1099–1102.

Cristallini, E. O. & Allmendinger, R. W. (2002). Backlimb trishear: a kinematic model for curved folds developed over angular fault bends. Journal of Structural Geology, 24(2), 289–295. https://doi.org/10.1016/S0191-8141(01)00063-3

Erslev, E. A. (1991). Trishear fault-propagation folding. Geology, 19, 617–620. https://doi.org/10.1130/0091-7613(1991)019<0617:TFPF>2.3.CO;2

Hardy, S. & Ford, M. (1997). Numerical modeling of trishear fault propagation folding. Tectonics, 16(5), 841–854. https://doi.org/10.1029/97TC01171

Zehnder, A. T. & Allmendinger, R. W. (2000). Velocity field for the trishear model. Journal of Structural Geology, 22, 1009–1014.